Frequency-Reconfigurable Low-Profile Omnidirectional Antennas

by

Ken Paramayudha

B. Eng. (Electrical Engineering),
Bandung Institute of Technology, Indonesia, 2009

Thesis submitted for the degree of

Master of Philosophy

in

School of Electrical & Electronic Engineering
Faculty of Engineering, Computer & Mathematical Sciences
The University of Adelaide

2019

Supervisors:

Prof. Christophe Fumeaux, School of Electrical & Electronic Engineering

Dr. Withawat Withayachumnankul, School of Electrical & Electronic Engineering

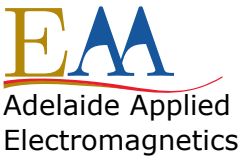

Contents

Abstract

THE high demand of today's wireless technologies has resulted in increasing research efforts dedicated to modern antenna designs. A "smart" antenna with abilities to tune its performance properties into a new environment can significantly increase communications reliability and decrease systems costs. Therefore, reconfigurable features have become a new standard of antenna designs, particularly when stringent performance indicators are required to keep up with increasing system demands. Owing to the radiation characteristics of antennas, an omnidirectional pattern is one that is widely sought after by antenna designers. Due to their uniform coverage, omnidirectional antennas are an ideal choice for numerous indoor or outdoor implementations.

In this context, this thesis investigates substrate-integrated, low-profile, and reconfigurable design solutions for omnidirectional antennas. Firstly, the thesis discusses the development of low-profile monopoles made of shorted patches, where the main objective of this work is to find via-less alternatives for the antenna shortings. Two alternative strategies, namely quarter-wave stubs and complementary split ring resonators, are deployed in substrate-integrated monopoles and are compared with the classical shorting pins in terms of performances. Secondly, the thesis focuses on the investigation of frequency-tunable antennas. The stub-loaded monopole from the first part of the thesis is further developed to create reconfigurable antennas. This work aims to provide multi-band reconfigurable devices with independent tunability between the operating frequencies. In this part, a novel method of designing reconfigurable low-profile monopoles is proposed based on independent magnetic current loops sharing the same thin aperture. Lastly, a circularly-polarized frequency-reconfigurable omnidirectional antenna is demonstrated as the final contribution of the thesis. The antenna operation principle is based on a combination of magnetic current sources, electric current sources, and phase compensation lines between them. Varactor-loaded slots are added to the structure to enable frequency reconfigurability. Moreover, a description of the antenna feeding aspects to maintain the circular polarization in real conditions is presented.

Overall, this thesis provides different designs of high performance low-profile omni-directional antennas. The results suggest that all the antenna designs are promising for numerous wireless applications. The benefits include simple antenna geometry, ease of fabrication, and low-profile. Importantly, the proposed design principles can be extended to other types of reconfigurable antennas.

Originality Declaration

I certify that this work contains no material which has been accepted for the award of any other degree or diploma in my name, in any university or other tertiary institution and, to the best of my knowledge and belief, contains no material previously published or written by another person, except where due reference has been made in the text. In addition, I certify that no part of this work will, in the future, be used in a submission in my name, for any other degree or diploma in any university or other tertiary institution without the prior approval of the University of Adelaide and where applicable, any partner institution responsible for the joint-award of this degree.

I acknowledge that copyright of published works contained within this thesis resides with the copyright holder(s) of those works.

I also give permission for the digital version of my thesis to be made available on the web, via the University's digital research repository, the Library Search and also through web search engines, unless permission has been granted by the University to restrict access for a period of time.

	10/08/2019
Signed	Date

Acknowledgments

First and foremost, praise is due to almighty Allah for giving me the strength, knowledge, ability, and opportunity to complete this Master thesis. Without His blessings, this achievement would not have been possible.

I would like to express my deepest gratitude to my supervisors Prof. Christophe Fumeaux and Dr. Withawat Withayachumnankul. Back in 2016, Prof. Fumeaux was the one who replied to my inquiry and offered me an opportunity to join his prestigious research group, Adelaide Applied Electromagnetics. It is because of his generous help I can pursue my dream to study at The University of Adelaide. Prof. Fumeaux has been a very supportive and approachable supervisor for my Master of Philosophy study. He is always happy and positive minded, always believe and encourages me that I could do more. He has taught me that everything is possible when we believe in ourselves. From the deep inside my heart, I would like to thanks Prof. Fumeaux for all the knowledge, experience, funding, and opportunity.

Dr. Withawat is an outstanding scholar who is a role model for me. His vast knowledge of everything related to microwave devices is essential to my research study. In each weekly meeting, his suggestions and constructive critics to my work were very valuable. I truly enjoyed every discussion with him. Not only that, I remember when the times were stressful and exhausting, he always reminds me to give it a rest and take it easy. I much appreciate this little thing, which kept me going at times.

I also wish to express my appreciation for Dr. Shengjian Jammy Chen for being a generous mentor during my candidature. Every time I faced technical difficulties regarding my research, I can always ask for his help. It is because of him I can finally complete this thesis. Thank you, Jammy!

During my study, I have received valuable help from many friends and colleagues. First of all, I would like to thank the members of the Applied Electromagnetic Groups at the University of Adelaide, Dr. Shengjian Jammy Chen, Dr. Thomas Kaufmann, Dr. Wendy Suk Ling Lee, Dr. Sree Pramod Pinapati, Siti Nailah Zainarry, Ali Malakooti, Weijie Gao, Xiaolong You, Xiaojing Lv, and Jin Huang. I truly enjoyed our group meetings and discussions. I would also like to thank Dr. Thomas Kaufmann, who has provided valuable comments on my writing. In addition, I also acknowledge the

staff of the school, IT officers, workshop colleagues for all their assistance throughout my study, namely Prof. Cheng-Chew Lim, Assoc. Prof. Wen Soong, Dr. Brian Ng, Dr. Damith Ranasinghe, Ms. Jodie Schluter, Ms. Laura McNamara, Mr. Alban O'Brien, Mr. Danny Di Giacomo, Mr. Norio Itsumi, Mr. Brandon Pullen, and Mr. David Bowler. I am also strongly indebted to my good friend from the school, Muhammad Saeed Aslam, who has helped me through the thesis submission process.

To my Adelaide-Indonesian family, thanks for being my support system in this country far away from home. I appreciate all the togetherness and all the good times we spent. Though there are many people to thanks, here are special mentions: my housemate during these two years: Rizky Poer Setyaji, Dewi Retno Pamungkas, Satriyo Krido Wahono and Heri Aprianto; my best friends: M. Naufal Fadhil, Jerryanda Pratama Putra, Igor Ritonga, Dewi Karlina Batubara, Teuku Rifqy Ratzarsyah, Dimas Yudo Bramantyo, and Chaerul Umam; and also Mas Berry Jatnika for the opportunity to join this great band "Rhythmnesia".

I gratefully acknowledge the financial support from the Indonesian Ministry of Research, Technology and Higher Degree Education through the Riset-PRO scholarship, without which I would not have been able to carry on the research.

Now to the most important part of my life, my family. Above all, I would like to send my deepest gratefulness and love to my parents who have always loved me unconditionally. Thanks to my sister, Ken Parimita, and my cousin, Refiyanti, who took care of my parents when I was abroad. I also wish to express my sincere appreciation to my parents-in-law and brothers-in-law, who supported me the best they can.

Last but not least, I would like to express my heartfelt and warmest appreciation to my little family. My lovely wife and daughter, Wigi and Shafiya, who always stands by me in ups and downs, loves, supports and believes in me unconditionally. Bunda, thanks for being a wonderful mother to Shafiya. You two (and soon to be three) are the world to me!

Ken Paramayudha
August 2019
Adelaide, Australia

Thesis Conventions

The following conventions have been adopted in this Thesis:

Typesetting

This document was compiled using LaTeX2e. TeXstudio is used as text editor interfaced to LaTeX2e. Inkscape was used to produce schematic diagrams and other drawings.

Referencing

The referencing and citation style adopted in this thesis are based on the Institute of Electrical and Electronics Engineers (IEEE) style.

System of units

The units comply with the international system of units recommended in an Australian Standard: AS ISO 1000–1998 (Standards Australia Committee ME/71, Quantities, Units and Conversions 1998).

Spelling

American English spelling is adopted in this thesis.

Abbreviation

AR	Axial Ratio
CPW	Coplanar Waveguide
HMSIW	Half-Mode Substrate-Integrated Waveguide
LHCP	Left-Hand Circular Polarization
LP	Linear Polarization
PCB	Printed Circuit Board
PEC	Perfect Electrical Conductor
PIFA	Planar Inverted-F Antenna
RF	Radio Frequency
RFID	Radio Frequency Identification
RHCP	Right-Hand Circular Polarization
SIW	Substrate-Integrated Waveguide
SMA	SubMiniature Version A
TEM	Transverse Electromagnetic
THz	Terahertz
TM	Transverse Magnetic
UWB	Ultra-Wideband
VSWR	Voltage Standing Wave Ratio

List of Figures

List of Tables

Chapter 1

Introduction

THIS introductory chapter presents a short overview of low-profile monopole antennas with frequency tunability. An overview of the objectives and motivations of the thesis will also be presented. Finally, the structural organization of the thesis is outlined with the highlights of original contributions.

1.1 Introduction and Motivation

The miniaturization and integration of antennas has been the focus of numerous research in the last decades. It is known that compact and low-profile antennas provide structural benefits, in particular for mountable wireless applications such as vehicular communications systems. Low-profile antenna structures are less noticeable, highly portable, and can be easily integrated on vehicles within a limited surface area. Nonetheless, it is noted that there are trade-offs between antenna size and performances, namely radiation efficiency and gain. A physical limitation to the miniaturization of antennas has been investigated in the classical paper [1]. One method to miniaturize the antenna is by increasing the radiation resistance using shorting wires [2, 3]. The method has been adapted into numerous antenna designs, in particular low-profile monopoles [4–9].

The demands in wireless technologies for compact antennas with an omnidirectional pattern make the low-profile monopoles a perfect choice for many communications systems. However, this type of antenna has narrow-band characteristics, which makes the antenna not suitable for advanced applications that require a broad frequency coverage. For this type of applications, one can design a wideband omnidirectional antenna. Nevertheless, such design may require to sacrifice the compactness and low-profile, as a large thickness is usually required to operate at a wide bandwidth [4, 8, 9]. An alternative solution is to make the antenna frequency-tunable. This feature can be achieved by incorporating active tuning elements such as varactor diodes into the antenna structure. Frequency reconfigurability allows the antenna to operate at a wider bandwidth than a static one while remaining low-profile. Furthermore, compared to wideband antennas, a frequency-tunable antenna can reduce unwanted interferences from unused bands, and thus limit the use of RF filters in the system.

In advanced applications, such as software-defined radios or carrier-aggregation systems, antennas with frequency reconfigurability and multi-band feature are required. Besides, multi-band antennas should have a tuning independency between the bands. Designing this kind of antennas is complicated, as several aspects must be carefully considered, such as satisfactory matching and radiation pattern and polarization consistency. Until now, only a few existing antennas can fulfil this requirement [10–15], with only one of these designs intended to radiate omnidirectionally [15]. Another desirable feature may be that the antenna can have circularly polarized radiation. This

mode of wave polarization has advantages over a linearly polarized one, namely robustness to interferences, fading, and misorientation between transmitting and receiving antennas.

In this mentioned context, this thesis will firstly investigate shorting techniques in low-profile monopole antennas by comparing the performances between antennas using via- and via-less shortings. The investigated antenna structures then will be used to design multi-band frequency reconfigurable low-profile monopole antennas. Following this, a concept of circularly polarized frequency reconfigurable antenna with omnidirectional pattern will be proposed.

1.2 Objectives

Three main objectives of the thesis are described in details in the following.

- **To realize via-less low-profile monopoles**

  As mentioned earlier, one of the methods to miniaturize the antenna is by employing shorting vias in the antenna structure. By using shorting vias, an antenna can radiate below its fundamental mode [2, 3]. Additionally, it has been demonstrated that physical vias integration enables a patch to radiate as a magnetic current loop, resulting in a monopolar radiation mode [5]. However, although vias integration into the patch has been demonstrated to be advantageous, one may argue about the increasing fabrication complexity. Besides, difficulties may arise in DC biasing, particularly in the context of reconfigurable antenna designs. Motivated by these challenges, the first objective of the thesis is to find via-less alternatives for the antenna shortings. Quarter-wave stubs and complementary split ring resonators (CSRRs) will be deployed in low-profile monopoles as shorting alternatives. These two alternative strategies of shortings will be compared with the classical vias in terms of performances.

- **To design multi-band frequency reconfigurable low-profile monopoles with independent tuning capability**

  An essential feature of reconfigurable multi-band antennas would be to tune the antenna to a first band at a given frequency while being able to independently control other bands at other frequencies. To obtain this feature, several design

aspects must be studied carefully. This leads to the challenging task of designing multi-band frequency reconfigurable antennas with a completely separated link between their performance properties. In this thesis, multi-band frequency reconfigurable low-profile monopoles based on magnetic current loops will be investigated and developed to obtain the desired tuning independence.

- **To design a circularly polarized low-profile monopole antenna with a continuous tuning frequency**

  A circularly-polarized antenna has several benefits compared to an antenna that radiates with linear polarization [16]. For instance, an antenna with circular polarization is effective in mitigating multi-path interferences or fading [17, 18]. The main challenge of designing a frequency-reconfigurable low-profile monopole antenna with circular polarization is to maintain the axial ratio across the tuning ranges. Besides, stable monopolar patterns should be attained across the operating frequencies. In the last part of the thesis, a new concept of a circularly-polarized frequency reconfigurable antenna with omnidirectional patterns will be demonstrated.

1.3 Thesis Structure and Original Contributions

As depicted in Fig. 1.1, this thesis begins with introduction and background in the first two chapters, followed by two main contributions that are divided into three chapters, and summarized with a conclusion and future work discussion in the last chapter. The chapters are described in detail in the following:

Overview (Chapters 1 & 2). The first part of the thesis covers the current introduction chapter and Chapter 2, where the context and the background information required for the rest of the thesis are provided. The second chapter contains three major topics: i) a short review of image theory applied to dipoles and monopoles; ii) a brief literature review on low-profile monopole antennas, and iii) an investigation on published frequency-reconfigurable antennas, with a particular focus on monopolar antennas.

Low-profile antennas (Chapter 3). The second part of the thesis focuses on omnidirectional antennas based on substrate integrated cavities. As the first contribution

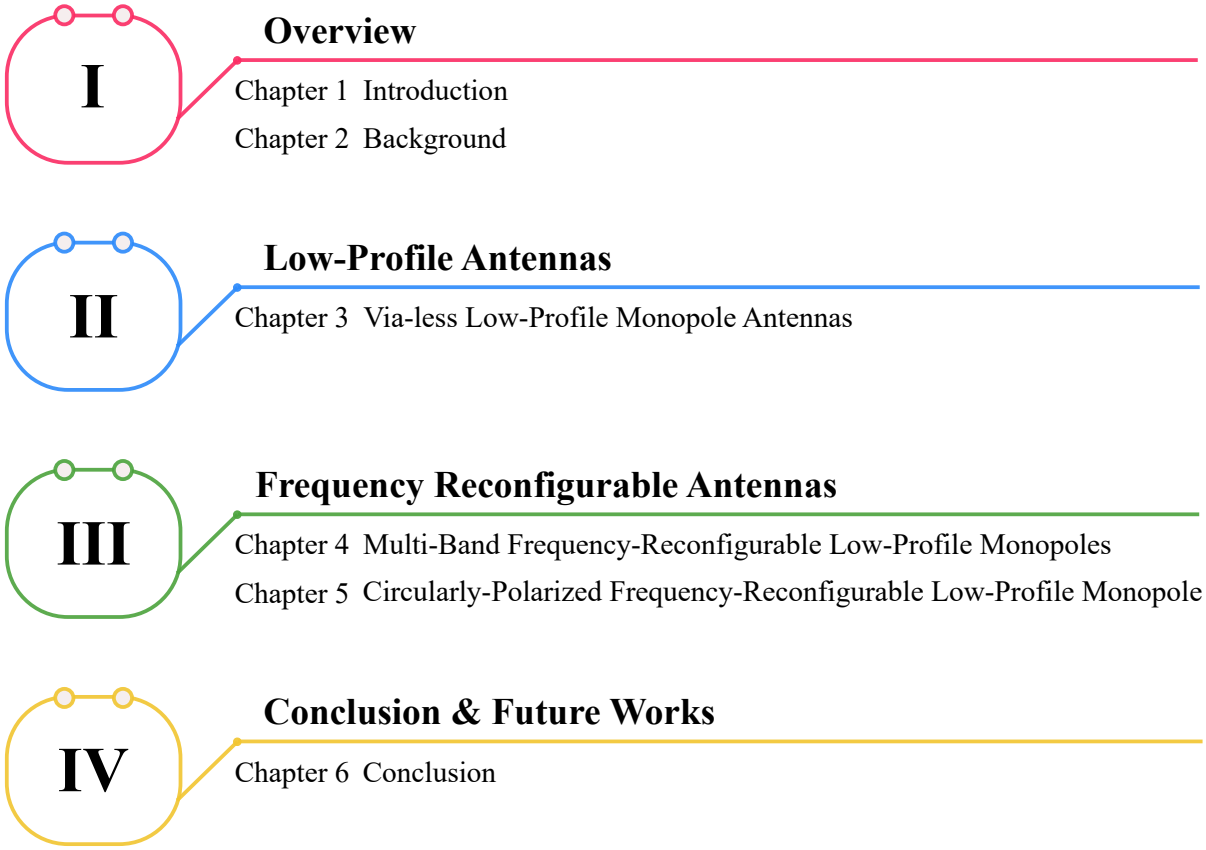

Figure 1.1. Thesis structure. The thesis comprises 6 chapters where the first two chapters are the overview of the thesis while the last chapter summarizes the thesis. The main chapters in between focus on the original contributions of the thesis.

of the thesis, three designs of low-profile monopole antennas realized using different shorting methods, namely vias, stubs, and CSRRs, are investigated. All designs use the same substrates and are optimized to operate at the dedicated short-range communications (DSRC) band. Via-less shortings on low-profile monopole antennas have advantages of simple fabrication and DC isolation. However, the results indicate that via-less structures come with trade-offs, particularly in size, bandwidth, and polarization purity. This work has been presented in *3rd Australian Microwave Symposium (AMS), 2018* under the title of "Low-profile monopole antenna with via-less shorting". The conference paper was one of the finalists for The Best Student Paper Award of AMS 2018.

Frequency reconfigurable antennas (Chapter 4 & 5). The next part of the thesis covers frequency reconfigurable antennas that radiate omnidirectionally. In particular, two antennas with different features are proposed: i) multi-band reconfigurable low-profile monopole with independent tunability, and ii) frequency-reconfigurable circularly-polarized monopolar antenna.

Chapter 4 is about multi-band reconfigurable antennas with independent tuning capability. As the second contribution of the thesis, multi-band frequency-reconfigurable low-profile monopole antennas with independently tunable bands are proposed based on the concept of independent magnetic current loops sharing a common thin aperture. Instead of using vias, groups of quarter-wavelength stubs are utilized to create sets of equivalent shorting points. The frequency tunability is achieved by employing varactor-diodes to control the current distributions of the antennas. The proposed concept is firstly validated by a dual-band frequency reconfigurable prototype and then extended to a triple-band device. The measurement shows that the tuning between bands is independent of the state of the other bands for all designs. Additionally, both antennas radiate omnidirectionally across the tuning frequencies. These results suggest that the proposed designs are suitable for advanced applications that require independent reconfigurability in multi-band operation. The designs have been submitted to *IET Microwaves, Antennas and Propagation* under the title of "Triple-band reconfigurable low-profile monopole antenna with independent tunability".

As the last contribution of this thesis, a circularly-polarized frequency reconfigurable low-profile monopole antenna is investigated in Chapter 5. The structure is based on center-fed circular patch surrounded by arc-shaped printed strips. Circular polarization is attained by the combination of two complimentary current sources. Electric current sources are originating from the arc-shaped strips, while slot cavities act as magnetic current sources. To achieve frequency-reconfigurability, varactor-loaded slots are included onto the patch. The result suggests that the variation of slots capacitance allows the resonance frequency of the antenna to be shifted. The antenna radiates omnidirectionally across the tuning frequencies. An article is in preparation on the basis of this chapter for submission to an antennas and propagation journal.

Conclusion and future works (Chapter 6). A summary of the thesis is included in the last chapter, as well as a perspective on future work.

Chapter 2

Background

OMNIDIRECTIONAL antennas with a capability to alter their frequency and radiation properties dynamically are beneficial to fulfill the demand of today's wireless communications systems. Such devices facilitate the reduction of user interferences resulting in high capacity and cost-effective systems. A low-profile monopole antenna is one type of antennas that can radiate omnidirectionally, and will be further investigated in this thesis. Therefore, the discussion of this chapter is related to the low-profile monopole antennas. The chapter first provides a background on the image theory, which is used frequently throughout this thesis to analyze the radiation patterns of the proposed low-profile monopole designs. A brief literature review on low-profile monopoles is then presented, followed by a discussion on frequency-reconfigurable antennas.

2.1 Introduction

Antennas are essential parts of wireless communications systems. From consumer devices, for example, mobile phones, TVs, radios, and laptops to high-performance military applications such as radar, all systems require an interface to wirelessly transmit and receive the electromagnetic signals. Antennas bridge the gap between electric currents that move in metal conductors and radio waves that propagate through free space. Based on reciprocity, antennas can transmit and receive signals in identical manner, which is described by a set of common performance measures. Until today, there are many types of antennas that have been well-developed to meet system specifications. However, demands still exist for antennas that are tailored to particular applications, with increasing performance indicators to keep up with increasing system demands. Besides, with the rapid growth of personal communications, the cost and performance of an antenna system are essential. Because of this, research efforts invested into reconfigurable antennas are rapidly increasing.

The development of reconfigurable antennas started with the idea of dinamically modifying the performance characteristics of the antenna. Resonance frequency, impedance bandwidth, polarization, and radiation pattern are examples of parameters that are often needed to be adapted in order to meet desired specifications. Rather than re-designing and re-building an antenna for each set of specifications, using a "smart" antenna with tuning properties appears a more time- and cost-effective alternative. Moreover, by altering the antenna performance, the capacity of the wireless communications can be improved since the interferences from other users can be in principle decreased. In most cases, this will reduce the overall cost of the system.

Recently, low-profile monopole antennas have become essential devices in microwave applications. Some of the examples include vehicle communications [19], aircraft applications [20], and sensor technologies [21]. The antenna can radiate omnidirectionally, which facilitates a uniform azimuthal coverage that is useful in conditions where the other transceivers are deployed randomly. The performance of a low-profile monopole antenna can be further improved by making it frequency tunable. This allows the antenna to cover a wide range of operation bandwidth while it remains low-profile.

In this chapter, a short explanation of the image theory will be firstly presented, with a focus on a dipole and a monopole. The principle will be used in this thesis to analyze the radiation characteristics of the proposed low-profile monopole antenna designs. Following this, a brief literature review on low-profile monopole antennas will

be discussed. The last section of this chapter will investigate frequency-reconfigurable antenna designs that have been previously published, with a particular focus on omnidirectionally reconfigurable antennas.

2.2 Image Theory

Image theory is used as a geometrical method to analyze the performance of an antenna radiating over a ground plane. Virtual sources are introduced to account for the reflections and these additional sources are combined with the real sources to form an equivalent system. This section briefly summarizes the method that can be found in textbooks [22, 23], with a focus on the antenna types that will be investigated in this thesis.

2.2.1 Image Theory Applied to a Dipole

Let us consider a vertically oriented electric dipole at a near distance h above an infinite perfectly electrically conducting (PEC) ground plane, as shown in Fig.2.1(a). Based on image theory, a virtual source is introduced below the ground plane to generate the reflections [22, 23]. According to the boundary conditions, there are no tangential components of the electric field on the PEC interface. Therefore, to satisfy the boundary conditions and to excite the same polarization of the reflected waves, the virtual source is also vertical and with the same polarity as the actual vertical source. The virtual dipole is combined with the real one to form an equivalent model. On and above the conductor, the equivalent model gives the same radiated field as the original problem with a ground plane. Meanwhile, the actual fields below the interface are zero, hence the model is not valid below the ground plane.

Using the same principle, an arrangement of a horizontal electric dipole produces the equivalent model shown in Fig.2.1(b). As $h \rightarrow 0$, horizontal electric dipole over ground plane will not radiate because the sum of the real and image currents nullifies each other. In another case, if the orientation of the dipole is arbitrary, the dipole currents can be decomposed into vertical and horizontal components.

LIBRARY NOTE:

This diagram has been removed due to copyright.

Figure 2.1. Image theory on electric dipoles. (a) Vertical and (b) horizontal electric dipoles above an infinite, flat, perfect electric conductor. Re-drawn from [22].

2.2.2 Image Theory Applied to a Monopole

The equivalent model can also be applied to explain a monopole antenna as shown in Fig. 2.2. Using image theory, the equivalent model of a monopole becomes a dipole that is driven by a voltage source V. In the actual condition, a voltage source has to be $V/2$ to obtain the same current I on both arms of the dipole (real and image). As a result, the characteristics of a monopole can be derived from a dipole. The input impedance of $\lambda/4$ monopole above a ground plane can be determined by:

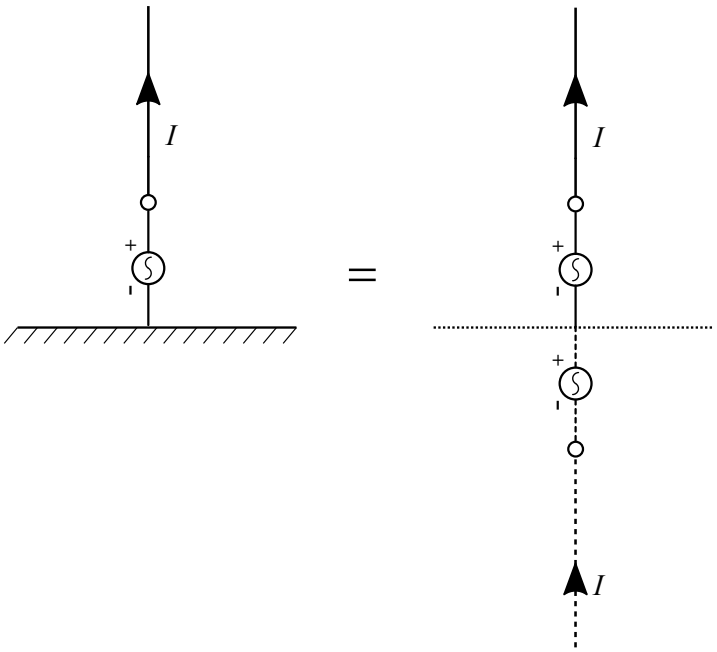

Figure 2.2. Image theory on a monopole antenna. Characteristics of a monopole can be derived from a dipole.

$$Z_{\text{monopole}} = \frac{V_{\text{monopole}}}{I_{\text{monopole}}} = \frac{\frac{1}{2}V_{\text{dipole}}}{I_{\text{dipole}}}, \tag{2.1}$$

with

$$I_{\text{monopole}} = I_{\text{dipole}}, \tag{2.2}$$

hence [22]

$$Z_{\text{monopole}} = \frac{1}{2}Z_{\text{dipole}} = 36.5 + j21.25\ \Omega. \tag{2.3}$$

From the image theory, it is also known that a monopole radiates the same fields over a ground plane as a dipole. The radiation intensity of a monopole $U(\theta, \pi)$ is the same as that of a dipole for $\theta \geqslant 90°$, with the fields below the ground plane being zero. Therefore, the average power radiated by a monopole is half that of a dipole. The directivity of the dipole is

$$D_{\text{dipole}} = \frac{U_m}{U_{\text{avg}}} = \frac{U_m}{W_d/4\pi}, \tag{2.4}$$

where W_d is dipole radiated power. Because a monopole only radiates half the power,

$$W_m = \frac{1}{2} W_d, \tag{2.5}$$

and

$$D_{\text{monopole}} = \frac{U_m}{W_d/8\pi}, \tag{2.6}$$

hence,

$$D_{\text{monopole}} = 2D_{\text{dipole}}. \tag{2.7}$$

In other words, the directivity of a monopole is two times that of a dipole or 3 dB higher.

2.3 Low-Profile Monopole Antenna

An early development of a monopole antenna with a low-profile feature was firstly introduced in the 1950s by Seeley [2]. The motive of the research was to reduce the size of a capped monopole by increasing the radiation resistance using a folded part. The folded part is technically a shorting wire connecting the patch and the ground. This technique was then re-introduced in the 1990s by Deleveaud *et al*. [3]. They miniaturized the monopoles using two shorting pins. Until the present time, the use of the shorting posts for the low-profile configuration of the monopole has been further developed into many designs [4–9].

In [4], Nakano *et al*. show the functionality of conducting pins and a capacitive gap to adjust the input resistance of the monopole. In principle, the capacitive gap, which is a cut ring slot in the patch monopole as illustrated in Fig. 2.3, is included to add capacitances. On the contrary, the conducting pins are used to increase the input resistance by adding inductances into the antenna. The combination of both elements has been proven effective as design technique to improve the impedance matching of the antenna. Therefore, similar design techniques will be widely applied in this thesis as essential method to attain a desired impedance matching of the proposed antennas.

An antenna structure that is based on a square substrate-integrated cavity with shorting vias was introduced in [5]. The shorting pins were positioned along the cavity side walls to form four slot aperture, in which four equivalent in-phase magnetic current are created. The structure then can be seen as a magnetic current loop antenna that radiates omnidirectionally as a monopole. This approach of employing shorting vias

to open radiating apertures provides a new perspective to the design of low-profile monopole antenna. Of particular interest in this thesis, this perspective has become a fundamental principle to the design of antennas in Chapters 3 and 4. The proposed concept is depicted in Fig. 2.4.

In a more recent publication, Nguyen-Trong *et al*. proposed a design of low-profile wideband monopolar antenna based on edge-shorted patch with four additional symmetrical tapered slots on the patch to reduce the overall antenna size [8]. Figure 2.5 shows the geometry of the antenna. The radiation of the antenna was based on magnetic current loop similarly as the previous example [5]. A wide impedance bandwidth

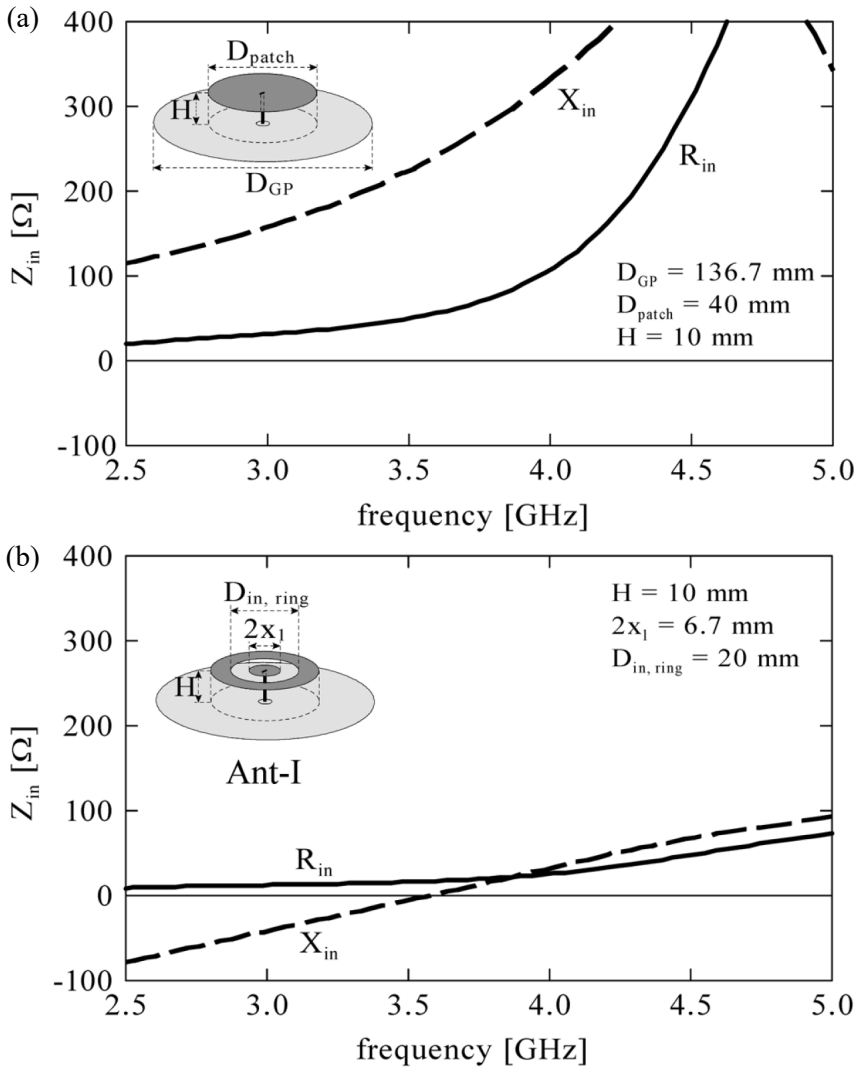

Figure 2.3. Capacitive gap on a monopole. Input impedances of (a) the original patch and (b) patch with a capacitive gap. Adopted from [4].

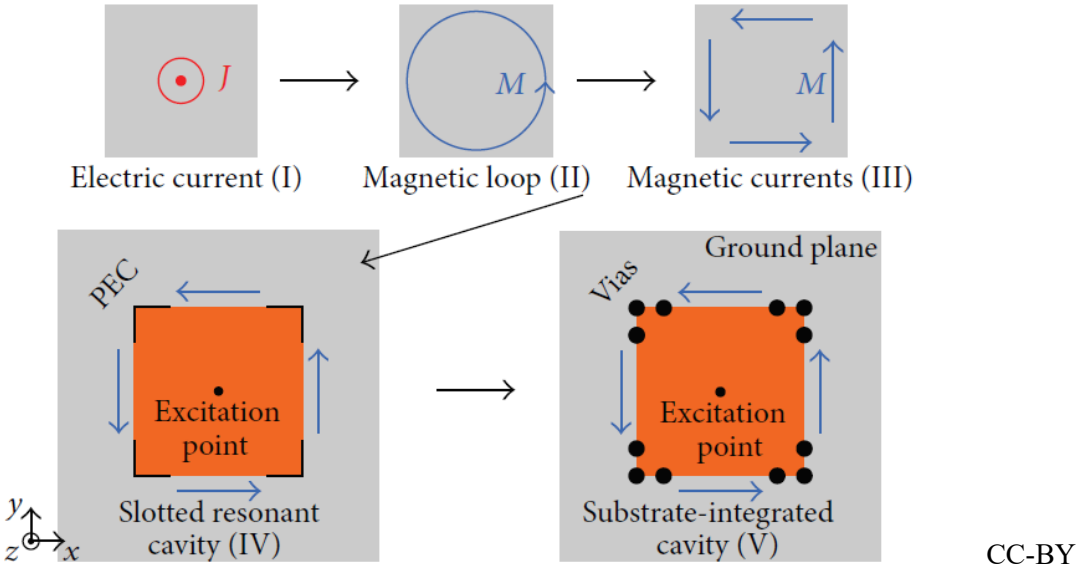

Figure 2.4. Radiation principle of low-profile antenna with omnidirectional monopole pattern. Evolution from electric current perpendicular to a ground plane to a slotted substrate-integrated cavity. Adopted from [5].

of about 3:1 was obtained after the slots size and the height of the antenna were optimized. It has been shown in the paper that by increasing the antenna height, the bandwidth could be further enhanced.

2.4 Frequency-Reconfigurable Antenna

The rapid growth of wireless communication systems has resulted in congestions of the available electromagnetic spectrum. To deal with this issue, a system that is cognitive and reconfigurable is advantageous. In the context of antennas, reconfigurability is the ability to change the radiation characteristics through electrical, mechanical, or other means [24]. These radiation characteristics include the resonance frequency, polarization, radiation pattern, or their combinations. Typically, a single reconfigurable antenna can produce the same RF performances compared to more than one single-purpose traditional antenna. As a result, a significant system cost saving will become realizable. Furthermore, reconfigurable antennas can potentially be used in different systems and applications and this features enable them to cope with increasing demands in mobile communications.

Multi-band and wideband antennas can operate across a wide range of frequencies. However, they cannot provide noise rejection in the bands that are not in use unlike

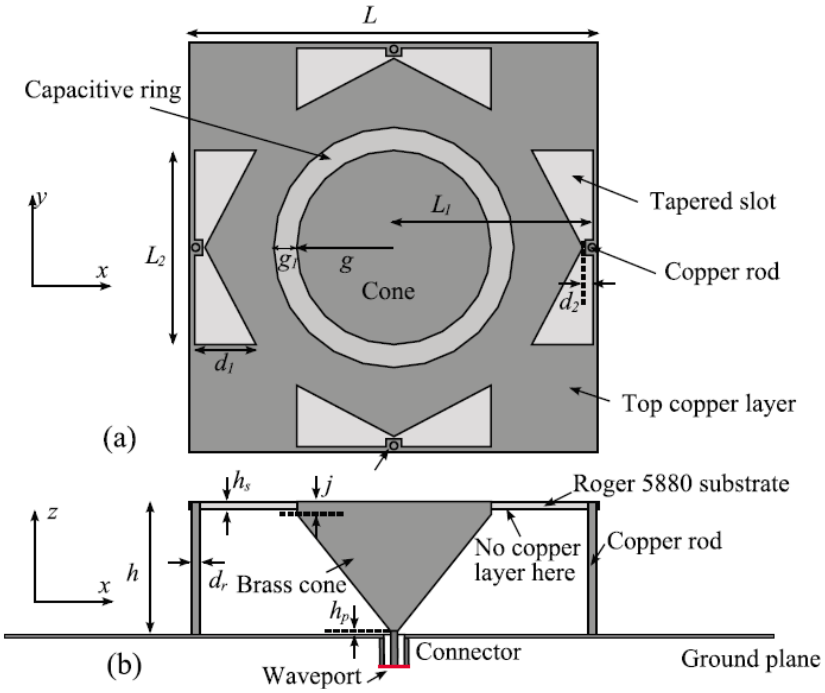

Figure 2.5. Design of a wideband low-profile monopolar antenna. (a) Top view and (b) side view. Adopted from [8].

frequency-reconfigurable antennas. In addition, although reconfigurable antennas are typically narrowband [10–15, 25], they provide a first means to reduce the possibility of jamming signals. This is essential for high-security applications such as military wireless communications. Naturally, a system consisting of a wideband antenna plus tunable filter can be used in this type of applications. Nonetheless, filters may add complexity and reduce the gain of the system as they come with size and cost. While the usage of filters in wireless communication system can not be avoided, it is certain that a frequency-reconfigurable antenna could ease requirements on additional RF filters.

In a large number of cases, a change in the resonance frequency of an antenna will affect other radiation characteristics or vice versa [24]. This performance linkage is inevitable and has become a relevant challenge for the designers with the aim of making it separable. Nevertheless, some approaches have been taken in the literature. The first approach consists in coping with the unwanted changing characteristics and associated performance degradation while focusing on one main property of interest. A second approach is to exploit the change as an advantage, through adjusting different performance parameters to accommodate user requirements. Lastly, a third strategy is

to design an antenna with a completely separated link between its performance properties. The latter feature has received significant attention recently, particularly in the context of multi-band antennas [10–15]. A desirable feature of reconfigurable multi-band antennas would be to tune the antenna to a first band at a fixed frequency while being able to control other bands at other frequencies. This is not a straightforward task, as many aspects must be considered in the antenna design to achieve the tuning independency. These aspects include the position of the active elements, the coupling between antenna elements, and the location of the highest current density.

Based on the type of tunability, frequency-reconfigurable antennas are classified into two different mechanisms, namely discrete and continuous tuning. Discrete tuning can be achieved by using PIN diodes or RF-MEMS switches. This type of tuning utilizes a switching mechanism in the structure of the antenna to obtain a multi-band performance. For the second mechanism, i.e. continuous tuning, the use of varactors diodes allow for smooth transitions across the tuning frequency by changing the biasing voltage to control capacitance. With the continuous frequency tuning capability, a wide range of operation bandwidth can be covered by the antenna. For the case of low-profile monopoles, this could mean that the device could cover a wide instantaneous bandwidth while remaining low-profile. This performance characteristic is one of the requirements of the antenna designs in this thesis.

2.4.1 Discrete Frequency Tuning

Discrete tuning occurs when the change of the resonance frequency of the antenna is discrete. This means that the operating frequency is fixed, and can only change between a finite number of bands, as shown in Fig. 2.6, for a case where the antenna has three switchable bands. A discrete frequency tuning can be obtained by incorporating active switches such as PIN diodes or RF-MEMS switches in the structure of the antenna. The switching mechanism enables a change in the operating frequency by adding or removing shapes of the radiating area or altering the current distributions of the antenna.

A PIN diode is a semiconductor device that acts similarly as a current-controlled resistor at microwave frequencies. The amount of current injected through the Intrinsic (I) region is inversely proportional with the RF resistance. PIN diodes also can be used as a switch and limiter. The popularity of PIN diodes is increasing for microwave circuit

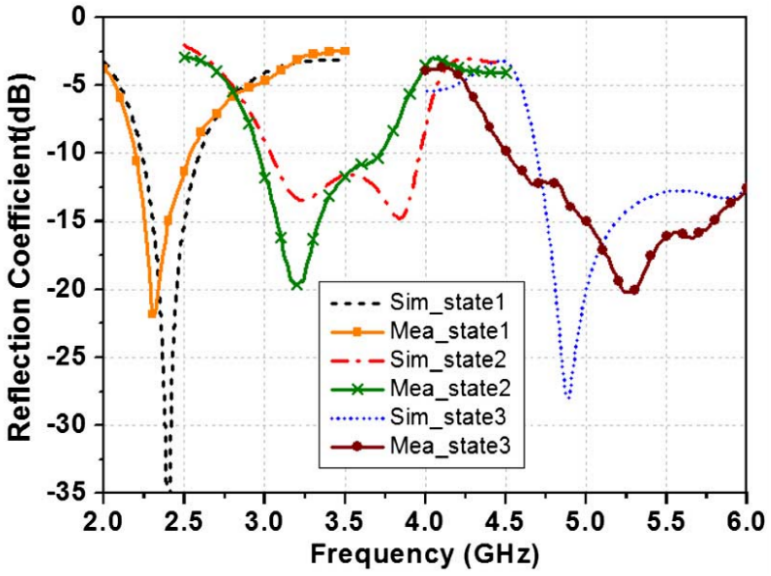

Figure 2.6. Reflection coefficients of a discrete frequency tuning antenna. The antenna can operate in three switchable bands: Bluetooth, WiMAX and WLAN. Adopted from [26].

applications due to their quick switching times and relatively high current handling capabilities. The structure of a PIN diode is depicted in Fig. 2.7.

The acronym "PIN" is indicative of the stack of *P*-type, *I* region, and *N*-type material semiconductor. The *P* contact is the anode, and the *N* contact is the cathode. The *I* region is between the *P* and *N* region. The width of the *I* region plays a vital role in the performance of the PIN diode. A PIN diode allows RF energy to flow when it is forward biased (ON state), and when it is reverse biased (OFF state), it blocks the RF energy flow. The electrical model of a PIN diode in the forward bias mode is similar to an inductor in series with a resistor, as shown in Fig. 2.8(a). In the reverse bias mode, a PIN diode is equivalent to an inductor in series with parallel capacitor and resistor, as depicted in Fig. 2.8(b). PIN diodes offer excellent linearity and are suitable for RF applications. However, frequency-reconfigurable antennas that employ PIN diodes typically have a lower radiation efficiency and realized peak gain compared to

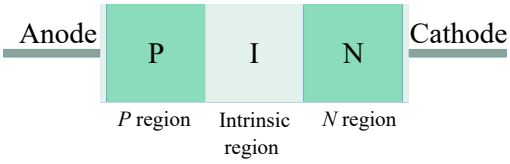

Figure 2.7. PIN diode structure.

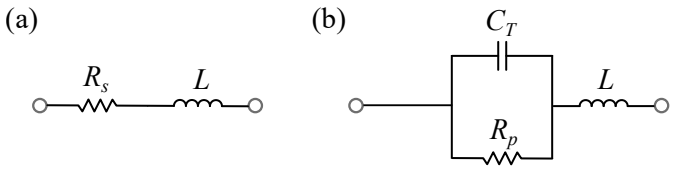

Figure 2.8. PIN diode electrical model. (a) Model of the PIN diode in forward bias mode (ON state) and (b) reverse bias mode (OFF state). R_s is the (low) resistance of the diode in forward bias mode; L is the parasitic inductance of the package; C_T is the sum of the diode junction capacitance and the parasitic capacitance of the package; and R_p is the (high) resistance of the diode in reverse bias mode.

a static antenna. This is because of relatively high ohmic losses when the RF signal pass through the PIN diodes in ON state. Nonetheless, PIN diodes have been widely used in many frequency-reconfigurable antenna designs during the last decades [26–32].

In [27], four PIN diodes were employed to create frequency diversity in a monopolar patch antenna. By switching the PIN diodes states, the frequency modes of the antenna can be tuned to eight different modes ranging from 1820 to 2480 MHz. The same number of PIN diodes was also used in the slotted ground structure of a monopole antenna, as reported in [28], which enables five switchable states: ultrawideband (UWB), three narrow bands, and one dual-band. The antenna design is shown in Fig. 2.9. In another recent publication, two PIN diodes were software-controlled to enable four distinct bands in a printed monopole [32]. This experiment aimed to simulate a cognitive radio network. The software automates activation of two switches based on users activity in a simulated environment.

Another switching technology that is typically used to design an antenna with a discrete tuning capability is based on RF-MEMS switches. Compared to semiconductor switches, RF-MEMS switches have a lower insertion loss due to low ON state resistance. They also provide large isolation due to a small parasitic capacitance. Nevertheless, their switching time is relatively slow, which may degrade the RF performance of the switches when they are utilized in a reconfigurable antenna. In [33], a single RF-MEMS switch was deployed in a planar inverted-F antenna (PIFA) to alter the current flow path. This resulted in a change in resonance frequency with a ratio of 7 between the two operating bands. In another reference, MEMS were integrated into an UWB single-sided monopole to obtain a frequency rejection [34]. The RF-MEMS was biased

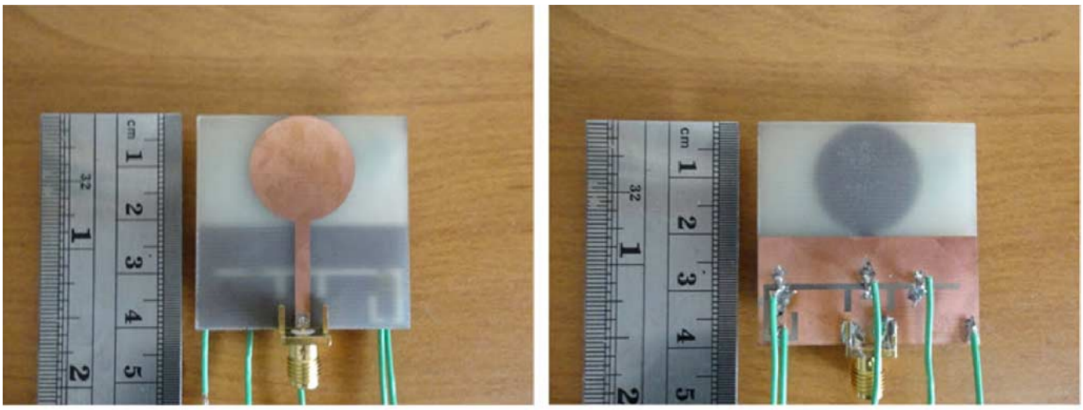

(a) (b) © 2015 IEEE

Figure 2.9. Frequency-reconfigurable monopole using PIN diode switches in the slotted ground structure. (a) Top and (b) bottom views. Adopted from [28].

with high-resistive lines on SiO_2 (Quartz) substrate. This arrangement does not require a backside ground plane which single-sided monopoles do not have. The RF-MEMS integrated antenna is depicted in Fig. 2.10.

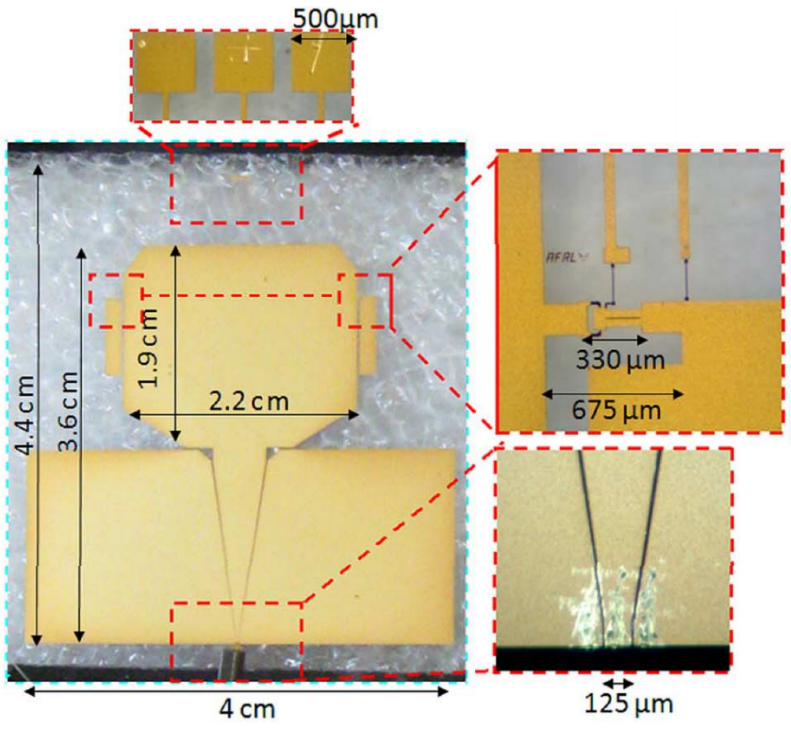

© 2014 IEEE

Figure 2.10. RF-MEMS integrated frequency-reconfigurable monopole. Top view of the fabricated antenna showing the RF-MEMS switch, feeding taper, and DC bias pads. Adopted from [34].

2.4.2 Continuous Frequency Tuning

A continuous frequency tuning means that the operating frequency of the antenna can have any value within the tuning range with a fine resolution. This is illustrated in Fig. 2.11, where the operating frequency can shift between 1.60 GHz and 2.23 GHz. Typically, a continuous frequency tuning can be attained by altering the effective electrical length of the antenna. To change the electrical length of the antenna continuously, one can incorporate devices with a continuous range of values into the antenna. To fulfill this requirement, varactor diodes are commonly used.

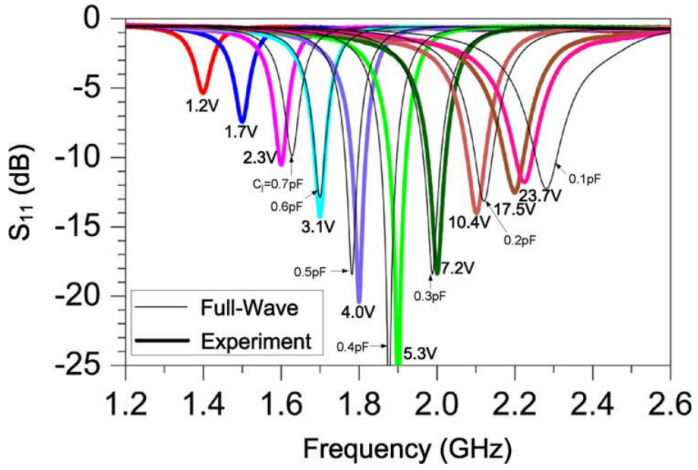

Figure 2.11. Reflection coefficients of a continuous frequency tuning antenna. The antenna can operate in frequencies between 1.6 GHz and 2.23 GHz. Adopted from [35].

Varactor diodes are diodes with a very thin depletion layer that can act as capacitors. They are usually based on silicon or gallium arsenide semiconductors. The equivalent circuit of a varactor diode is shown in Fig. 2.12. The capacitance value of a varactor diode varies depending on the applied reverse bias voltage. When the voltage gets larger, the capacitance of the varactor diodes decreases and vice versa. The type of varactors that are used throughout the thesis is based on hyperabrupt p-n junction. This varactor diodes provide greater capacitance change for the given voltage change than the abrupt types. The capacitance C can be calculated as [36,37]:

$$C(V) = \frac{C_{JO}}{(1 + V/V_J)^M} + C_{\text{par}}, \tag{2.8}$$

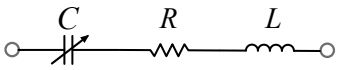

Figure 2.12. Varactor diode electrical model. The capacitance value C varies depending on the applied reverse bias voltage, R and L are the intrinsic resistance and inductance of the varactor.

Table 2.1. MACOM MA46H120 varactor parameter values. Adopted from [36].

R	L	C_{JO}	V_J	M	C_{par}
2 Ω	0.05 nH	1.2 pF	4.155 V	1.97	0.1044 pF

where junction capacitance C_{JO} and junction voltage V_J are constant, M is greater than 0.5 for hyperabrupt p-n junction and C_{par} is the parasitic capacitance of the varactors. The varactor type that is used for the antenna designs in this thesis is MA46H120 from MACOM Technical Solutions. The values of the varactor parameters were measured and derived in [36], and are summarized in Table 2.1. The varactor capacitance C varies from 1.30 to 0.15 pF when biased with 0 to 18 V voltage.

Numerous frequency-reconfigurable antennas designs using varactor diodes are available in the literature [10–15, 25, 36, 38–53]. Different type of antenna structures were used for these designs, namely dipole, patch, half-mode substrate integrated waveguide (HMSIW), PIFA, and low-profile monopole. A single frequency-reconfigurable low-profile monopole was presented in [53]. The antenna consists of a circular patch surrounded by four sector-shaped patches. Two varactor diodes bridge the gap between the circular patch and the sector patch. The varactor diodes function to control the current distribution of the antenna, which can alter the resonance frequency. The tuning range was from 1.64 to 2.12 GHz and controlled by changing the reverse bias voltage from 0 to 20 V. Figure 2.13 shows the antenna design and the tuning range.

A concept of frequency-reconfigurable low-profile monopole antenna with two independent tuning bands was introduced in [15]. Two independent magnetic current loops were created using four shorting rods at the antenna edges and four symmetrical slots on the patch. These two magnetic current loops radiate almost independently to

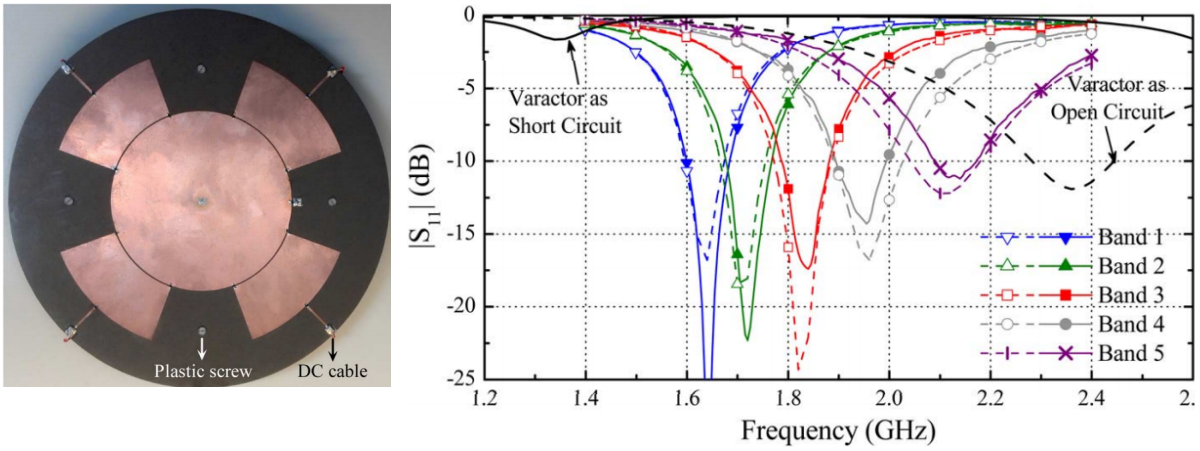

Figure 2.13. Single frequency-reconfigurable low-profile monopole antenna. Antenna geometry and tuning range of the antenna. Adopted from [53].

each other. Two sets of varactor diodes were utilized to control the resonance frequencies of the two bands, and thus allowing instantaneous coverage of a wide bandwidth. The antenna achieves tuning ranges of 31% and 22% centered at 0.9 and 1.7 GHz. The configuration of the antenna is depicted in Fig. 2.14.

These two examples of continuous frequency-reconfigurable low-profile monopole antenna have similar characteristics of their radiation patterns. Stable omnidirectional patterns on the azimuth plane were obtained across the tuning ranges. This performance is desirable and has become a fundamental requirement when designing a frequency-reconfigurable monopolar antenna.

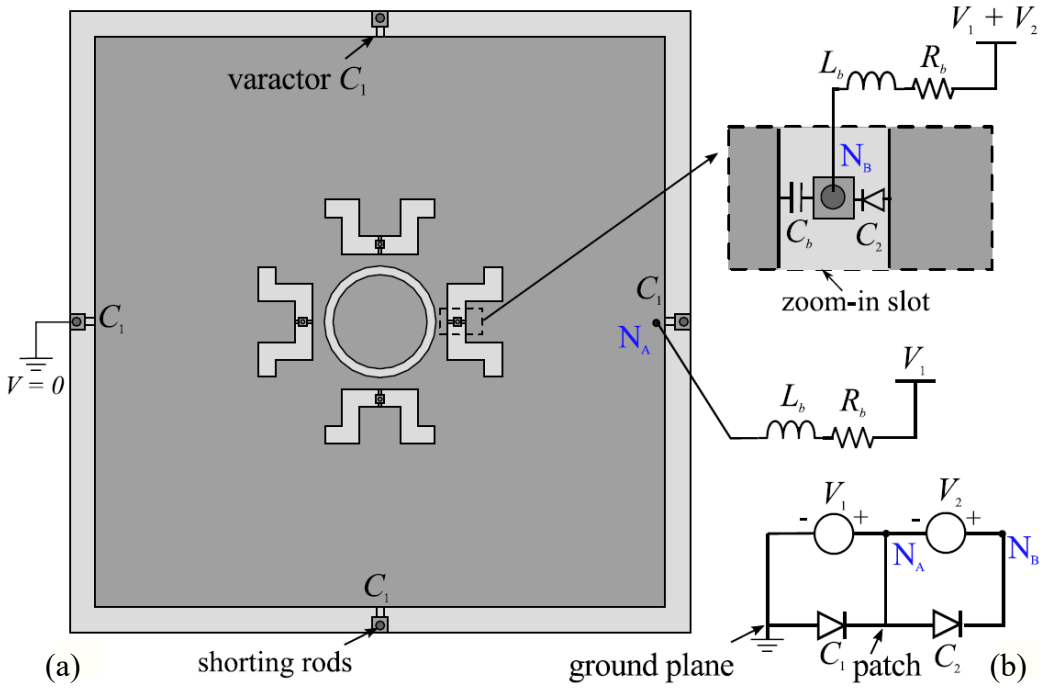

Figure 2.14. Dual-band frequency-reconfigurable low-profile monopole antenna. (a) Antenna geometry. (b) Diagram of the varactors voltage bias. Adopted from [15])

2.5 Summary

This section has presented a short review of image theory, in particular in relation to dipoles and monopoles. The theory can explain the radiation characteristics of a low-profile monopole antenna. A brief literature review on low-profile monopole antennas and frequency-reconfigurable antennas has also been presented, with some examples of existing designs that are related to the antenna designs that will be proposed in this thesis.

Chapter 3

Via-less Low-Profile Monopole Antennas

THIS chapter proposes variations of low-profile monopole antennas using via and via-less shorting methods. The methods are compared in terms of performance, namely bandwidth and radiation patterns. Stubs and complementary split ring resonators are used as via-less shorting to replace classical vertical pins. All designs use the same substrate and are optimized to operate at the same frequency. Measurement results from fabricated prototypes show good agreement with simulations. This via replacement study on low-profile monopole antennas aims to investigate the performance tradeoffs between via and via-less shorted antennas.

3.1 Introduction

With their omnidirectional pattern and vertical polarization characteristics, low-profile monopole antennas are suitable for many communications systems. One of the examples is for vehicle to vehicle (v2v) safety system in the dedicated short-range communications (DSRC) band that requires compact antennas to be deployed on car tops. Based on the IEEE 802.11p standard, the frequency range of 5.850–5.925 GHz is allocated for wireless access in DSRC.

For compactness and bandwidth enhancement, shorting vias have been integrated into low-profile monopole antennas [2, 4, 8]. As demonstrated in [4], the shorting vias add parallel inductances to the antenna capacitance so to enable the antenna to operate in a resonance frequency below the fundamental mode. The resonance frequency of the antenna is primarily set by the surface of the patch, the antenna height, the substrate permittivity, and the number of shorting vias.

It also has been shown that a rectangular patch that is shorted at its edges can radiates as a magnetic current loop similarly to an electric monopole [5]. In this reference, shorting vias were used to open four radiating slots along the side of the patch, resulting in an equivalent monopole antenna that is radiating omnidirectionally.

These published results suggest that shorting vias integration into the low-profile monopole is beneficial. Nevertheless, one may argue that the realization of antennas with physical vertical connections will increase fabrication complexity. Besides that, shorting between the patch and the ground plane may cause difficulties in DC biasing for integration with active components. In particular, these difficulties may arise when the shorting vias are utilized in reconfigurable antenna designs.

One solution to address these issues as mentioned earlier is to replace vias with quarter-wave stubs. Stubs are placed at the edge of the patch so that the apparent impedance at this location is zero. This concept has been used in [54, 55], in which a series of stubs replaced the via walls in a substrate integrated waveguide (SIW) as shown in Fig. 3.1(a). Another approach to via-less shorting is through the use of metamaterial resonators [56, 57]. In these references, the authors demonstrated that complementary split ring resonators (CSRRs) arranged side by side in series were able to confine propagating waves in a SIW as depicted in Fig. 3.1(b). It should be noted that these two via-less realizations present a trade-off in terms of bandwidth limitation.

(a)

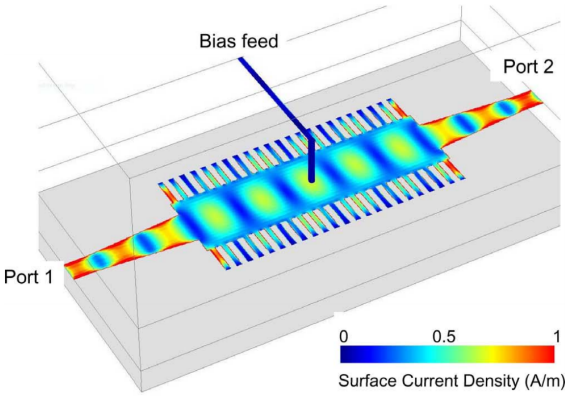

(b)

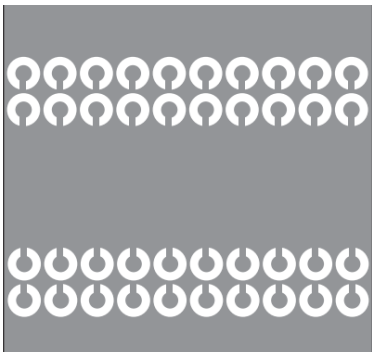

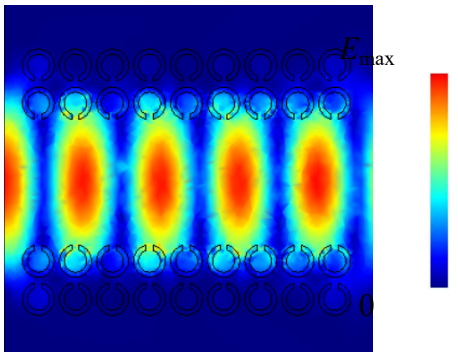

Figure 3.1. Via-less SIW. (a) Corrugated SIW (CSIW) and the simulated surface current density on the top of CSIW. Adopted from [54, 55]. (b) SIW with CSRRs etched on metal planes and the simulated E-field distribution at substrate mid-plane. Adopted from [56, 57].

In this chapter, three designs of low-profile shorted-patch monopole antennas that use via and via-less shorting methods are investigated. The first part of the present chapter focuses on the antenna designs. A monopole with shorting vias design will be presented, followed by the stub-loaded monopole and CSRR-loaded monopole. In the second part of the chapter, the simulated and measured results of these three optimized designs are compared to understand the performance trade-offs between via and via-less antennas.

3.2 Antenna Designs

Three low-profile monopole antennas have been designed using different types of shortings including vias, stubs, and CSRRs, as shown in Fig. 3.2. All design are based on a Rogers Duroid 5880 substrate with a thickness of 3.18 mm (about $\lambda_0/16$), relative permittivity $\varepsilon_r = 2.2$ and loss tangent $\tan\delta = 0.0009$. The targeted frequency is 5.9 GHz with a required bandwidth of 75 MHz correspondings to a fractional bandwidth of 1.3%. The shape of the ground plane for all proposed designs is circular with a 55-mm diameter in order to have a symmetrical radiation pattern. SMA connectors are used for probe-feeding the antennas.

3.2.1 Via Monopole

The first type of low-profile monopole design is created based on the antenna proposed in [5]. The main difference of this via monopole compared to their design is on the number of shorting pins and the shape of the patch. A circular patch is used for the design instead of a rectangular one, with three single vias positioned at the edge of the patch acting as a metallic wall. The vias are fabricated using rivets that are soldered to the PCB. The angular separation between vias is 120°, in order to open three radiating apertures. These apertures are similar to thin slots which induce equivalent magnetic currents. The basic via monopole design is shown in Fig. 3.3.

In this antenna, the resonance frequency is influenced by the cavity size D_{cavity}, the substrate permittivity ε_r, and the slot length l_{slot} which is determined by the diameter of the via d_v [5]. Based on [58], a change on the cavity size enables the antenna to resonates at a different frequency. This is supported by simulation results shown in Fig. 3.4. On the other hand, a variation of the via diameter affects the slot length and thus shift the operation frequency. A smaller via diameter result in an increased slot aperture size, and hence increase the extent of fringing fields and lower the resonance frequency as shown in Fig. 3.5. For a fixed cavity size, a higher substrate permittivity will lower the resonance frequency but with trade-offs in higher losses and reduced bandwidth.

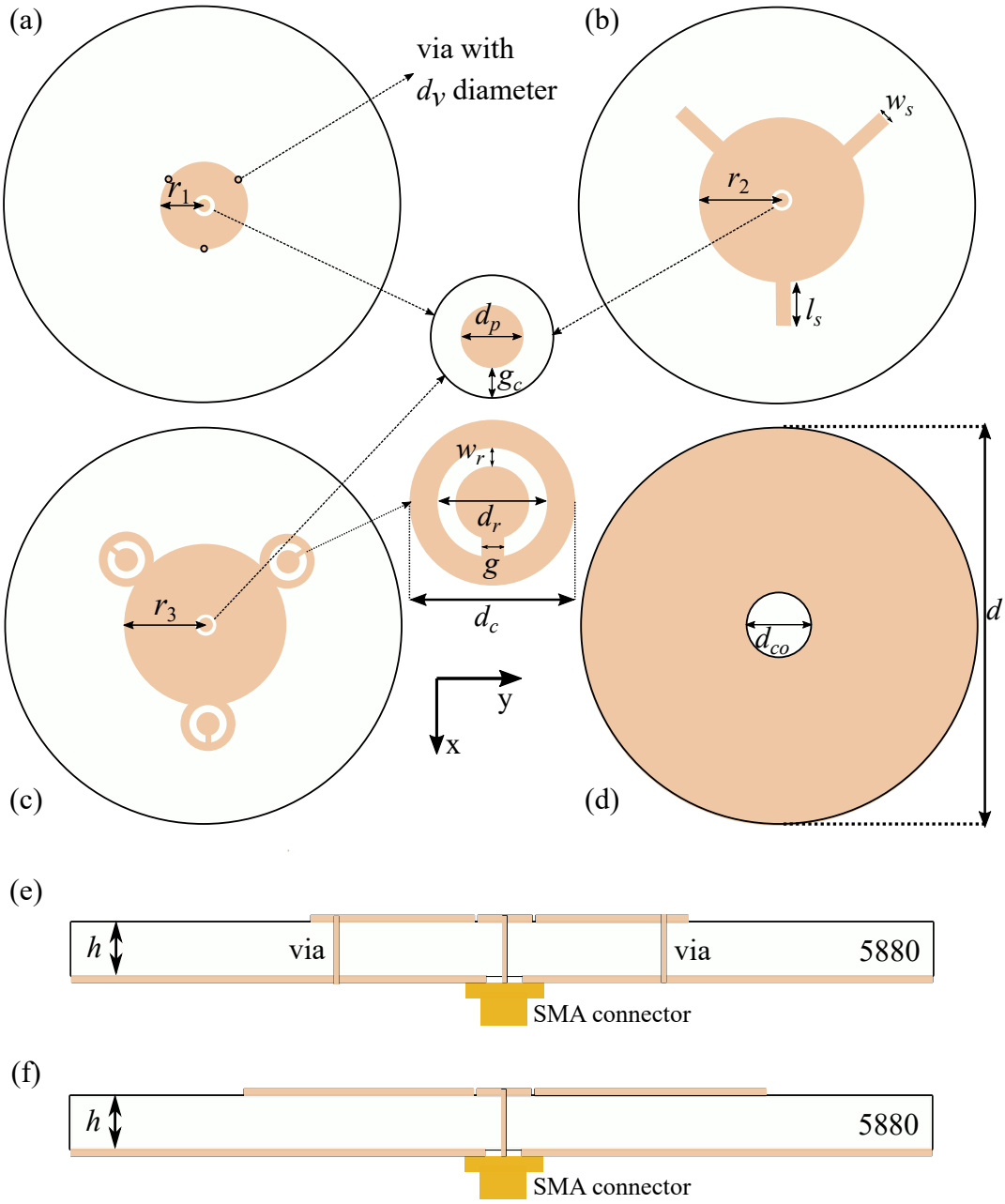

Figure 3.2. Low-profile monopole antennas design geometry. Top views of (a) via monopole, (b) stub monopole, (c) CSRR monopole, (d) Ground plane for all antennas. Side views of (e) via and (f) via-less monopole. Dimensions (mm): $d_p = 1.27$, $d = 55$, $d_{co} = 4.5$, $r_1 = 6.3$, $g_c = 0.57$, $d_v = 1$, $r_2 = 10.8$, $g_c = 0.27$, $l_s = 6.93$, $w_s = 2.7$, $r_3 = 11$, $g_c = 0.37$, $d_c = 6.4$, $d_r = 3.3$, $g = 0.95$, $w_r = 0.95$ and $h = 3.18$.

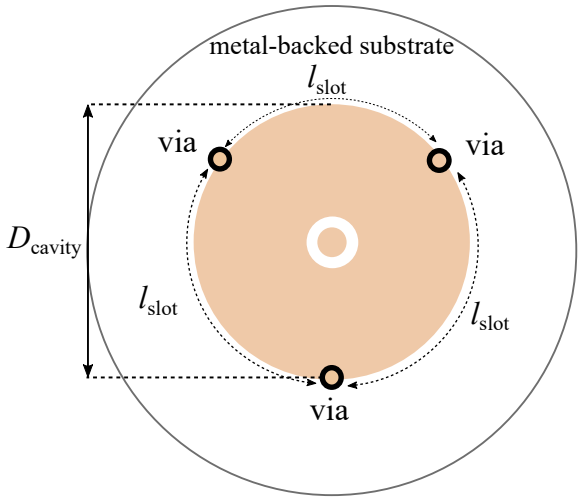

Figure 3.3. Basic via monopole design.

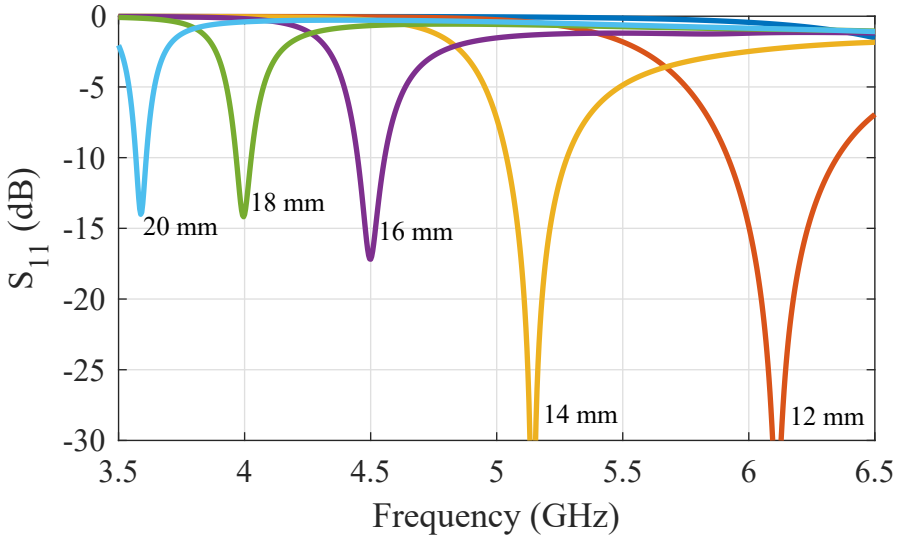

Figure 3.4. Reflection coefficients of via monopole when D_{cavity} is varied.

3.2.2 Stub Monopole

In the second design shown in Fig. 3.2(b), the shorting vias are replaced with quarter-wavelength stubs, resulting in a structure that is completely DC isolated from the ground plane, as shown in Fig. 3.2(f). Based on the transmission line theory, a quarter-wavelength stub can change the state of a circuit from open to short or vice versa. Because of this, stubs are placed at the periphery of the patch in order to change the impedance state from open to short. These stubs provide zero impedance at their connection to the patch for a particular frequency. The condition is similar to when the patch is shorted with physical vias. The angular separation between the shorting stubs

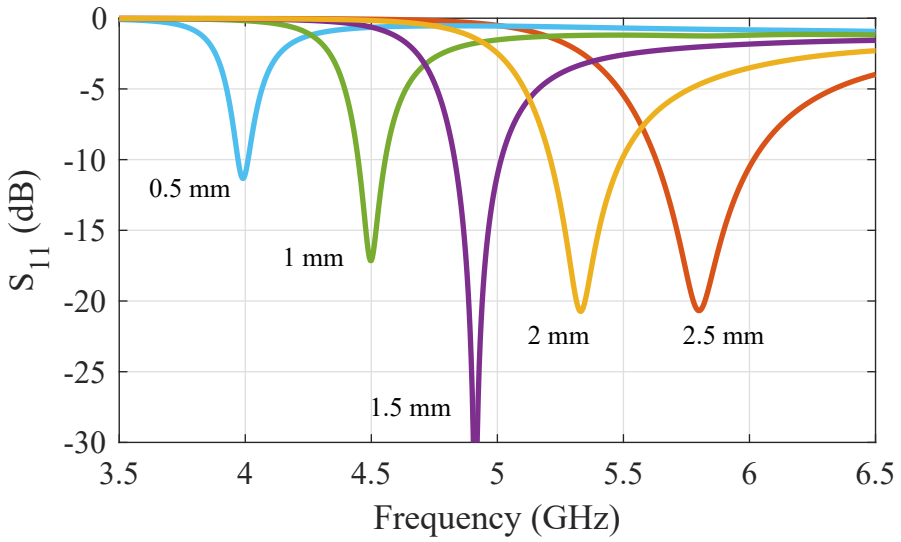

Figure 3.5. Reflection coefficients of via monopole when d_v is varied.

is also 120°, which open three radiating magnetic slots since the substrate height is sufficiently thin compared to the slot length.

In this design, the size of the patch cavity and the length of the stubs influence the resonance frequency. The cavity size determines the slot aperture size, while the shorting stubs influence the effective aperture of the slots which in turn affect the operation frequency of the antenna. This is supported by the parametric simulation shown in Fig. 3.6. In that simulation, the length of the stubs l_s is varied with a fixed cavity size D_{cavity}.

3.2.3 CSRR Monopole

In the last proposed design shown in Fig. 3.2(c), CSSRs are utilized as shortings. They are placed in the same location as previous shorting elements. CSRRs are essentially resonant tanks that can be excited by an axial electric field [59]. In this type of low-profile monopole, each CSRR work as a small electric dipole that couples with a normal electric field emerging from the feed. On resonance, the field undergoes phase reversal, similarly to a physical via. In CSRRs, the *E*-fields are localized in the center of the ring slot opposite to the gap, and hence the shorting mechanism starts from this area of the ring. The CSSRs are thus positioned with their slot gaps facing towards outside of the antenna to create shorting at the circular island in the middle of the ring.

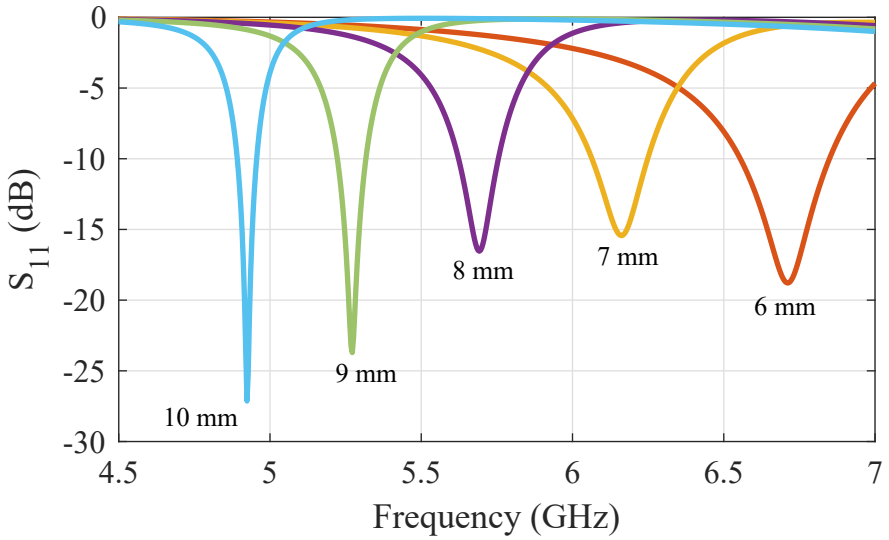

Figure 3.6. Reflection coefficients of stub monopole when l_s is varied. D_{cavity} is set to 16 mm.

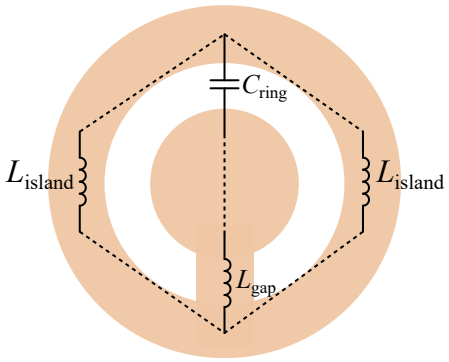

Figure 3.7. Simple electrical model of a CSRR. The slot ring and the metal part determine the capacitance C_{ring} and the inductances L_{gap} and L_{island} of the resonator.

The simple electrical model of a CSRR is depicted in Fig. 3.7. As shown in this model, the capacitance of the resonators is determined by the slot ring, namely the width w_r and the diameter d_r, while the inductance is influenced by the metal area of the CSRR. By varying the capacitance and the inductance of the CSRR the working frequency of the antenna can be altered. As an example shown in Fig 3.8, variation of the diameter of the slot ring d_r enables to shift the working frequency of the antenna.

Comparisons of E-fields simulations are illustrated in Fig. 3.9 to support the concept of via-less shorting in low-profile monopole antennas. The E-fields are captured when the maximum magnitude is at the center of the patch, illustrated as red areas. The shorting mechanism, which is equivalent to the E-field phase reversal, is clearly identified as blue areas. This demonstrates that the stubs and CSSRs act similarly as physical vias

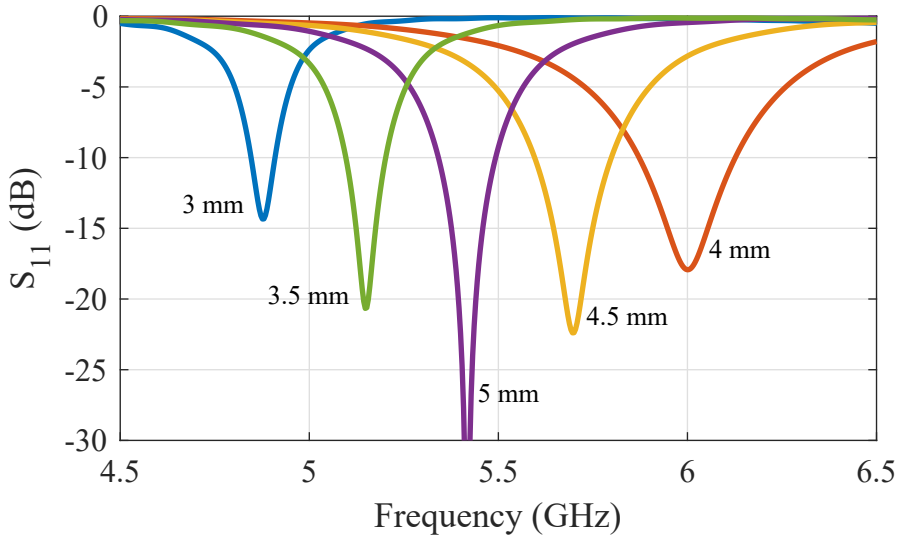

Figure 3.8. Reflection coefficients of CSRR monopole when d_r is varied.

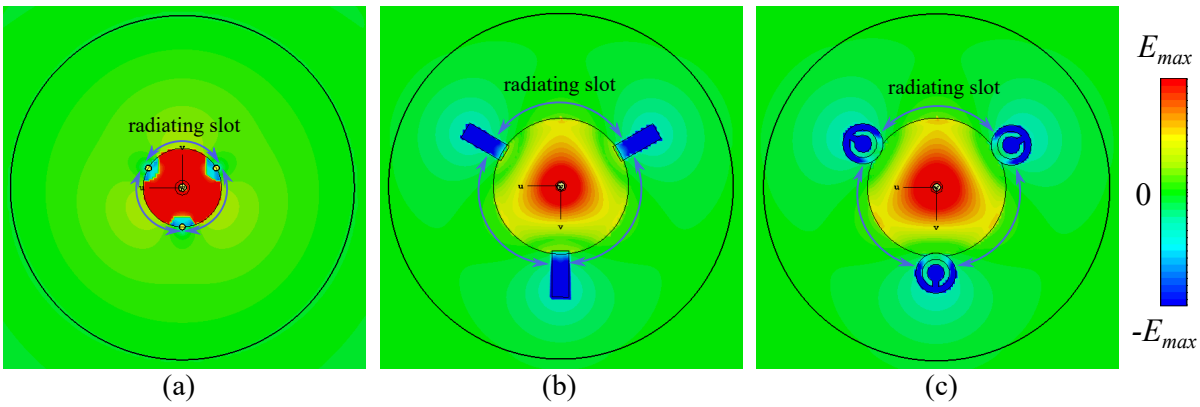

Figure 3.9. Instantaneous E-fields distribution in saturated scale. (a) Monopole with vias, (b) stubs, and (c) CSRRs.

to realize shortings in a low-profile monopole antenna. It is also noted from Fig. 3.9 that the radiating slot aperture of the via-less antennas are not as well defined as that of the via one. However, it is seen from Fig. 3.9(b) and (c) that the maximum of the E-fields occurs at the middle between the via-less shortings. This means that the radiating slot aperture of the via-less monopoles is located between the shorting elements. Further explanation is described in Fig.4.2 in Section 4.2.

Bandwidth optimization has been performed for the via-less monopoles by adjusting the diameter of the circular patch. In addition, to attain a good matching in the proposed designs, a coaxial gap between the probe and the patch is used to control the input impedance [4,5]. The coaxial gap size g_c shown in Fig. 3.2 influences the input

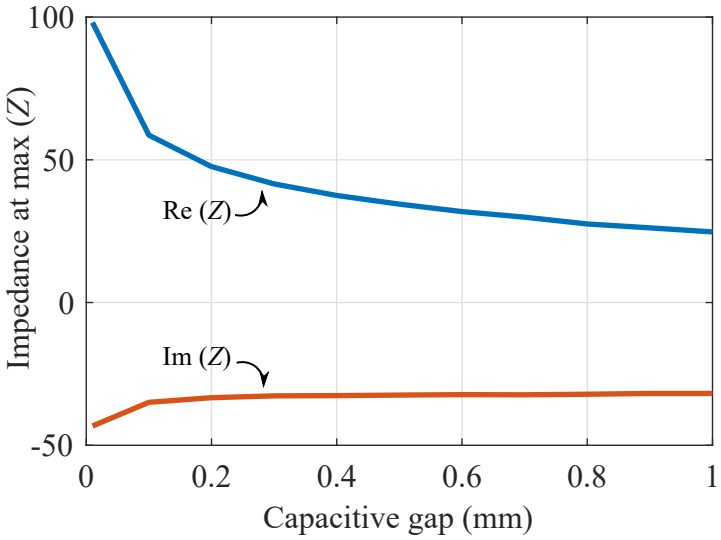

Figure 3.10. Impact of capacitive gap on the input impedance of the stub monopole antenna.

impedance of the antenna. As an example, a parametric simulation on a stub monopole with g_c variation is shown in Fig. 3.10. It can be seen that the magnitude of the input resistance decreases for increased capacitive gap size. The input resistance Re(Z) when g_c = 0.01 mm is 89 Ω, and decreases to 24 Ω at g_c = 1 mm. A similar trend is also observed in the input reactance Im(Z) which has a negative value. The capacitive gap size has been optimized for a matched impedance of 50 Ω at the operation frequency of 5.9 GHz.

3.3 Experimental Validation

The discussed designs have been fabricated and are shown in Fig. 3.11. The simulated and measured reflection coefficients of the designs are compared in Fig. 3.12. The resonance frequencies slightly vary from the target frequency by 1% due to imperfect probe positioning in the prototypes. The measured bandwidth for via, stub and CSRR monopoles are 360, 210, and 195 MHz equal to a fractional bandwidth of 6.2, 3.5, and 3.3%, which all cover the DSRC band generously. Bandwidths for via-less monopoles are narrower than the via version due to the higher radiation Q factor from the stubs and the CSRRs.

The normalized simulated and measured radiation patterns of each antenna design are depicted in Fig. 3.13. A good qualitative agreement is observed between the simulation and measurement. The patterns are omnidirectional in the xy-plane with less than

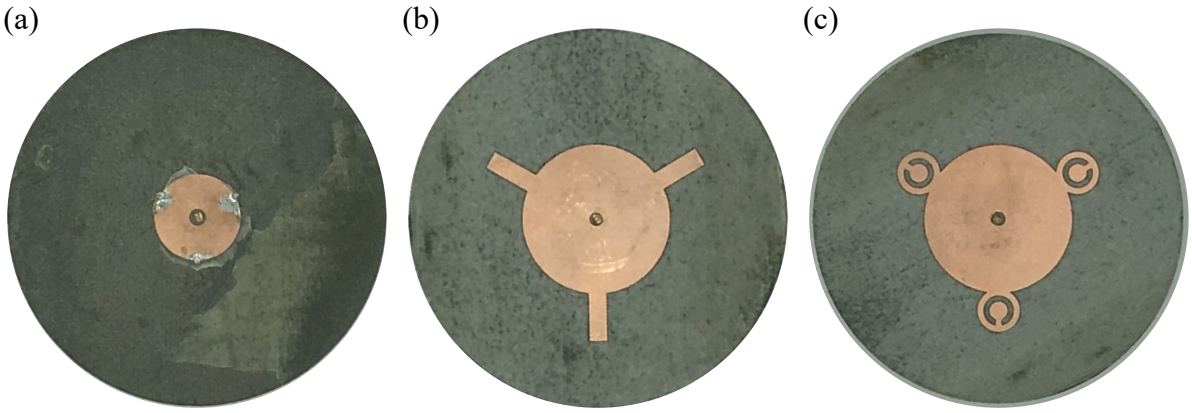

Figure 3.11. Photographs of the fabricated antennas. (a) Via, (b) stub, and (c) CSRR monopoles.

1 dB variation, while in the elevation yz-plane, the radiation patterns are conical due to a finite ground-plane effect. The simulated maximum gain of the via monopole is 3.68 dBi, while that of the stub- and CSRR-monopoles are 4.40 and 4.31 dBi. The simulated gain and the cross-polarization components in the via-less monopoles are higher because they have larger overall sizes as a result of the optimization process. It is noted that the large patch size results to a higher current distribution for the radiation of the orthogonal polarization.

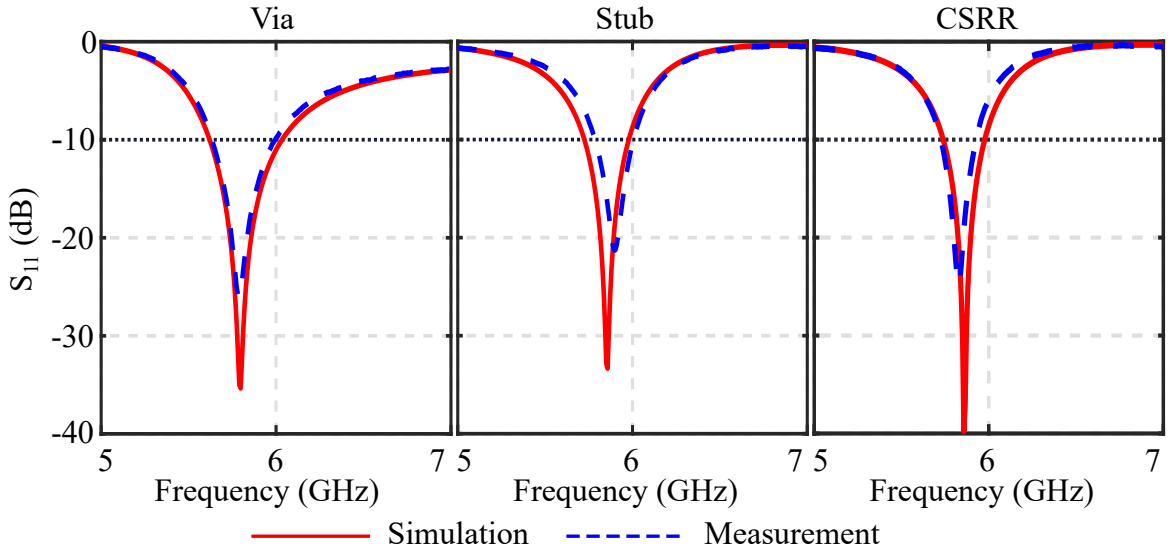

Figure 3.12. Simulated and measured reflection coefficients of all proposed monopole designs.

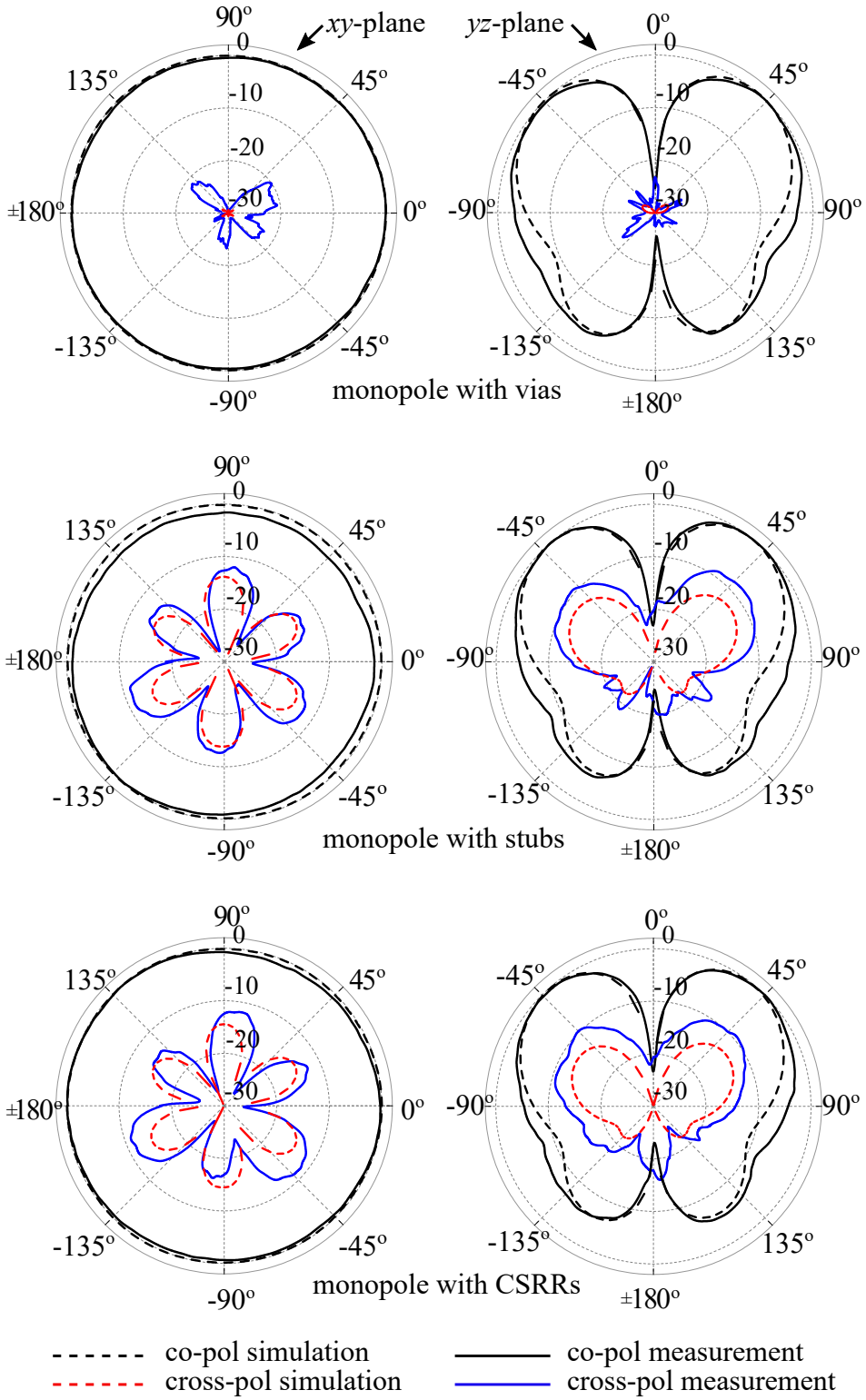

Figure 3.13. Normalized radiation patterns in the xy- and yz-planes.

3.4 Conclusion

Three designs of low-profile monopole antennas realized using different shorting methods have been investigated. These antennas are based on the concept of magnetic current loops on a thin aperture. The measured bandwidth for the optimized designs of via, stub and CSRR monopoles are 360, 210, and 195 MHz at a center frequency of 5.9 GHz. All these designs exhibit omnidirectional radiation patterns in the xy-plane with less than 1 dB variation, and conical patterns in the elevation yz-plane. Via-less shorting monopole antennas offer simple fabrication with better isolation between the top and bottom layers. However, those via-less structures have trade-offs in size, bandwidth, and polarization purity.

Chapter 4

Multi-Band Frequency-Reconfigurable Low-Profile Monopoles

THIS chapter presents the original contributions of the thesis dedicated to multi-band frequency-reconfigurable low-profile monopole antennas with independent tuning capability. The antennas are based on the concept of a center-fed patch with shortings to achieve omnidirectional radiation patterns. Instead of using vias, varactor-loaded stubs are utilized to create reconfigurable equivalent shorting points. The proposed concept is firstly validated by a dual-band frequency-reconfigurable prototype and then extended to a triple-band device. The triple bands can be achieved by using three sets of stubs. This configuration results in three magnetic current loops that spatially overlap at different independently tunable frequencies. Measurement results show that the design obtains three independent tunable operation bands. The antenna radiates omnidirectionally with vertical polarization in the three sweeping bands.

4.1 Introduction

In recent decades, the demand in wireless communications has risen significantly. This has brought upon increasing congestion of the available radio spectrum. Therefore, it is desirable to have antennas that can cover several allocated frequency bands simultaneously. To accomplish the goal, wideband antennas with a low-profile monopole structure are often desired due to their omnidirectionality, low-cost, and fabrication simplicity [4, 6, 8, 9, 60–64] . Another solution is to use frequency-agile antennas that have been widely developed recently. Compared to wideband antennas, a frequency-reconfigurable antenna can mitigate undesirable interference from unused bands, thus ease requirements on additional RF filters in the system.

Frequency-reconfigurability can be obtained by modifying the antennas electrical properties with the assistance of active elements such as PIN diodes [26, 28–30, 32], RF-MEMS switches [33, 34, 65–67], varactor diodes [13, 15, 38–40], or their combinations [50, 51]. In [28], PIN diodes were used in the slot of a planar monopole ground plane to switch the antenna states into a single-band, dual-band, or ultrawideband, while in [66], an RF-MEMS switch was utilized in the slot of a patch antenna to switch the operation frequency. In varactor-loaded antennas, varying the bias voltage leads to a progressive variation in the diode capacitance that can create a continuous frequency tuning. Because of this feature, adopting varactors to create frequency-reconfigurable antennas is beneficial, in particular for applications that require a large number of operating bands with continuous tunability.

Numerous concepts of antennas with continuous frequency tunability have been previously proposed in the literature. The structures used for the antennas were shorted patches [38–40], slotted patches [10–14, 41–44], dipoles [45–47], planar inverted-F antennas (PIFA) [48], half-mode substrate integrated waveguides (HMSIW) [36,49], multi radiators [50, 51], and low-profile monopoles [15, 25, 52, 53]. Nonetheless, only a few of those proposed antenna designs are able to cover more than one band at the same time [10–15, 25, 41]. In the case of multi-band reconfigurable antennas, the independency of frequency sweeping is one desirable feature. Behdad and Sarabandi [13] demonstrated a broadside-pattern dual-band reconfigurable antenna with independent tuning of the bands. This was obtained by loading varactors onto a bent slot antenna. Recently, an antenna with tri-band independent tuning capability was presented by Bai et al. [14]. In this case, the design was specific for radio receivers with broadside radiation patterns and only -6 dB reflection coefficient. For low-profile

monopole antennas, the independent tunability of two frequencies was reported by Nguyen-Trong et al. [15]. For that dual-band design, stable omnidirectional patterns were achieved in all sweeping frequencies with relative tuning ranges of 31% and 22% in the first and the second bands.

In this chapter, multi-band frequency-reconfigurable low-profile monopole antennas are proposed based on the concept of independent magnetic current loops sharing a common thin aperture. The antenna is composed of a center-fed circular patch with groups of stubs located on the patch edge. Each set of stubs functions as equivalent shortings at a particular frequency to define a magnetic current loop at the perimeter of the patch [5, 68]. To achieve a continuous frequency reconfigurability, varactor diodes are placed between the patch and the stubs. These varactors are biased with DC control voltages to tune the frequencies independently. Monopolar radiation patterns with reasonable azimuthal variations are obtained across the tuning ranges.

This chapter will begin with an explanation on the operation principle of the antenna. In particular this includes an illustration of magnetic current loops that will play an important role in the multi-band radiation. Then, the concept of reconfigurability will be validated with a dual-band design. In the last section, the triple-band reconfigurable low-profile monopole antenna will be demonstrated, followed by concluding remarks.

4.2 Operation Principle

As shown in Fig. 4.1, the basic geometry of the single-band low-profile monopole antenna consists of a center-fed circular patch on a substrate with a ground plane underneath. The patch is surrounded by three stubs on its edge with 120° angular separation. The radiation principle of the antenna is based on the magnetic current loop formed by a low-profile shorted monopole antenna, as discussed in [5]. As shown in Fig. 4.2(a), we begin with a vertical electric current with density J that is equivalent to a magnetic current loop with constant density distribution M depicted in Fig. 4.2(b), both placed over a ground plane. The magnetic current loop M can be established with three in-phase magnetic current elements as shown in Fig. 4.2(c), which in theory can be realized from thin slots in a metallic cavity. For a substrate integrated design, such a slot aperture can be created between two adjacent vias shunting the top patch with the ground, as shown in Fig. 4.2(d). The substrate thickness should be sufficiently small so that a purely transverse electric field E is present in the slots. On resonance, each

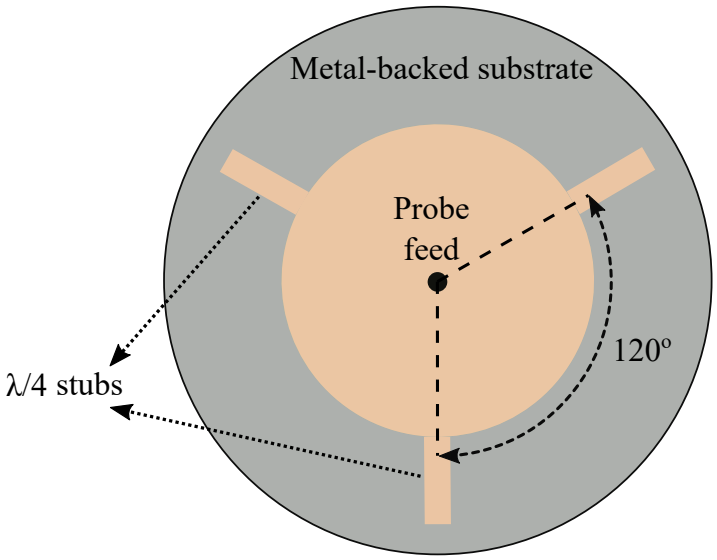

Figure 4.1. Basic geometry of a single-band low-profile monopole antenna with stubs for shorting. The figure shows the top view, where the ground plane is hidden.

of these slots can be considered as a $\lambda/2$ transmission line (slot line) that is shorted at its two ends. As a result, three slot apertures are formed between three shorts, with the highest E-field magnitude occuring in the middle of the slots. Furthermore, as has been demonstrated in the previous chapter and in [54, 68], vias can be replaced by quarter-wavelength stubs as shown in Fig. 4.2(e). It is noted that for this antenna configuration, the slot and the stub lengths influence the effective size of the cavity and thus the resonance frequency [68].

To open a second band, an additional set of three shorting stubs with a specific length determined by the targeted frequency is interlaced with the original set. This basically defines two sets of slots that radiate at different frequencies. A preliminary simulation of this concept has been carried out in CST Microwave Studio with the results shown in Fig. 4.3. The base antenna is designed with a diameter of 36 mm, while the lengths of the longer and shorter stubs are l_1 = 20 mm and l_2 = 16 mm, respectively. Dual-band performance is then observed in the frequencies of around f_1 = 2.8 GHz and f_2 = 3.9 GHz. The longer stubs are responsible for the lower operation frequency f_1 as indicated in the E-field simulation shown in Fig. 4.3(c). In contrast, the three shorter stubs are responsible for the resonance at the higher frequency f_2 as illustrated in Fig. 4.3(d). It is important to note that in this structure, the two sets of magnetic current elements M_1 and M_2 work independently. This concept is further supported

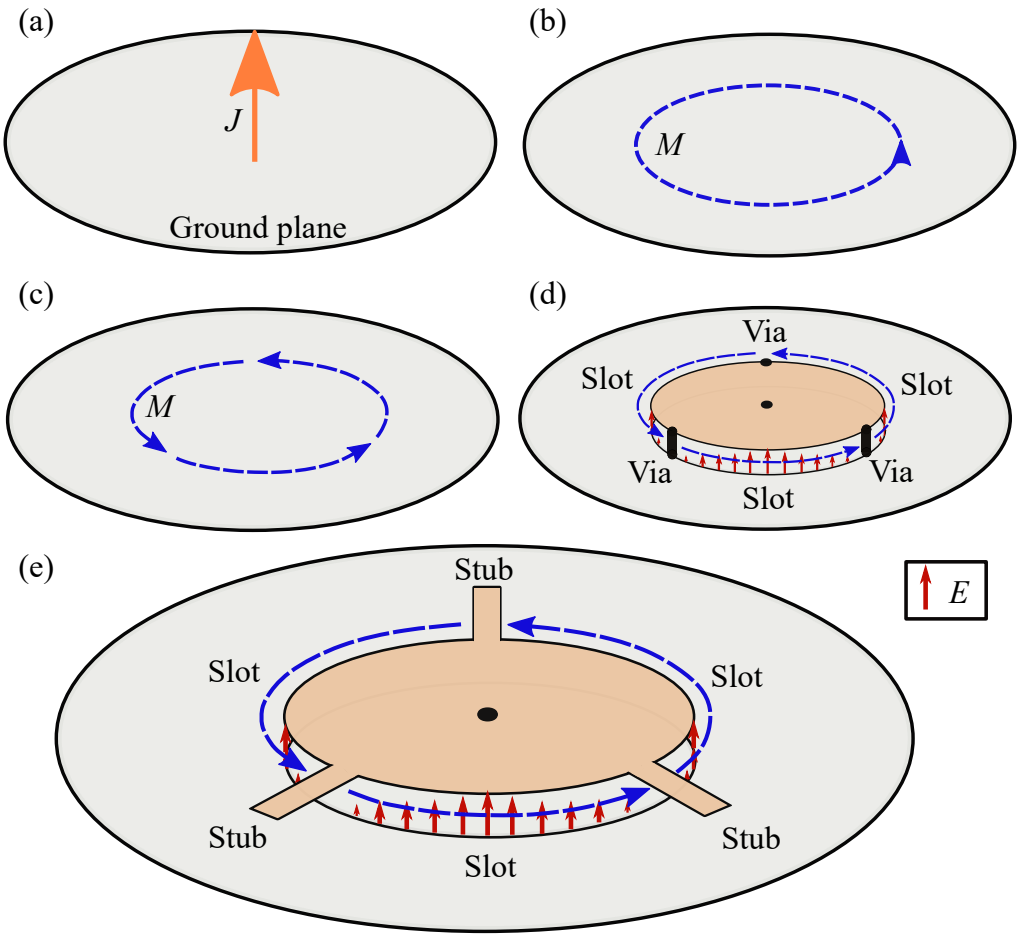

Figure 4.2. Operation principle of the proposed low-profile monopole antenna based on magnetic current loop. (a) Electric current and (b) its equivalent magnetic current loop, (c) discretization of magnetic currents, (d) realization in a center-fed patch with vias, and (e) with quarter-wave open stubs.

by the parametric simulation depicted in Fig. 4.3(b). In this scenario, the variation of the stub length l_1 shifts the resonance frequency f_1 while f_2 remains nearly unchanged. The concept can potentially be extended to more bands by adding additional sets of stubs. Extending the concept, a third band can be opened with the introduction of additional independent magnetic currents by simply adding a third set of stubs as shown in Fig. 4.4, where a third magnetic current loop M_3 with similar E-field distribution as depicted in Fig. 4.4(e) is found in the simulated reflection coefficient, as illustrated in Fig. 4.4(b). The number of bands is limited by the efficiency and the impedance matching of each band. Therefore this chapter will limit the discussion to dual-band and triple-band designs.

Instead of varying the stub length, the resonance frequencies of the multi-band antenna can be tuned independently by varying the stub impedance, which can be implemented by integration of varactor diodes [36]. Separate sets of varactors are placed between the patch edge and the stubs to control the current flows. As a result, changing the capacitance of one set of varactors can shift the frequency in one band while the other band remains unaffected. In addition, it is worth mentioning that the monopolar radiation pattern with vertical polarization is expected to be maintained in all bands as the magnetic current slots remain the predominant radiating sources.

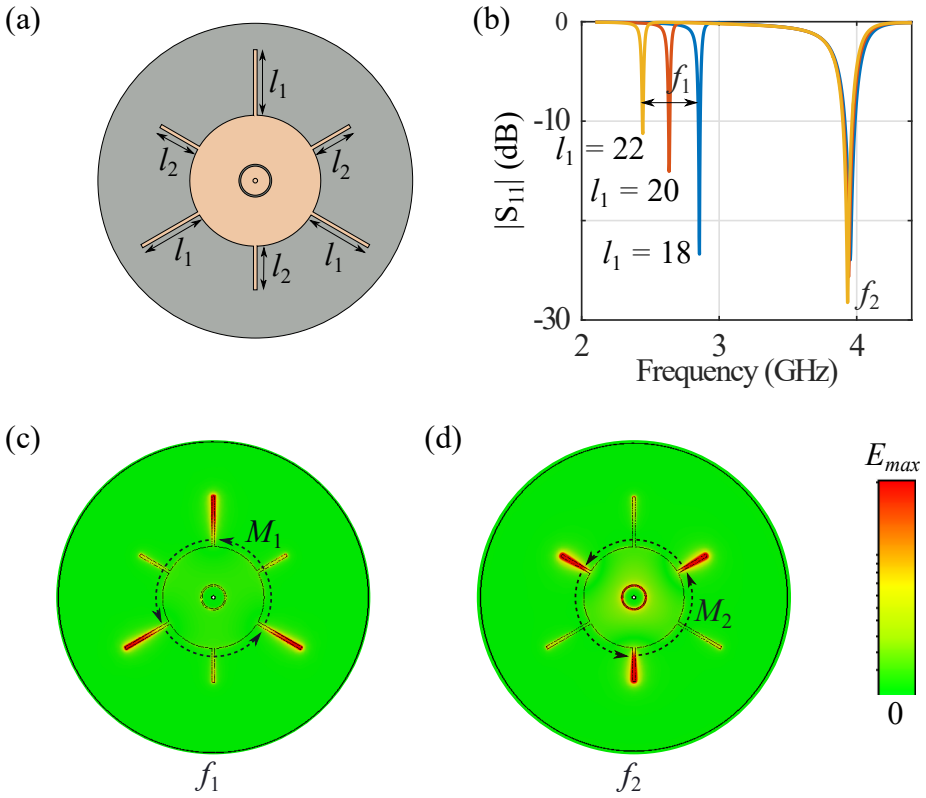

Figure 4.3. Dual-band low-profile monopole with stub shortings. (a) Antenna geometry. (b) Reflection coefficient of the antenna when $l_1 = 18$, 20, and 22 mm. (c,d) Instantaneous E-field in the substrate at resonance frequencies of f_1 and f_2.

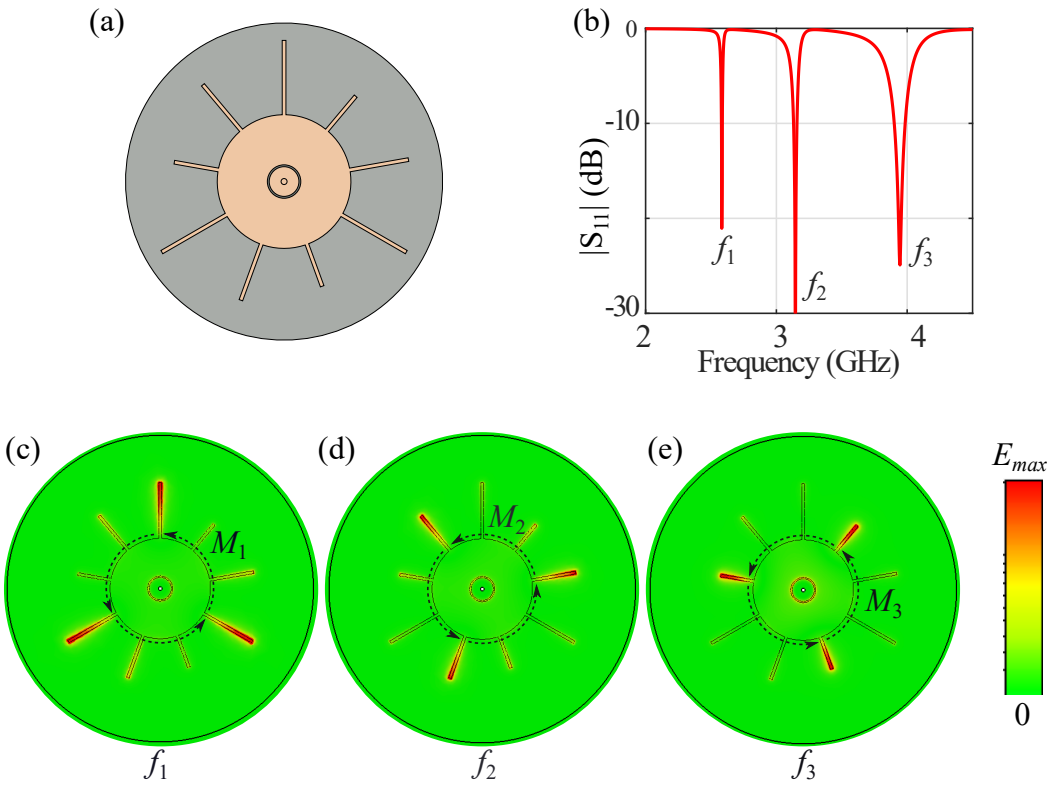

Figure 4.4. Triple-band low-profile monopole with stub shortings. (a) Antenna geometry. (b) Reflection coefficient of the antenna. (c–e) Instantaneous E-field in the substrate at three different frequencies.

4.3 Dual-Band Reconfigurable Design

4.3.1 Antenna Geometry

The design and the photographs of the fabricated antenna are depicted in Fig. 4.5 and Fig. 4.6, respectively. The dual-band design is created on Rogers Duroid 5880 substrate with a relative permittivity of $\epsilon_r = 2.2$ and a loss tangent of $\tan\delta = 0.0009$. The thickness of the substrate is chosen to be 3.18 mm (or about $0.03\lambda_{\text{min}}$). Two sets of stubs are included for dual-band operation. The width of these stubs should be sufficiently narrow so that the stubs do not radiate. For that reason, a stub width $w = 1$ mm is used in the design. The angular separation between consecutive stubs is set to be 60°, and six varactors bridge the six stubs and the patch. The center pin as a probe feeding is created from a 50-Ω SMA connector through the ground plane. The ground plane is circular for symmetry with a diameter of 135 mm. The bias network is implemented on another layer below the ground plane using an FR-4 substrate with a thickness of

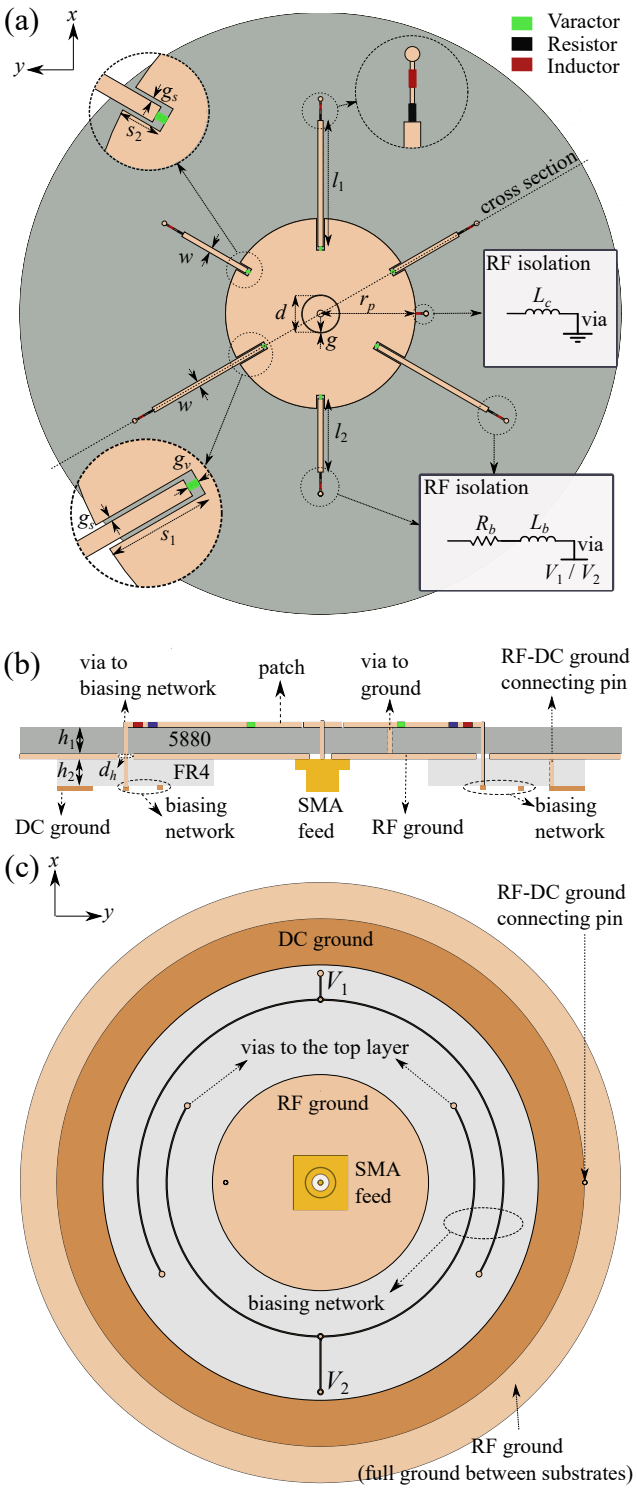

Figure 4.5. Dual-band reconfigurable antenna design. (a) Top, (b) cross-sectional, and (c) bottom views. Dark grey color is the 5880 substrate, light grey color is the FR-4 substrate, light brown color is copper on 5880 substrate, and dark brown color is copper on FR-4 substrate. The dimensions (mm) are: $l_1 = 24$, $l_2 = 14$, $s_1 = 6$, $s_2 = 2.5$, $w = 1$, $d = 7$, $r_p = 18$, $g = 0.1$, $g_v = 0.66$, $g_s = 0.25$, $d_h = 1.8$, $h_1 = 3.2$, and $h_2 = 1.6$.

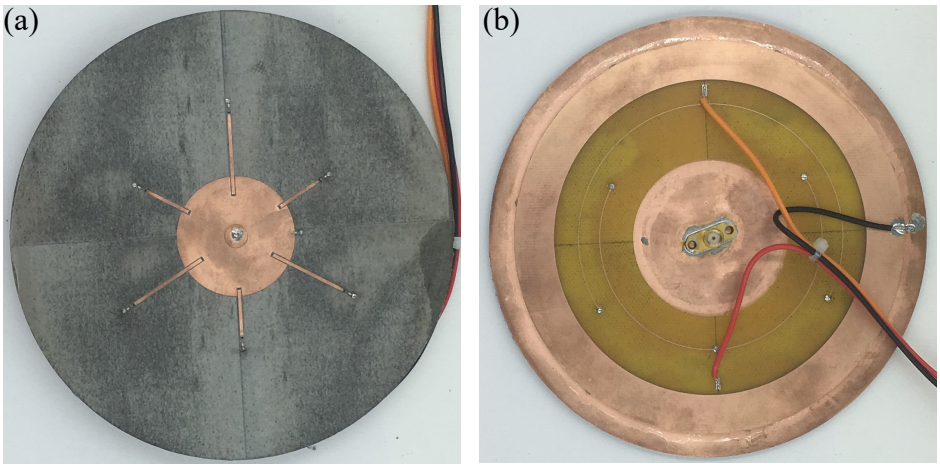

Figure 4.6. Photograph of fabricated dual-band reconfigurable design. (a) Top and (b) bottom views

1.6 mm. Separating the DC circuitry from the RF board avoids the effect of bias lines that can disturb the radiation pattern of the antenna.

For impedance matching purpose, the capacitive gap around the probe and the recesses around the stubs are created and optimized. The probe cap with a diameter of d can be seen as a radial inductor while the circular ring gap g adds the capacitance as explained in [4]. The recess configuration for the stubs is adopted from the well-known impedance matching technique for patch antenna feeding [22]. The depths of the recesses are shown in Fig. 4.5 as s_1 and s_2.

4.3.2 Bias Circuit

The varactors used in the design are MA46H120 from MACOM Technical Solutions. The capacitance of this type of varactor ranges from 1.30 to 0.15 pF when reverse-biased at 0 to 18 V [36] . The varactor internal resistance is approximately R_v = 2 Ω, and varies with the bias voltages as explained in [69]. These varactors are divided into two sets, one set being placed between the patch and the longer stubs, while the other is for the shorter stubs. These two varactor sets are biased separately by DC voltages V_1 and V_2, which are applied from the bottom layer through vias. An RF choke is implemented by using a resistor with high resistance R_b = 1 MΩ followed by an inductor with a value L_b = 100 nH. In addition to impedance matching, the capacitive gap at the feed blocks the DC current from flowing to the probe. A single via together with an RF choke L_c = 100 nH shown on the right side of the patch in Fig. 4.5(a) is used to

DC-ground the circular patch.

4.3.3 Reflection Coefficient

The measured and simulated reflection coefficients for the dual-band antenna design with different bias voltages (V_1 and V_2) are shown in Fig. 4.7 and Fig. 4.8. In the first case illustrated in Fig. 4.7, the lower band is tuned by fixing the voltage V_2 = 18 V (C_2 = 0.15 pF) while the voltage V_1 is set to 5 different values (0, 1.66, 3.77, 7.97 and 18 V). Meanwhile, for the second case plotted in Fig. 4.8, V_2 is varied to tune the upper band while keeping V_1 = 0 V (C_1 = 1.30 pF). The measured results agree well with the simulated ones in both cases, with just a small frequency shift amounting to less than 2% observed in the upper bands. The independence of two frequency bands is achieved in both scenarios confirming operation of distinct radiating magnetic current loops in the lower and upper bands. The measured −10 dB tuning range for the first

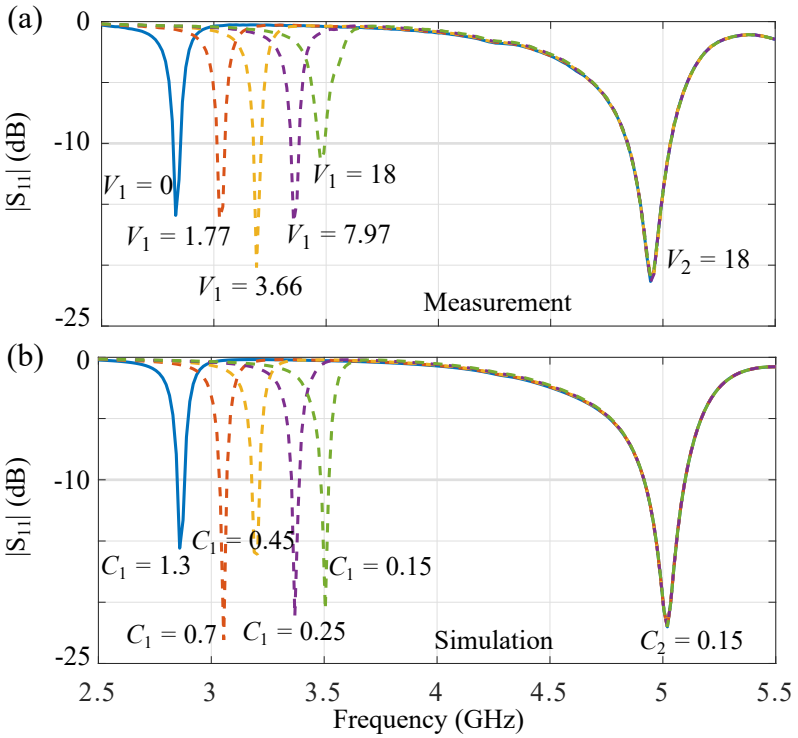

Figure 4.7. Reflection coefficients of the dual-band reconfigurable low-profile monopole design for fixed V_2 and varying V_1. (a) Measurement and (b) simulation results. The unit for the voltages is Volt, and the unit for the capacitances is pF.

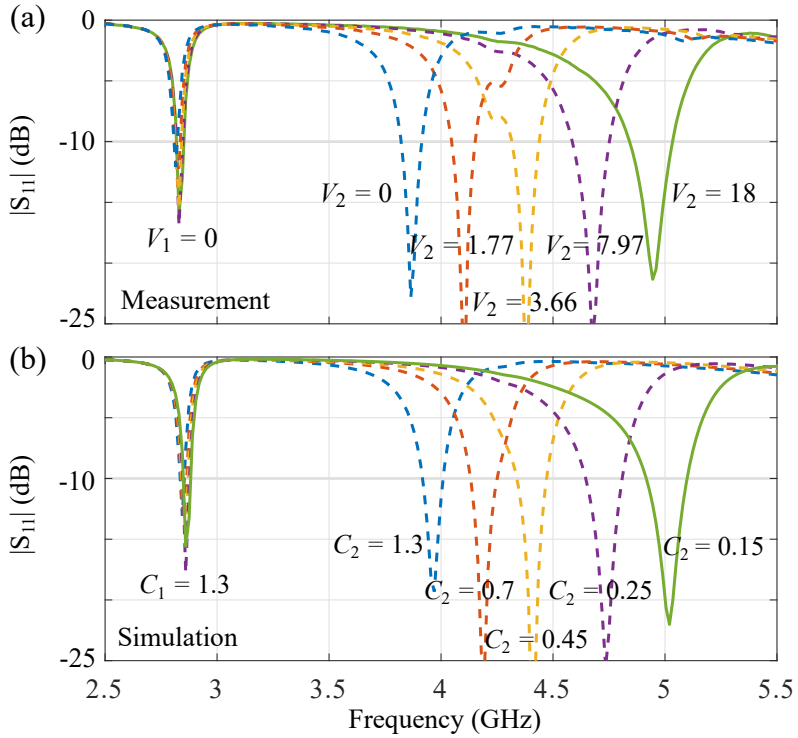

Figure 4.8. Reflection coefficients of the dual-band reconfigurable low-profile monopole design for fixed V_1 and varying V_2. (a) Measurement and (b) simulation results. The unit for the voltages is Volt, and the unit for the capacitances is pF.

band centered at 3.16 GHz is 21.2% (f_1 = 2.82–3.49 GHz), while it is 27.1% (f_2 = 3.82–5.02 GHz) for the second band centered at 4.42 GHz. The instantaneous impedance bandwidth of the lower band is maintained at approximately 1%, whereas in the upper band it increases from 2.3% to 4% with increasing resonance frequency.

4.3.4 Radiation Pattern, Gain and Efficiency

The normalized simulated and measured radiation patterns of the dual-band design are shown in Fig. 4.9. The patterns are for the lower and the higher limits for each band. A good agreement between the simulation and measurement results is achieved. In the azimuth *xy*-plane, stable monopole-like radiation patterns are obtained at all sweeping frequencies, while in the elevation *yz*-plane, the radiation patterns are conical as a result of the finite ground plane similarly as in [8,9,61,63,70]. It is emphasized that the co- and cross-polarizations in the omnidirectional *xy*-plane patterns were measured at the horizon, i.e., $\theta = 90^\circ$.

!h

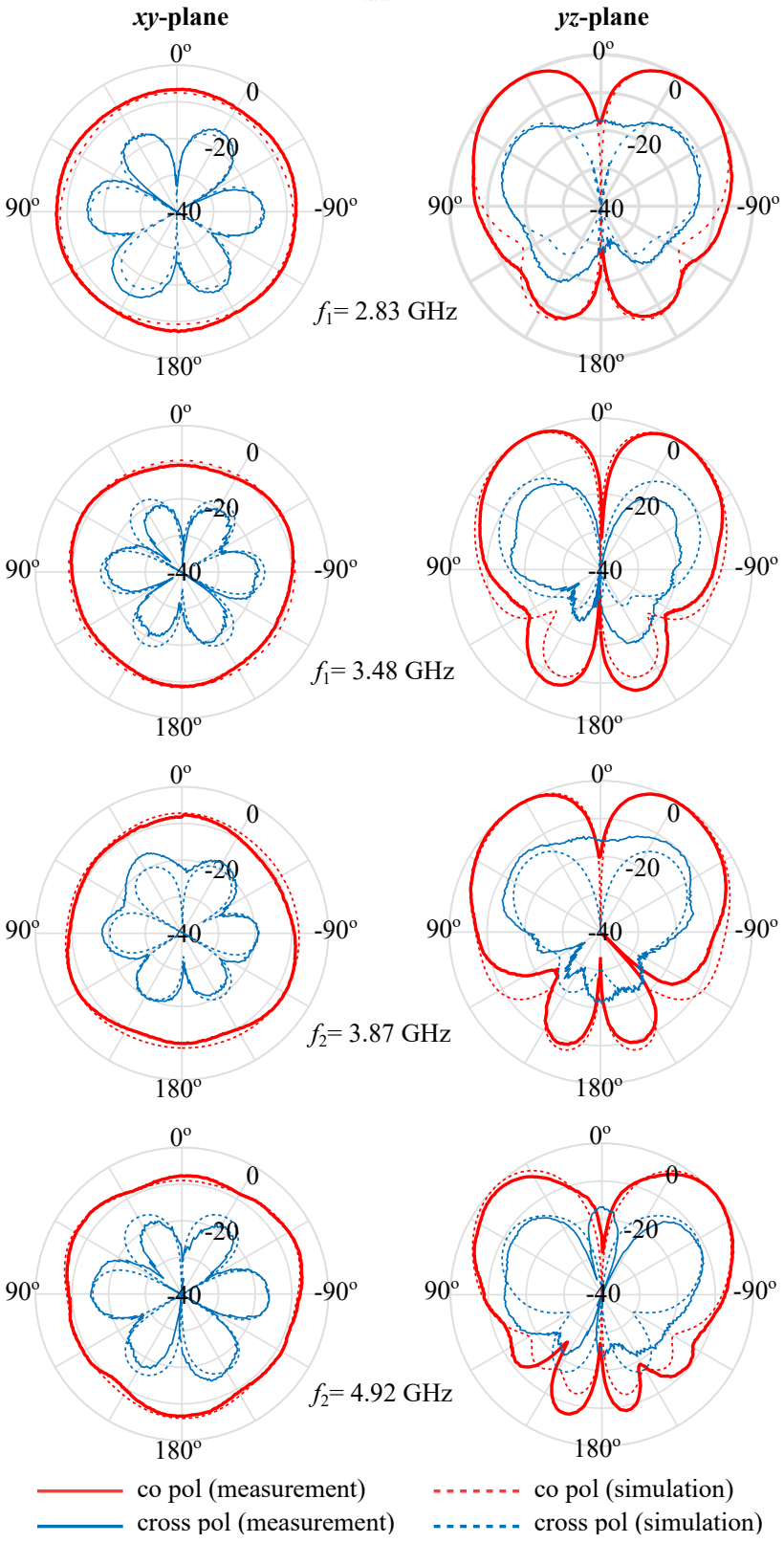

Figure 4.9. Normalized radiation patterns of the dual-band reconfigurable low-profile monopole antenna.

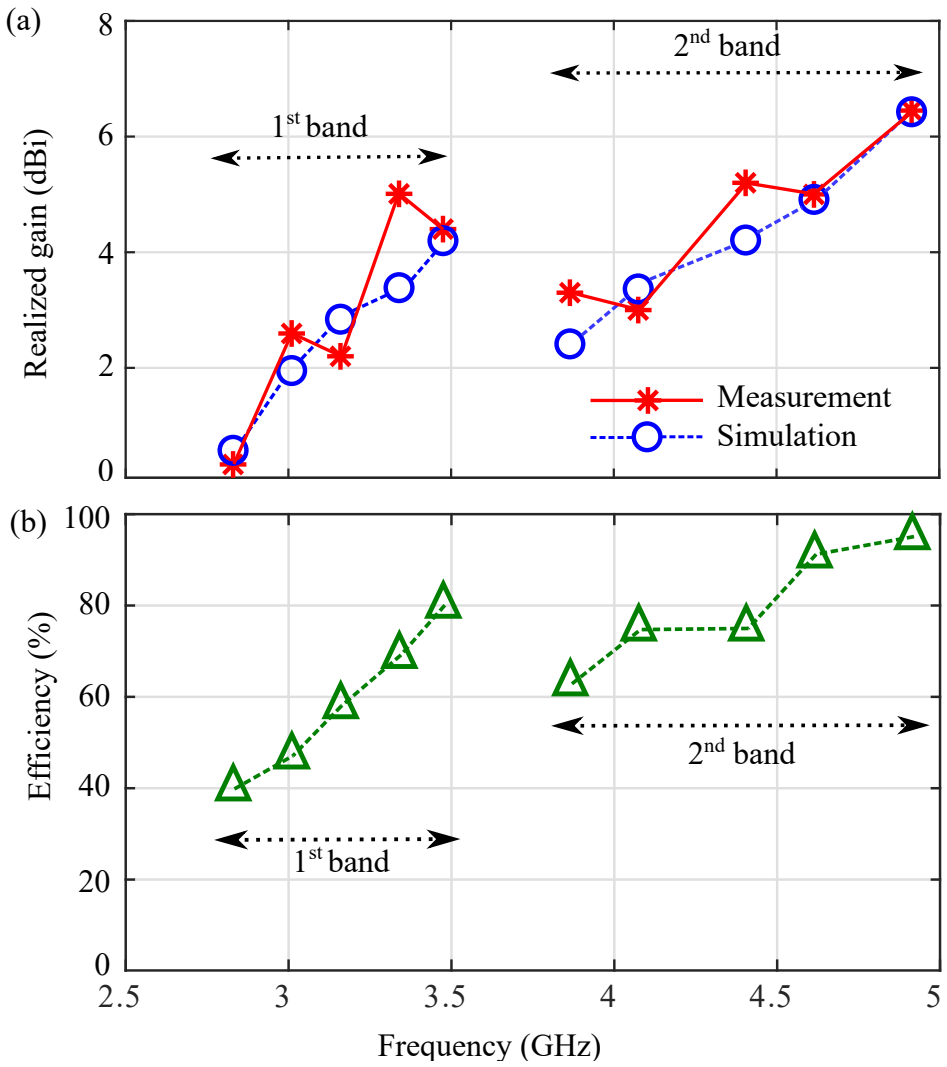

Figure 4.10. Gain and efficiency of the dual-band design. (a) Realized gain across the two tuning ranges. (b) Simulated total efficiency across the two tuning ranges.

The simulated and measured realized gains for both bands are shown in Fig. 4.10(a), while the simulated antenna efficiencies are depicted in Fig. 4.10(b). For the first band, the realized gain generally increases from 0.33 to 4.40 dBi as the resonance frequency increases. In the second band, the measured gain rises from 3.30 to 6.45 dBi when the antenna is tuned from the lowest to the highest frequencies. At higher frequencies, the patterns become more conical because the ground plane is electrically larger and this leads to a higher gain. The efficiency of the antenna also increases with the increasing frequency. At the first band, the efficiency is from 40% to 80%, while in the second band the efficiency increases from 63% to 95%. The lower antenna efficiency is mostly because of the higher loss in the internal resistances of the varactors. In the lowest

frequency, a higher current flows through the varactors when the capacitance is at the highest value (1.30 pF). The capacitance drops by one order of magnitude to 0.15 pF at the highest tuning. This condition resembles closely as an open circuit, resulting in almost no current flowing through the varactors. The actual radiation efficiency of the antenna is expected to be close to the simulated one, considering the agreement between the simulated and measured realized gains.

4.4 Triple-Band Reconfigurable Design

The previous section validated the concept of independent magnetic-loops in the dual-band reconfigurable design. In this section, the extension of the principle into a triple-band device will be demonstrated, with emphasis on the design difference compared to the previous one.

4.4.1 Antenna Geometry and Bias Circuit

The design and the photographs of the fabricated triple-band reconfigurable antenna are depicted in Fig. 4.11 and Fig. 4.12. This triple-band reconfigurable design is created on Rogers Duroid 5880LZ substrate with a relative permittivity ϵ_r of 2.0, $\tan\delta$ = 0.0027 and a thickness of 4.32 mm (or about $0.032\lambda_{\text{min}}$). A thick substrate is required to attain good impedance matching in each of the three bands and to improve the radiation efficiency. The antenna is center-fed with a 50-Ω SMA connector. The diameter of the ground plane is set to 150 mm. An FR-4 substrate with a thickness of 1.6 mm is also used to realize the biasing network in a separated layer underneath the ground plane. The most noticeable difference compared to the previous dual-band design is in the configuration of the stubs. Nine stubs divided into three sets of different lengths are utilized to introduce three shorting conditions at three particular frequencies. In addition, these three sets of stubs are not evenly angularly distributed.

Based on our investigation, a larger number of stubs increase mutual coupling effects, which in turn affect the tuning independence. The coupling is not only between adjacent stubs but also between the inactive stubs and the active radiating slots. It is known from a typical slot antenna that the highest amplitude of the *E*-field occurs in the middle of the slot when it resonates in its fundamental mode. Because of this, it is advisable to avoid placing inactive stubs close to the middle of an active radiating slot. A parametric optimization of the design has been carried out to balance trade-offs between

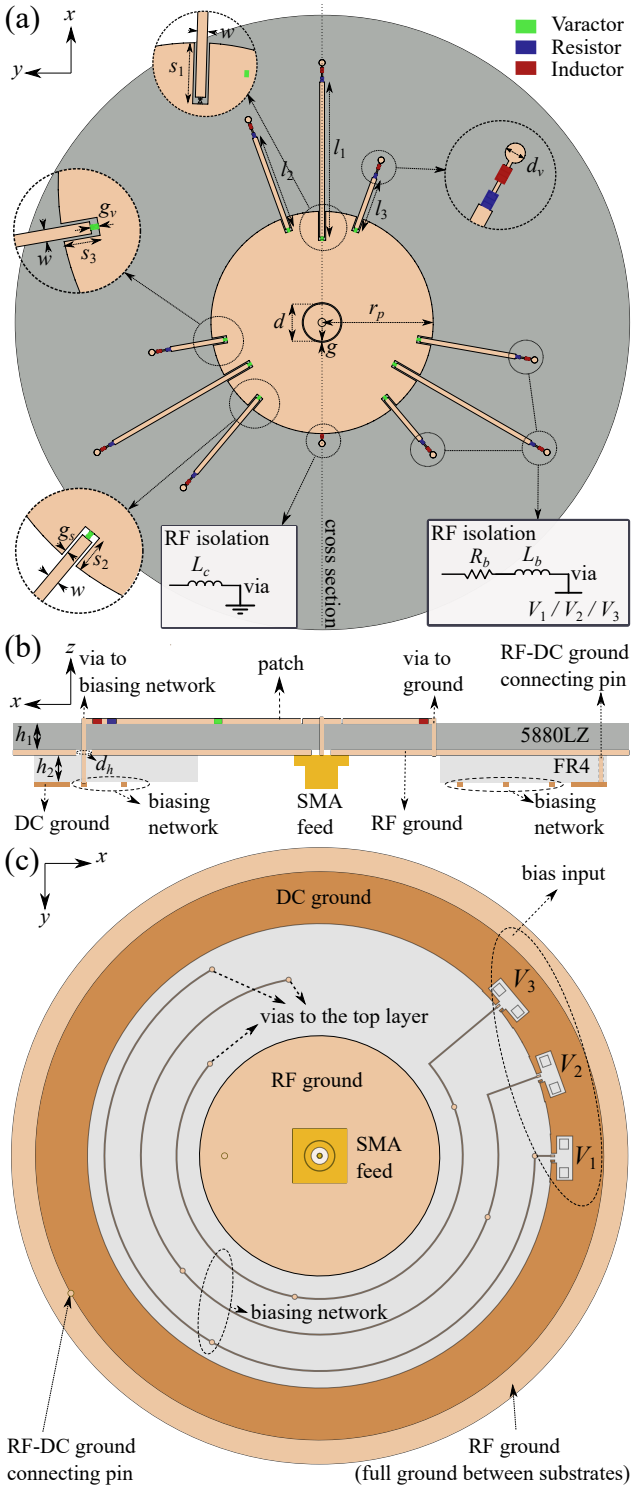

Figure 4.11. Triple-band reconfigurable antenna design. (a) Top, (b) cross-sectional, and (c) bottom views. Dark grey color is the 5880LZ substrate, light grey color is the FR-4 substrate, light brown color is copper on 5880LZ substrate, and dark brown color is copper on FR-4 substrate. The dimensions (mm) are: $l_1 = 32$, $l_2 = 20$, $l_3 = 11$, $s_1 = 6$, $s_2 = 3$, $s_3 = 3$, $w = 1$, $d = 8$, $r_p = 23$, $g = 0.1$, $g_v = 0.66$, $g_s = 0.25$, $d_v = 0.9$, $d_h = 1.8$, $h_1 = 4.32$, and $h_2 = 1.6$.

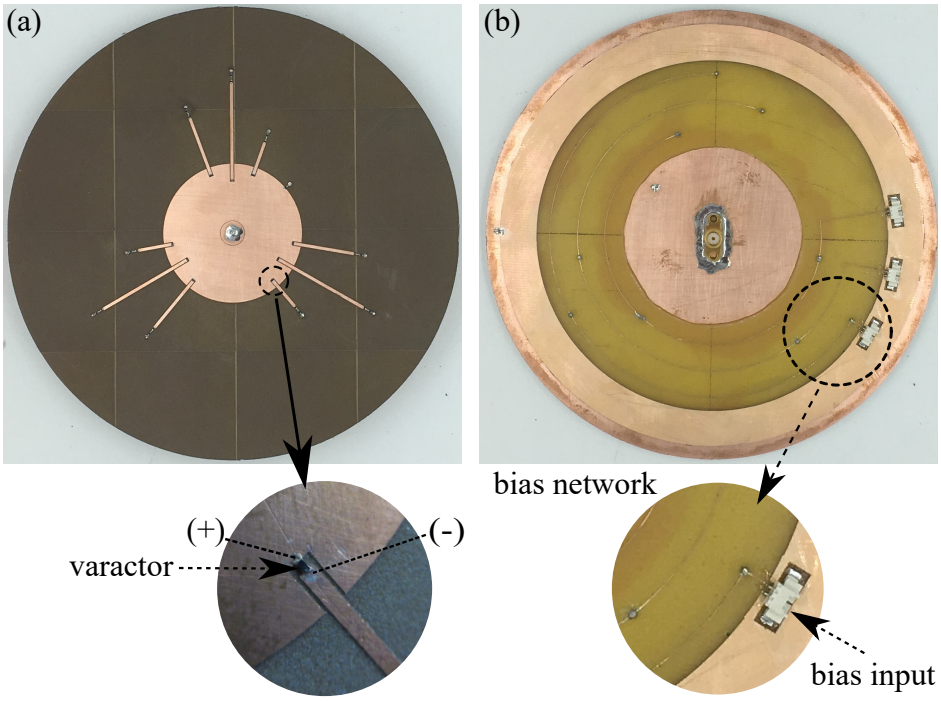

Figure 4.12. Photograph of fabricated triple-band reconfigurable design. (a) Top and (b) bottom views.

stub-to-stub and stub-to-slot coupling, and an optimal angle between the consecutive stubs is found to be 20°. It is noted that a similar optimization of the angular degree between the stubs can also be performed for the dual-band design. Nevertheless, this optimization was not specifically required in this previous case, since a good tuning independence with a very small discrepancy of less than 1% was already obtained.

To achieve reconfigurability, nine varactors MA46H120 are located between the patch and the stubs. These varactors are divided into three sets, one for each group of same-length stubs. These three varactor sets are biased separately by DC voltages V_1, V_2, and V_3, which are applied from the bottom layer through vias. A 1 MΩ resistor followed by an inductor is located after each stub as the RF choke. The inductors are L_b = 100 nH for the shortest and the longest stub and L_b = 24 nH for the middle-length stubs. These two inductors are found appropriate taking into account their self resonant frequency. A single via together with an RF choke L_c = 100 nH is used to DC-ground the circular patch. A full RF ground plane is used between the two substrates. To allow the vias connecting the patch to the biasing network layer, circular holes with diameter d_h = 1.8 mm (about $0.013\lambda_{\text{min}}$) are created on the RF ground plane. The size of these

holes is set to be sufficiently small to avoid a detrimental effect on the radiation patterns of the antenna.

4.4.2 Reflection Coefficient

Measured and simulated reflection coefficients with different bias voltages V_1, V_2, and V_3 agree well, as shown in Fig. 4.13. The three bands are centered at 2.51, 3.56, and 4.62 GHz. In each scenario, only one band is tuned while the other two are fixed. It can be seen from all the scenarios that the tuning of one band does not affect the other two. Hence, the independence of frequency tuning is achieved for this triple-band antenna design. The measured -10 dB tuning ranges are 22.8% for the first band (2.22–2.79 GHz), 22.8% for the second band (3.15–3.96 GHz), and 16.7% for the third band (4.23–5.00 GHz). An instantaneous impedance bandwidth of about 1% is obtained in the first band, 1% to 2% in the second band, and around 4% in the third band. This narrow-band feature is typical for multi-band reconfigurable antennas [10–15,25]. Nevertheless, with the wide and continuous frequency tuning capability, this antenna can cover a large operation bandwidth with an excellent frequency selectivity and remains low-profile owing to the narrow-band feature. This characteristic is highly desirable for applications such as cognitive radio.

Figure 4.14 shows two scenarios when the tuned resonances are close to each other. In the first scenario, the first band is tuned to the maximum bias voltage V_1 = 18 V and the second band is tuned to the minimum voltage V_2 = 0 V. For the second scenario, the second band is at the highest tuning voltage V_2 = 18 V and the third band at the lowest tuning voltage V_3 = 0 V. It is observed from the two scenarios that the antenna still maintains a satisfactory impedance matching with reflection coefficient below -10 dB. It is also noticed that there are separations of 360 MHz and 270 MHz between the first-second bands and the second-third bands respectively. In these two scenarios of Fig. 4.14, the predominant radiating sources are still the magnetic current slots. Therefore, the antenna radiates omnidirectionally and is not compromised by the coupling. We note that it would be possible to design a seamless tuning without gaps between consecutive bands, although with trade-offs in the tuning independence between adjacent bands.

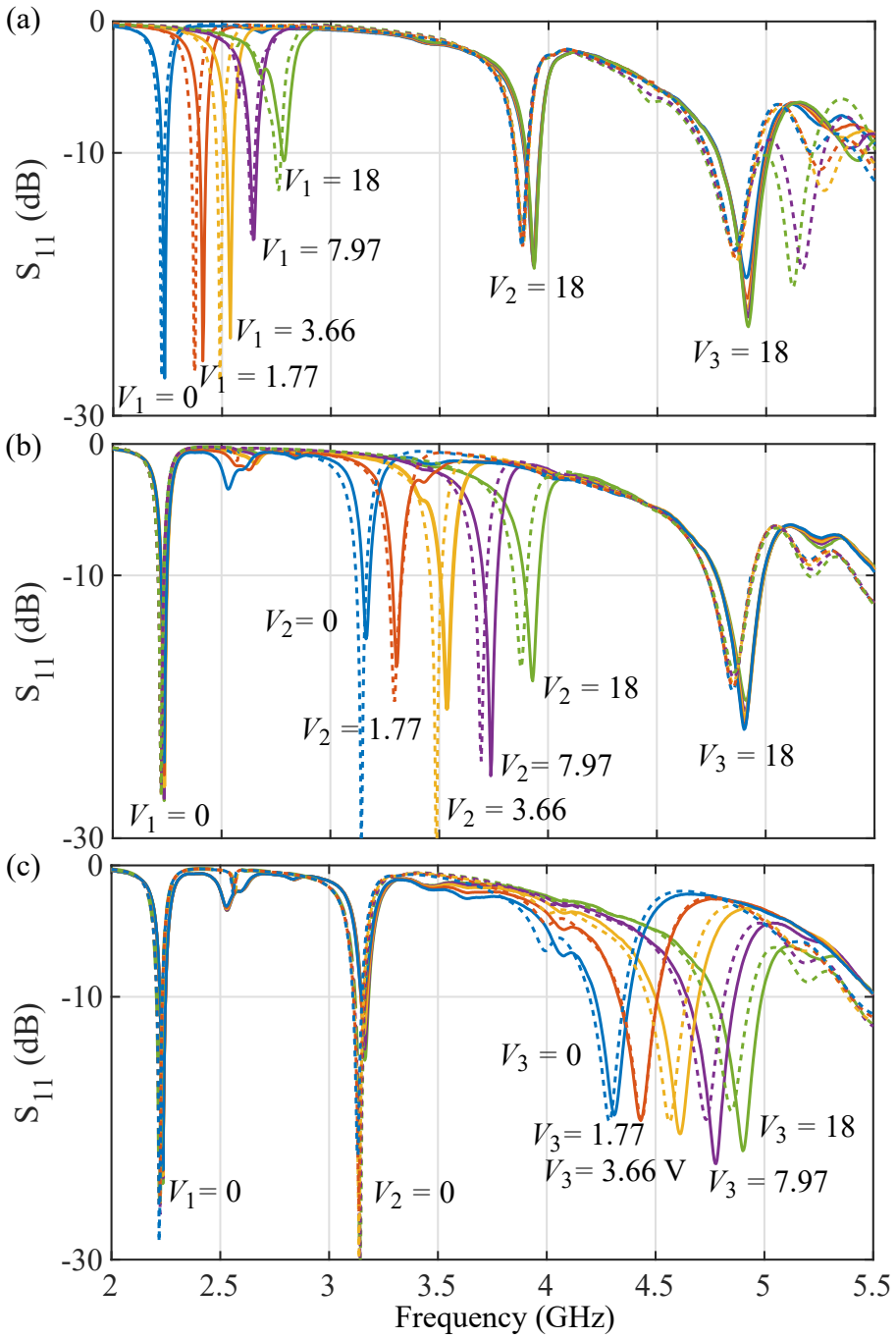

Figure 4.13. Measured (solid lines) and simulated (dotted lines) reflection coefficients of the triple-band reconfigurable low-profile monopole design. (a) Varying the first band (V_1), (b) varying the second band (V_2), and (c) varying the third band (V_3). The unit for the voltages is Volt.

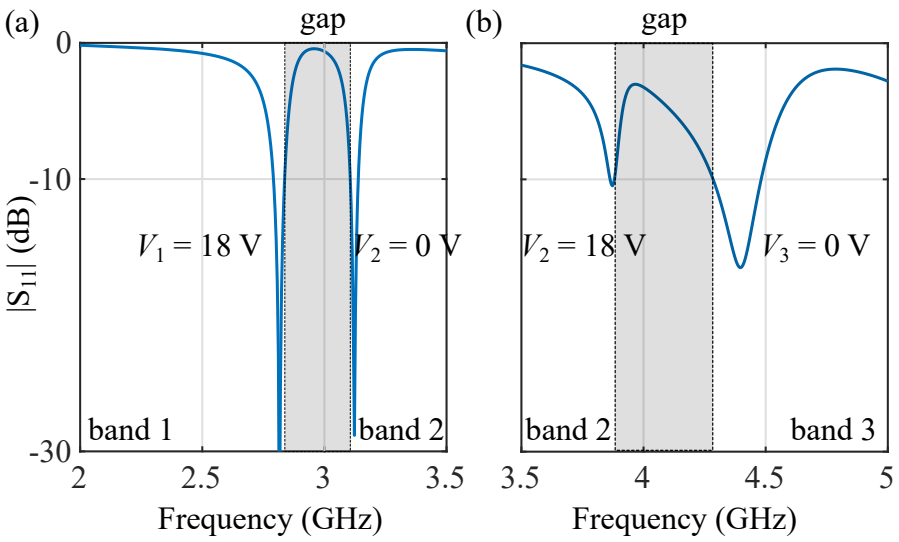

Figure 4.14. Reflection coefficients when the tuned resonances are close to each other. (a) First band is tuned with the maximum bias $V_1 = 18$ V and second band is tuned with the minimum bias $V_2 = 0$ V. (b) Second band is tuned with maximum bias $V_2 = 18$ V and third band is tuned with the minimum bias $V_3 = 0$ V.

4.4.3 Surface Current Distribution

Figure 4.15 shows two examples of surface current distributions of the active tuning stub at the lowest band. In Fig. 4.15(a) the varactor on the longest stub is biased with the minimum tuning voltage $V_1 = 0$, resulting in a capacitance of 1.30 pF. At this minimum tuning frequency $f_1 = 2.23$ GHz, the current density in the stub is depicted in Fig. 4.15(c) with the maximum approximately at the beginning of the stub (patch edge) and the minimum at its end. This suggests that the stub works equivalently as an opened $\lambda/4$ transmission line that effectively creates a short near the edge of the circular patch. On the other hand, for the case when f_1 is tuned to the maximum of 2.75 GHz with the varactor capacitance set to 0.15 pF, the current density is shown in Fig. 4.15(b) and Fig. 4.15(d). In this condition, the location where the stub has the maximum current density is shifted toward the center, indicating that the impedance at the beginning of the stub is increased due to the smaller varactor capacitance. The varactor can be considered as a loaded impedance at the antenna aperture as explained in [36]. The variation of the impedance affects the fringing field and thus the resonance frequency is shifted. Simulated surface current distributions with a short and an open circuits are included as dotted lines in Fig. 4.15(c) and Fig. 4.15(d). They are added to show comparisons with the two extreme scenarios of the varactors.

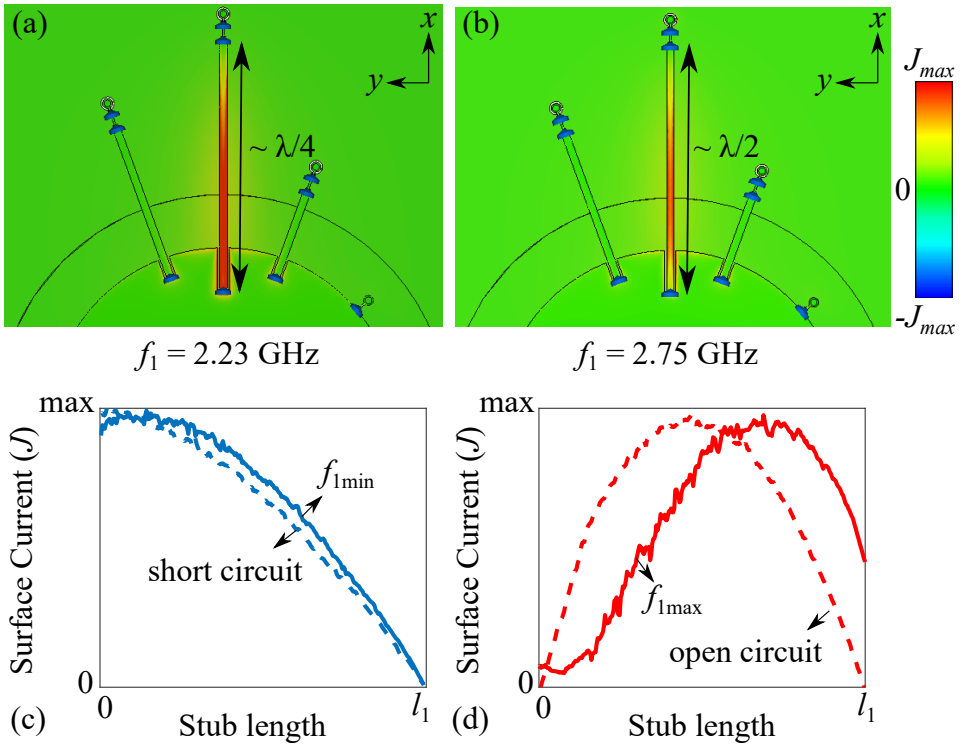

Figure 4.15. Simulated surface current distribution. (a) f_1 tuned to the minimum and (b) maximum. (c, d) Normalized surface current density along the length of the stub for the case shown in (a, b), respectively. The blue and red solid lines illustrate the simulated surface current density when the capacitance of the varactors are tuned to the minimum and maximum, respectively. The dotted lines depict the simulated surface current density when the varactors are substituted with short circuit (blue) and open circuit (red) for comparison.

4.4.4 Radiation Patterns

The photographs of the radiation patterns measurement setup in the chamber are illustrated in Fig. 4.16. The normalized simulated and measured radiation patterns at the minimum and maximum tuning frequencies for each of the three bands are depicted in Fig. 4.17. A good qualitative agreement is observed between simulation and measurement. In the azimuth xy-plane, monopole-like radiation patterns are obtained at all sweeping frequencies, while in the elevation yz-plane, the radiation patterns are conical as a result of the finite ground plane similarly as monopole antennas that were proposed in [4, 8, 63, 64, 70]. The omni-directional radiation patterns are required for applications where a large coverage in the azimuthal plane is needed. It is emphasized that the co- and cross-polarizations in the omnidirectional xy-plane patterns are measured at the horizon, i.e., $\theta = 90°$, as can be seen in Fig. 4.16(a). It is observed that at the

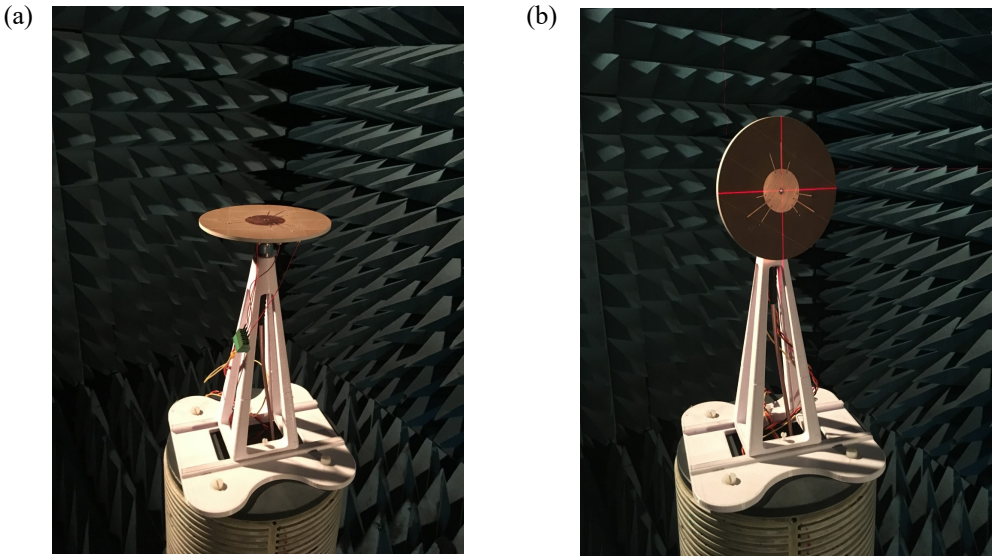

Figure 4.16. Antenna radiation patterns measurement setup. (a) Azimuth xy-plane measurement, and (b) elevation yz-plane measurement.

highest tuning frequency in the second and the third band, the patterns in the xy-plane become more directive towards the active shorting stubs. Ideally, from image theory it is known that the electric current flows over the stubs is canceled out by the reflected image from the ground plane (chapter 2.2). As a result there should be no substantial net radiation from the stubs. However, for these two particular tuning conditions, the separation between the antenna and the ground plane is becoming sufficiently large. As a result, parasitic radiations originating from the stubs can be observed. The stubs then can be seen as electric dipoles at a non-negligible distance above the ground plane, and together with the slots they contribute to the total radiation pattern. This pattern degradation should be considered and might set a limitation of the proposed design concept for further extension into a higher number of bands.

4.4.5 Antenna Efficiency and Gain

The measured and simulated realized gain profiles are compared in Fig. 4.18(a). The gain is generally increasing with frequency. For the first band, the measured gain is between 0.93 and 4.62 dBi, whereas the second one is between 2.42 and 6.00 dBi, and the third one spans from 4.77 to 8.50 dBi. The simulated radiation efficiency of the antenna is displayed in Fig. 4.18(b). In the first band, the efficiency ranges from 40% to 70%, for the second band the efficiency is between 50% to 87%, and increases from 77%

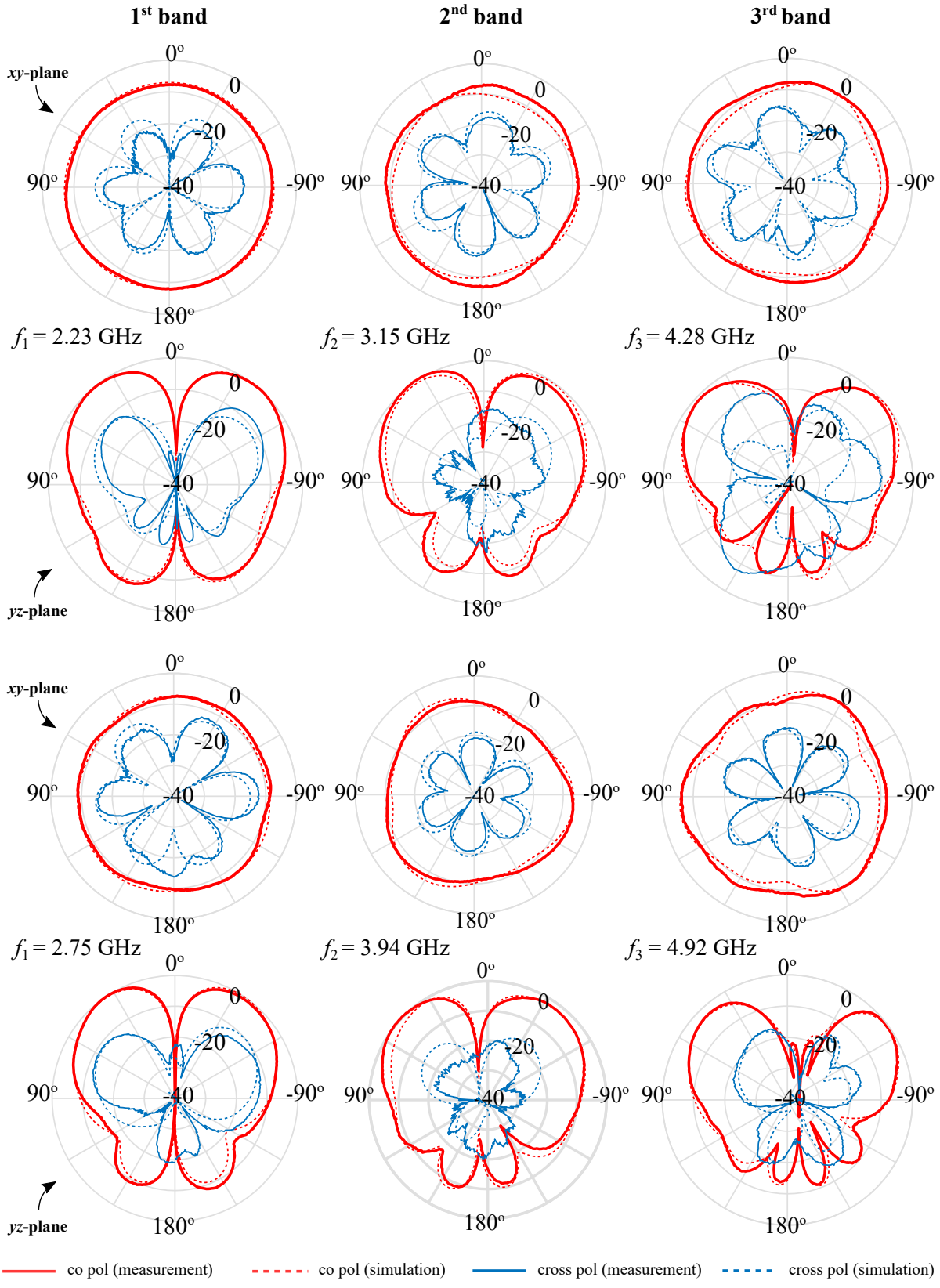

Figure 4.17. Normalized radiation patterns of the triple-band reconfigurable low-profile monopole antenna.

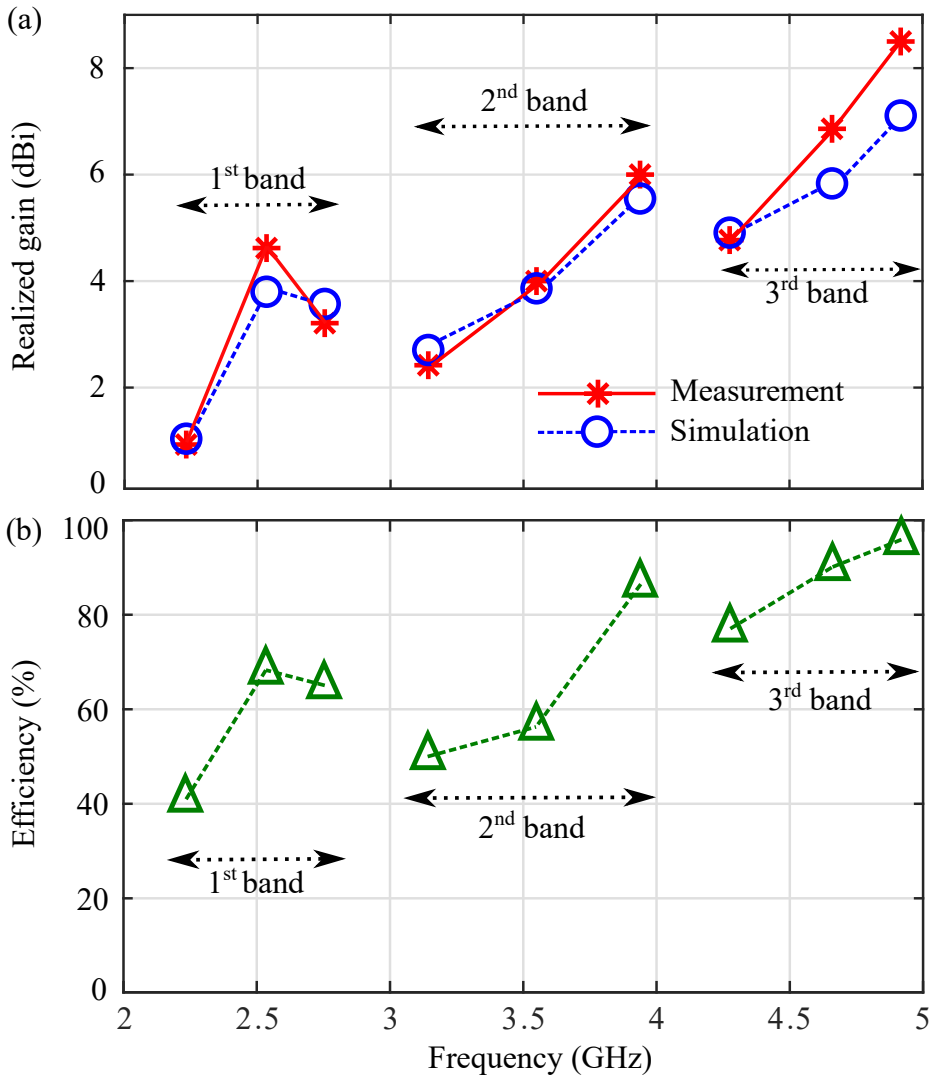

Figure 4.18. Gain and efficiency of the triple-band design. (a) Realized gain across the three tuning ranges. (b) Simulated total efficiency across the three tuning ranges.

to 96% in the third band. Similar to the previous dual-band design, at the lower end of the tuning range a higher current flows through the varactors, which results in the lowest efficiency, whereas, nearly no current flows through the varactors at the higher end, leading to the highest efficiency.

4.4.6 Comparison with Existing Designs

Table 4.1 shows a comparison on the performance of some typical reported antennas with frequency reconfigurability in multi-bands. The antenna reported in [10] offered the largest number of independent tunable bands among the others. However, the

highest band has a very small tuning range of 3%. In addition, the design did not consider the stability and nature of the radiation patterns. The shape of the patterns was undefined. Among the published designs with broadside patterns [11–14], the antenna in [14] featured the highest number of tunable bands. They proposed three independent tuning frequencies and the tuning ranges were measured for more than 34% for each band. Nonetheless, these ranges were calculated based on minimum −6 dB bandwidth. The proposed design is more suitable to be compared with antennas that also radiate omnidirectionally as in [15] and [25]. Between these two dual-band antennas, only the antenna in [15] can be tuned independently. Compared to these designs, the triple-band antenna in this chapter demonstrates a larger number of tunable bands with a higher measured maximum gain.

Table 4.1. Performance comparison between presented design and published frequency-reconfigurable multi-band antennas

Reference	No. of Bands (Tunable)	Tuning Range (%)	Independent	Pattern	Max Gain (dBi)
[10]	5 (4)	23.5 / 10.3 /13.5 / n.a. / 3	Yes	Undefined	-4.2 / 0.95 / 1.19 / 0.92 / 1
[11]	2 (1)	n.a. / 29,2	No	Broadside	7 / 6.8
[12]	2 (2)	n.a.	No	Broadside	n.a. / 2.7
[13]	2 (2)	19.7 / 51.3	Yes	Broadside	1.2 / 1.8
[14]	3 (3)	58.8 / 85.7 / 34.7 [a]	Yes	Broadside	-2.06 / -0.55 / 0.31
[25]	2 (2)	11 / 29.2	No	Monopolar	2.37 / -0.41
[15]	2 (2)	31 / 22	Yes	Monopolar	3.5 / 5.5
This work	3 (3)	22.8 / 22.8 / 16.7	Yes	Monopolar	4.62 / 6 / 8.5

[a] -6 dB bandwidth

4.5 Conclusion

In this chapter, frequency-reconfigurable low-profile monopole antennas with independently tunable bands have been presented. These multi-band antennas are based on the concept of a center-fed patch with shortings to create independent magnetic current loops sharing the same thin aperture. Groups of quarter-wavelength stubs are located at the patch edge with each set of stubs functioning as equivalent shortings at a particular frequency. Frequency-reconfigurability is achieved by placing sets of varactor diodes between the patch and the stubs. For the first design, the two independently tunable bands are centered at frequencies of 3.16 and 4.42 GHz with -10 dB independent tuning ranges of 21.2% and 27.1% respectively. The extension of the principle into a triple-band design demonstrates center operation frequencies at 2.51, 3.56, and 4.62 GHz with -10 dB independent tuning ranges of 22.8%, 22.8%, and 16.7% respectively. The number of bands is limited by the stub-stub and stub-slot couplings, and the electrical separation between the patch and ground plane. For the radiation patterns, both antennas radiate omnidirectionally with vertical polarization across the tuning ranges, indicating that the magnetic current slots remain the predominant radiating sources. All these results suggest that the proposed antenna designs are promising for advanced applications that require independent reconfigurability in multi-band operation, such as software-defined radio or carrier aggregation systems. The advantages include simple antenna geometry, ease of fabrication, and low profile.

Chapter 5

Circularly-Polarized Frequency-Reconfigurable Omnidirectional Antenna

This chapter presents the original contributions of the thesis dedicated to a circularly-polarized (CP) omnidirectional antenna with frequency tunability. The antenna is based on a center-fed circular patch surrounded by three arc-shaped strip lines. Three varactor-loaded slots are etched onto the patch to achieve a frequency tunability. Simulated results and experimental validation demonstrate that the antenna has a wide CP tuning range of 22.6% with stable omnidirectional patterns.

5.1 Introduction

Nowadays, low-profile monopole antennas are widely used in wireless technologies due to their compact size and omnidirectional radiation pattern. An omnidirectional antenna radiates the signal uniformly in the azimuth direction, making it very useful in conditions where the other transceivers are arbitrarily deployed. In addition, an antenna with a broadband operation or frequency agility is desirable to allow operation at different communications bands. It is noted that compared to a broadband antenna, a frequency-reconfigurable antenna is generally expected to have a more compact size for the same accessible operation bandwidth. A frequency-tunable antenna is also more robust to interferences than the passive wideband one due to its high isolation between communication channels. Because of this, various frequency-reconfigurable antenna designs have been proposed in the literature in the past few years [11, 12, 14, 15, 36, 38, 39, 44].

To further increases the robustness of a communications system with mobile users, it is often desirable to use an antenna which is capable of transmitting and receiving with circular polarization. A circularly-polarized (CP) antenna provides several advantages compared to a linearly-polarized antenna [16]. A CP antenna is effective in reducing multi-path interferences or fading [17, 18]. The incoming radio signal that is reflected from the ground or other objects will be reversely polarized, that is, from left-handed circular polarization (LHCP) to right-handed circular polarization (RHCP) or vice versa. This results in a decrease of multi-path interferences due to the rejection of signals from different polarization. A CP antenna is also effective in reducing 'Faraday rotation', an effect that occur when the radio signal travels through the ionosphere [71], making it suitable for space to Earth communications. Another advantage of antennas with circular polarization is that they are more robust to orientation misalignment between transmitting and receiving antennas compared to LP antennas. With CP, the received signal strength is independent of the antennas orientation.

For the CP antennas with frequency tunability, only a few designs have been reported until this present time [72–77]. In [72], a dual-band CP antenna was demonstrated. The reconfigurability was achieved by controlling the states of dual PIN diodes, resulting in a frequency ratio of 1.08. Another dual-band CP design with a higher frequency ratio of 1.6:1 was reported in [73]. In this design, RF-MEMS switches were incorporated into the antenna structure for controlling the operating frequencies. Both of the frequencies were RHCP with axial ratio below 3 dB. In a more recent publication [75],

four varactor diodes were integrated into a square patch antenna to tune the resonant frequencies of dual orthogonal resonant modes equally. This configuration allows the resonance frequency to be tuned continuously from 1.97 to 2.53 GHz. All of these published designs share a common characteristics, namely that they aim at directive radiation pattern in broadside direction. To date, there are however no records of existing frequency-tunable CP antenna designs with omnidirectional patterns.

In this chapter, a concept of CP frequency-reconfigurable low-profile monopole antenna is proposed. The antenna is based on a center-fed circular patch surrounded by three arc-shaped arms. The patch includes three varactor-loaded slots to define the frequency reconfigurability. By varying the capacitance of the varactors with a single DC voltage, the resonance frequency of the antenna can be tuned while still maintaining the 3-dB axial ratio criterion of the CP. The chapter begins with a description of the antenna geometry and its operation principle and then follows with practical aspects of the antenna design, including biasing wires and sleeve-balun integration. Afterward, the simulated and measured results of the prototype will be discussed, followed by the conclusion.

5.2 Operation Principle

The basic antenna geometry is adapted from [78], as shown in Fig. 5.1, while the antenna design evolution is depicted in Fig. 5.2. The antenna comprises three main elements: magnetic current sources, electric current sources, and phase compensation lines. Two identical circular metal patches are printed on both sides of the substrate. Three shorting vias connect the patches with 120° annular arrangement between consecutive vias. The overall structure is fed by a 50-Ω coaxial probe. This configuration can be seen as a parallel plate slot cavity. The thickness of the substrate, which is also the profile of the cavity, is sufficiently small compared to the wavelength. Hence, only transverse E-field will occur in the slot formed at the periphery of the patches, and thus the open aperture of the cavity can be seen as a magnetic current source M. Similarly, the arc-shaped arms can be considered as electric current line sources J because their width is small compared to the wavelength. Furthermore, double-sided meandered parallel strip lines are placed between the patch and the arms. These strip lines are functioning as phase compensation lines between the magnetic current sources and

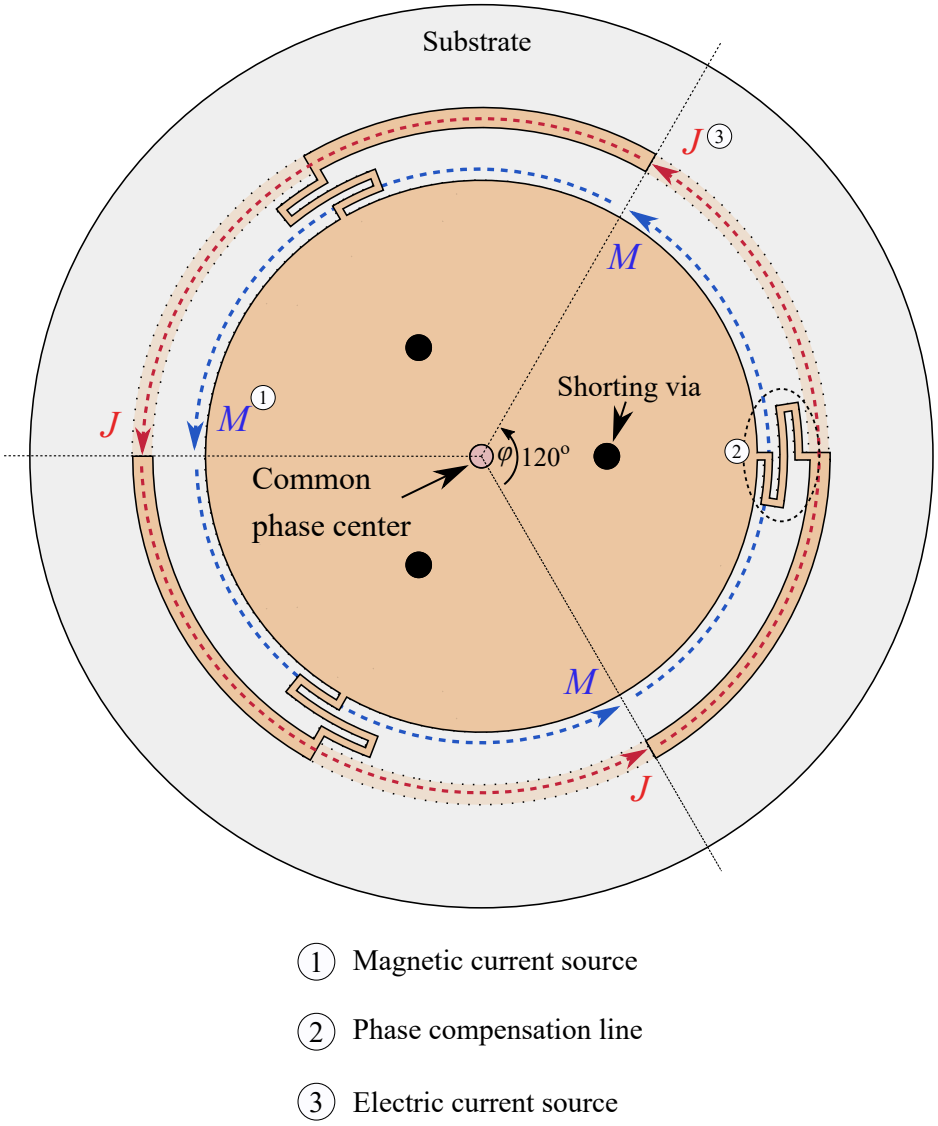

Figure 5.1. Basic antenna design with indication of the three main physical components for CP operation.

the electric current sources. To this end, magnetic current sources M and electric current sources J take part in the radiation of vertical electric fields E_θ and horizontal electric fields E_φ, respectively.

To determine the axial ratio of the antenna, we should define the magnitude ratio m and the phase difference δ between the two orthogonal electric fields components.

$$m = |E_\varphi|/|E_\theta|, \tag{5.1a}$$

$$\delta = \angle E_\varphi - \angle E_\theta. \tag{5.1b}$$

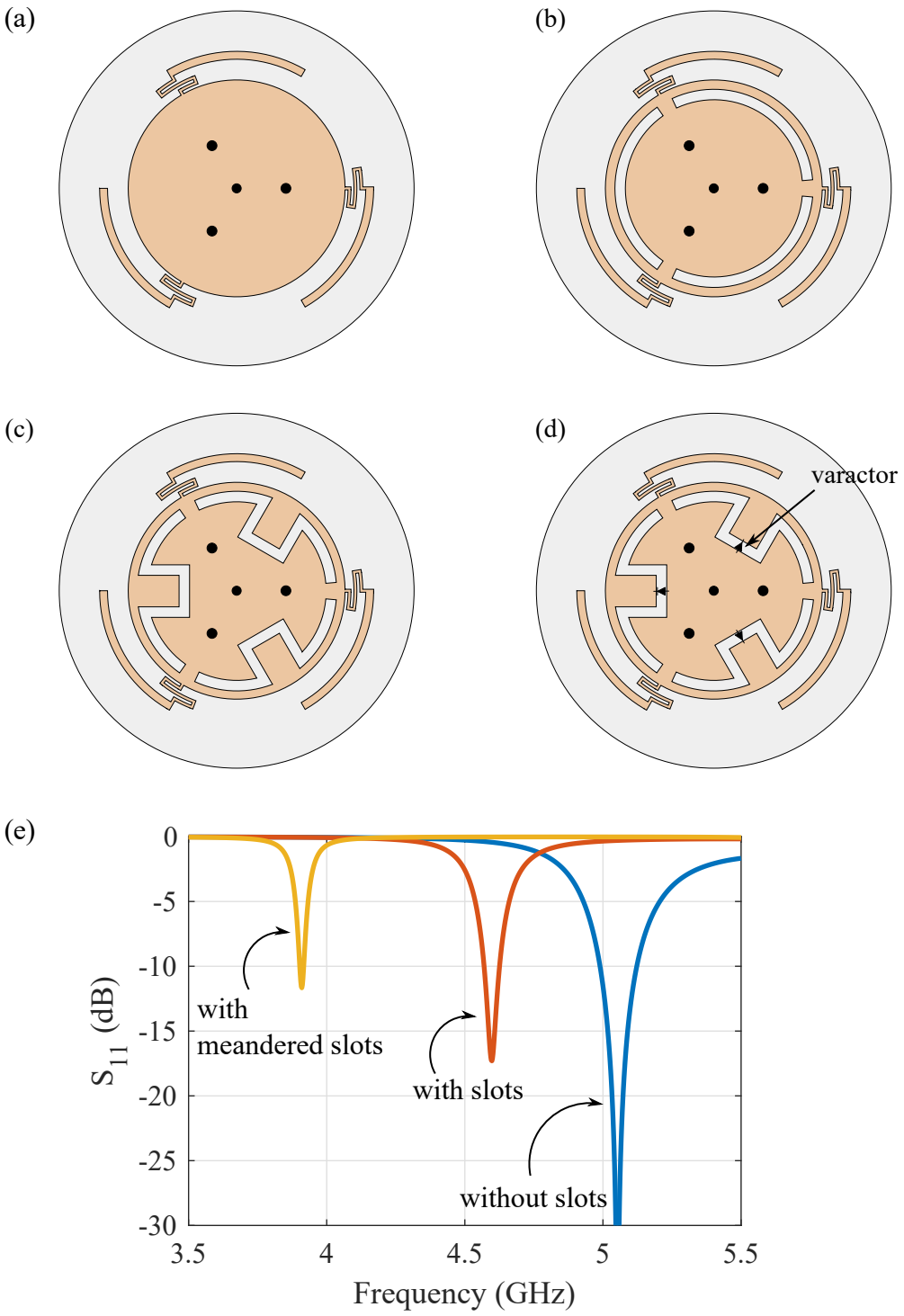

Figure 5.2. Design evolution. (a) Passive CP antenna [78], (b) CP antenna with arc-shaped slots, (c) CP antenna with meandered slots, (d) CP antenna with varactor-loaded slots. (d) resonance frequencies of CP antennas without slots, with slots and with meandered slots.

The axial ratio can be calculated as a function of m and δ as [78]

$$\mathrm{AR}(m,\delta) = \left| \frac{\sqrt{m^2+1-2m\cdot\sin\delta} + \sqrt{m^2+1+2m\cdot\sin\delta}}{\sqrt{m^2+1-2m\cdot\sin\delta} - \sqrt{m^2+1+2m\cdot\sin\delta}} \right|. \tag{5.2}$$

A perfect polarization purity corresponding to AR = 1 (0 dB) can be achieved if $m = 1$ and $\delta = (2n+1)\pi/2$ $(n = 0, 1, 2, 3, ...)$. Nonetheless, a typical design requirement for the axial ratio of a CP antenna is AR < 3 dB. By adjusting the design geometry of the patch, the meandered strip lines, and the arc-shaped arms, parameters m and δ can be optimized to meet the axial ratio requirement for CP.

The mentioned design principle of a basic passive CP antenna shown in Fig. 5.2(a) is further developed to design a frequency-reconfigurable version of the antenna. Firstly, three symmetrical arc-shaped slots are etched onto the top patch, as shown in Fig. 5.2(b). These slots introduce additional magnetic current sources that radiate in a linearly polarized manner. As a result, the introduction of the slots allows opening a higher frequency band, which will not be used directly. However, tuning this higher band affects the the original CP mode frequency, as pictured in Fig. 5.2(e). It is noted that the frequency shifting does not affect significantly the axial ratio of the CP mode. Furthermore, it is found that the length of the slots determines the frequency shifting. To extend the length of the slots, meandered slots are used as depicted in Fig. 5.2(c). This technique of meandering the slots to fit them within the constraint of a patch area also can be found in [15]. Lastly, by integrating varactor-diodes into the slots as illustrated in Fig. 5.2(d), the antenna can be made frequency-reconfigurable. The variation of capacitance in the slots enables the LP mode frequency to be tuned, which indirectly shifts the frequency of the CP mode. It is worth mentioning that the LP mode frequency will not be shown in the final results as it is not the intended mode.

Table 5.1. Design parameters of the proposed antenna.

Parameter	w_s	w_i	l_m	d_b	w_m	d_f	d_v	g_p
Value/mm	1	2.1	4.33	0.8	7	0.92	1	0.3
Parameter	w_p	w_a	g_e	h_s	r_s	r_p	r_a	d
Value/mm	0.3	0.8	0.5	1.575	13.9	11	5	36
Parameter	α_s	α_g	α_p					
Value/degree (°)	60	6	8					

5.3 Antenna Geometry

The optimized design geometry of the antenna is illustrated in Fig. 5.3 and the design parameters are summarized in Table. 5.1. The antenna is created on a Rogers Duroid 5880 substrate of thickness 1.575 mm, relative permittivity ϵ_r = 2.2, and loss tangent tanδ = 0.0009. The structure is based on a center-fed double-sided circular patch surrounded by three arc-shaped arms and is fed at the center by a 50-Ω coaxial probe. Three varactor-loaded slots are introduced onto the top patch to define frequency-reconfigurability. The varactor type for the design is MA46H120 from MACOM Technical Solutions. The anodes of the varactors are soldered to the patch side while the cathodes are soldered to rectangular 'islands' introduced in the center of the slots. To bias the varactors, voltages are applied through the bottom patch and substrate using vias, as shown in Fig. 5.3(c). The capacitance of the varactors C_v is varied from 1.30 to 0.15 pF when they are biased from 0 to 18 V. Inductors L_b of 47 nH are placed before the vias to block the RF current, while capacitors C_b of 10 pF allows the RF signal to propagate across the slots.

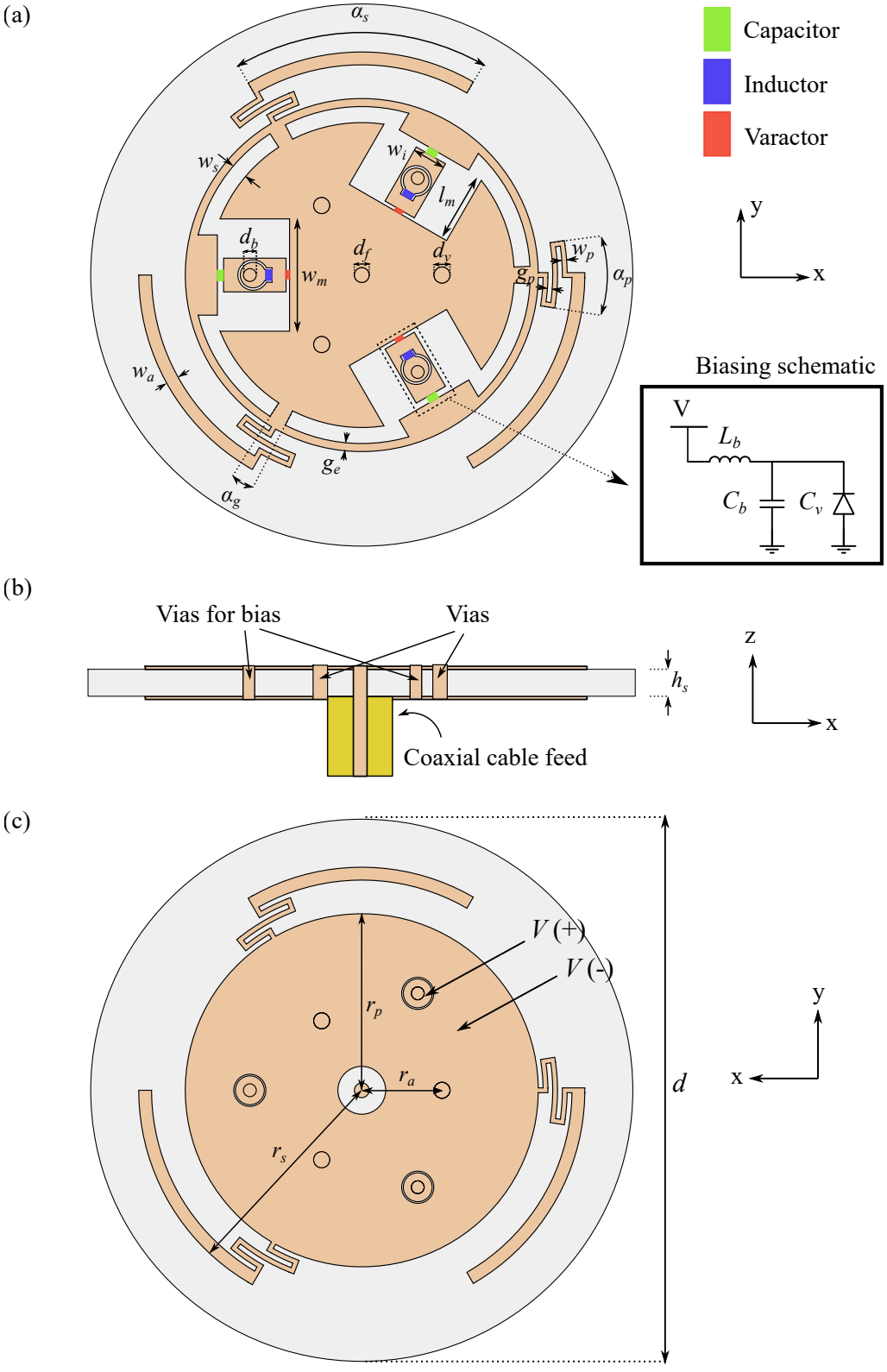

Figure 5.3. Antenna geometry. (a) Top, (b) side, and (c) bottom views. Light brown is copper, grey is the substrate.

5.4 Practical Aspects of the Design

There are two practical aspects of the design that need to be carefully considered before continuing to the prototype fabrication, namely DC biasing cable and the coaxial feed. In this section, the effect of these two elements to the performance of the antenna is discussed.

It is found that the use of standard straight DC biasing wires can degrade the axial ratio performance of the antenna. Although inductors have been used to block the majority of RF currents as shown in blue parts at Fig. 5.3, there is still leakage of surface currents from the top patch through the via bias due to the unavoidable electromagnetic coupling. The parasitic electric currents J_p continue to flow through the vertical cable, resulting in the excitation of parasitic E_θ radiation, as illustrated in Fig. 5.4(a). Besides, the near-field radiation from the antenna can couple back to these straight wires. which can also excite parasitic radiation. The unwanted radiation contributes to the total radiation of the structure and affecting the magnitude ratio between the two orthogonal E-fields. To mitigate this phenomenon, we replace the standard straight wires with wire coils, as shown in Fig. 5.4(b). It is noted that the wire coil is one form of an inductor. The inductance L_{coil} of this coil is proportional to the loop diameter d_l, and the number of turns N, which can be approximately calculated as [79]

$$L_{\text{coil}} \approx N^2 \mu_0 \mu_r \left(\frac{d_l}{2} \left[\ln \left(\frac{8 d_l}{d_w} \right) - 2 \right] \right), \tag{5.3}$$

where d_w is wire diameter, μ_0 is permeability of free space, and μ_r is relative permeability. In the proposed design, $N = 50$, $d_l = 1$ mm, $d_w = 0.2$ mm and $\mu_r = 1$ are used, resulting in an approximation of 2.65 μH wire inductance.

Another crucial design aspect that should be considered is relating to the coaxial cable that feeds the antenna. It is found that surface currents flowing on the outer conductor of the coaxial cable cannot be neglected, as they also contributes to the radiation of E_θ component of the field. Similar to the previous case, this radiation will affect the axial ratio of the antenna in a manner that is difficult to predict. To suppress this parasitic cable current, a sleeve balun is integrated into the coaxial cable as depicted in Fig. 5.5. A sleeve balun is one type of RF choke that is typically used in electrically small antenna measurement. This balun choke can suppress the unwanted currents on the outer conductor of the coaxial RF cable, as demonstrated in [80–82]. In addition, the choking characteristics of a sleeve balun were analyzed in [83]. For the proposed

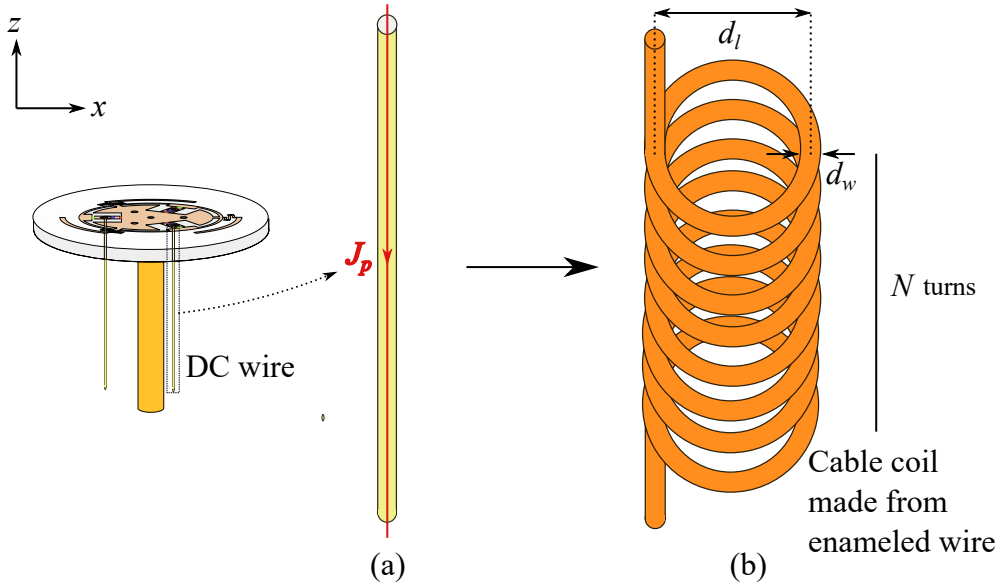

Figure 5.4. Wire configuration for biasing the varactors. (a) Straight biasing wire, (b) wire coil.

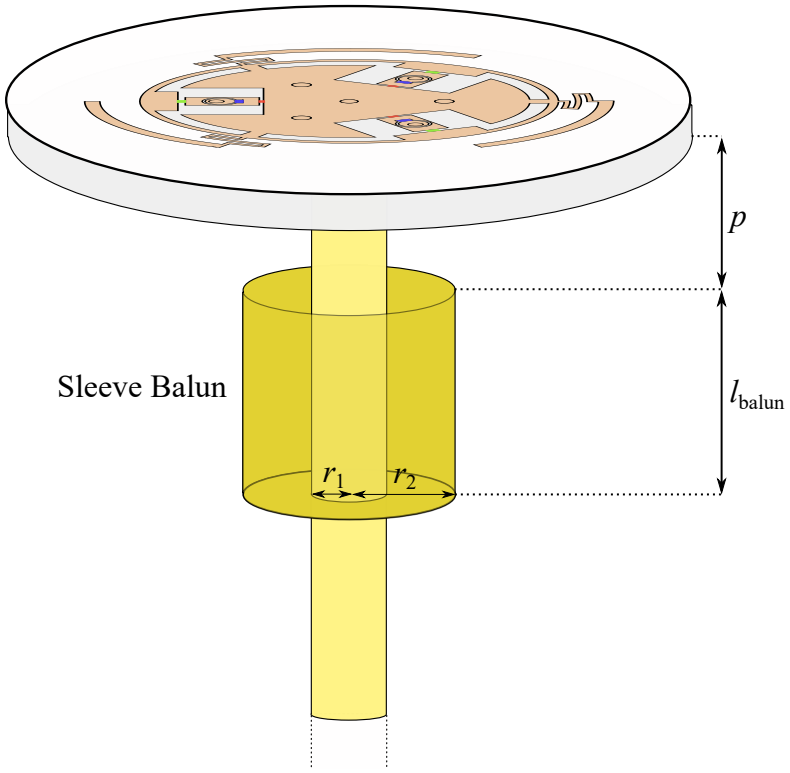

Figure 5.5. Sleeve balun configuration.

antenna design, it is found that to achieve an optimum surface current suppression at center frequency of 5.05 GHz, a ratio of r_2/r_1 should be equal to 3 with the balun length l_{balun} of 11 mm, and a distance between balun and the patch p of 10 mm. Figure 5.6

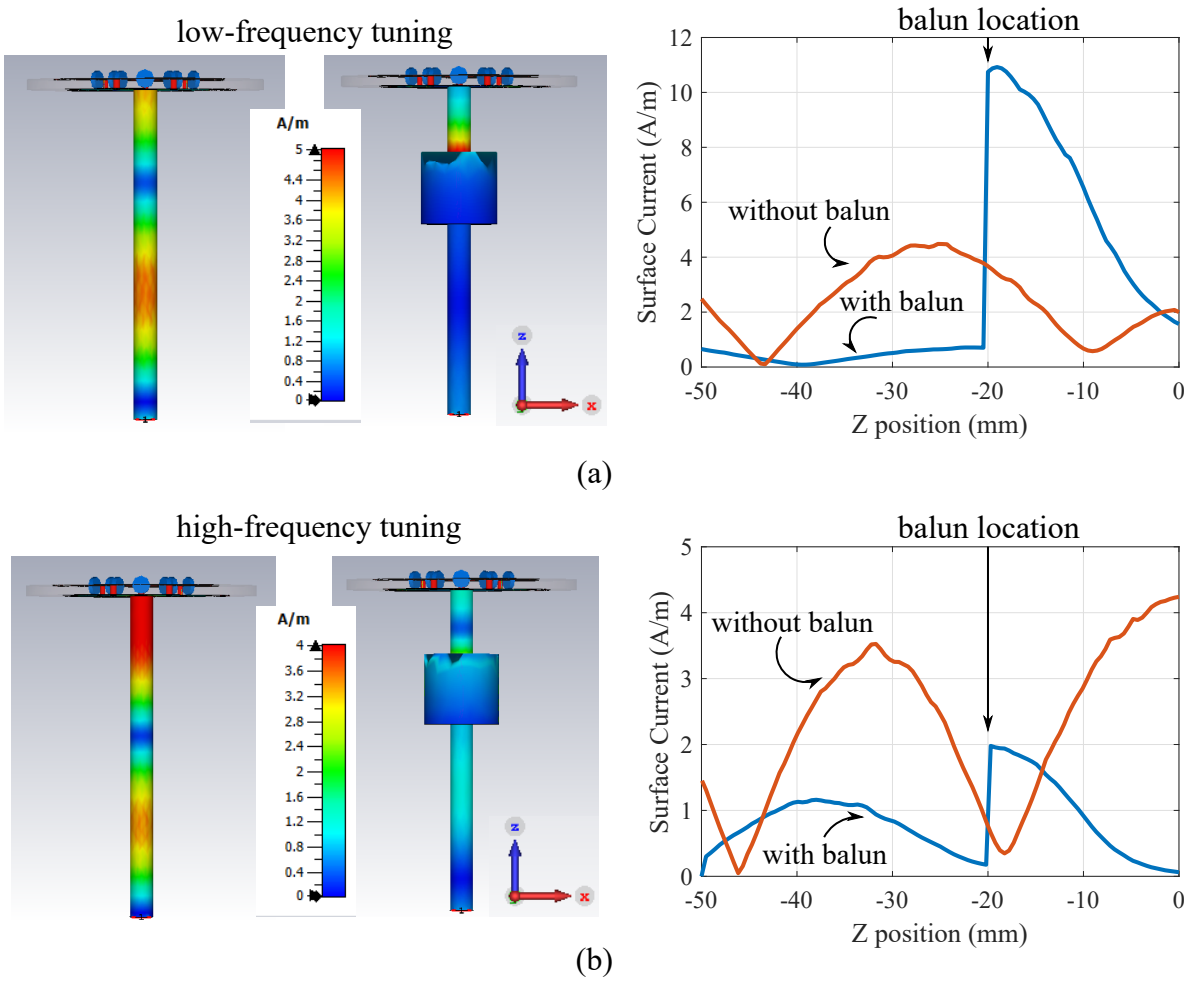

Figure 5.6. Comparison of simulated instantaneous surface current distributions on outer conductor of coaxial cable. With and without sleeve balun, at (a) low and (b) high-frequency tunings.

shows the effect of the sleeve balun on the suppression of the surface current at the low and high frequency-tuning scenarios of the proposed antenna. It can be seen that in both simulations, the balun integration reduces the magnitude of outer conductor current for about 70%.

5.5 Results

The antenna has been fabricated to verify the proposed operation principle and the prototype is shown in Fig. 5.7. The measured and simulated reflection coefficients $|S_{11}|$ are illustrated in Fig. 5.8. It is observed that both measured and simulated $|S_{11}|$ are in a very good agreement, with a measured tuning range of 22.6% from 4.48 to

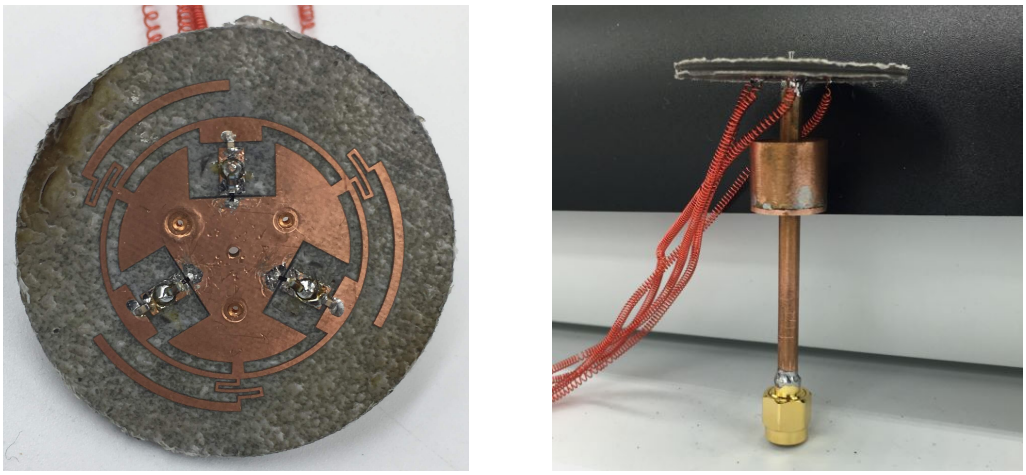

Figure 5.7. Photographs of the fabricated antenna. (a) Top and (b) side views.

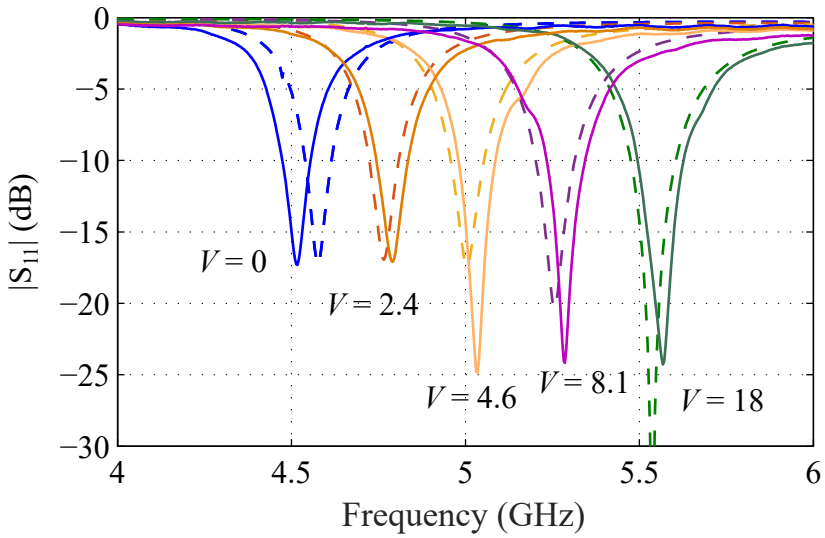

Figure 5.8. Measured (solid lines) and simulated (dotted lines) reflection coefficients of the antenna at five different biasing voltages. The unit for the voltages is volt.

5.62 GHz. The axial ratios of the antenna in the azimuth plane $\theta = 90^\circ$ are overall below 3 dB with minor breaches across the tuning range as depicted in Fig. 5.9. The discrepancies are mainly attributed to the imperfectly leveled antenna, which causes the variation of the measured axial ratios over the azimuthal angle φ. The plot of axial ratios at $\theta = 90^\circ$ and $\varphi = 0^\circ$ over frequencies in three different bands is illustrated in Fig. 5.10 . It can be seen from the graph that the antenna radiates in a CP mode across the reconfigurable tuning bands. Additionally, stable omnidirectional patterns in the azimuth $\theta = 90^\circ$ are achieved at the low, middle, and high tuning band and can be seen

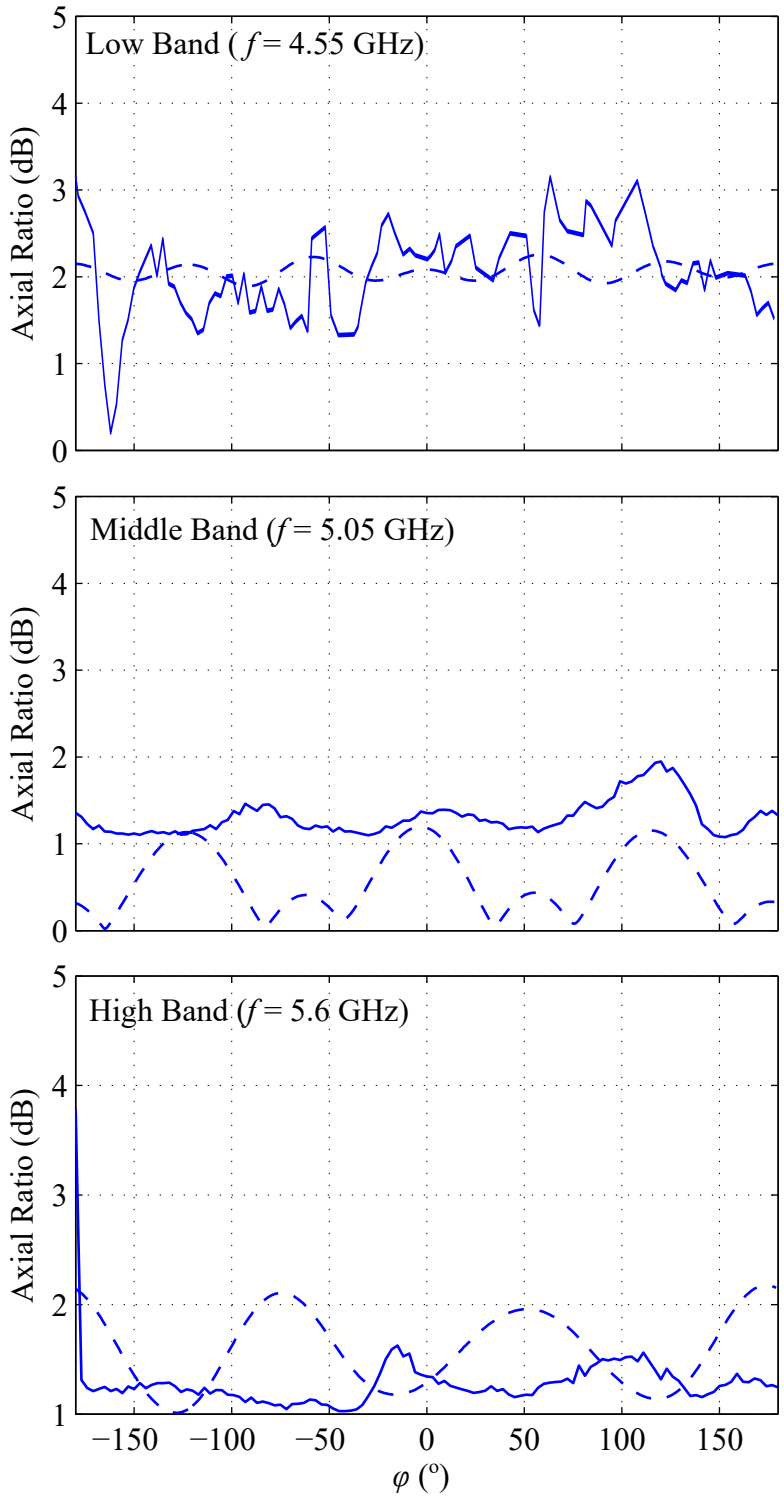

Figure 5.9. Axial ratios of the antenna. Measured (solid lines) and simulated (dotted lines) in the azimuth $\theta = 90^\circ$ at three different tuning bands.

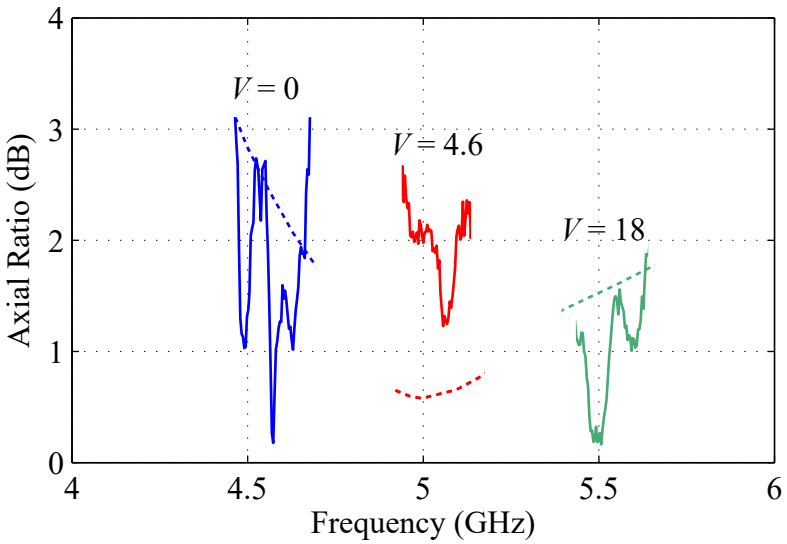

Figure 5.10. Axial ratios of the antenna across the tuning band. Measured (solid lines) and simulated (dotted lines) in the azimuth $\theta = 90^\circ$ and $\varphi = 0^\circ$ at three different tuning bands. The unit for the voltages is volt.

in Fig. 5.11. As shown in Fig. 5.12, the efficiency of the antenna increases from 56.8% to 88.2%. The low efficiency at the low tuning band is due to a higher ohmic loss of the varactor diodes at the low frequency compared to that of the higher band.

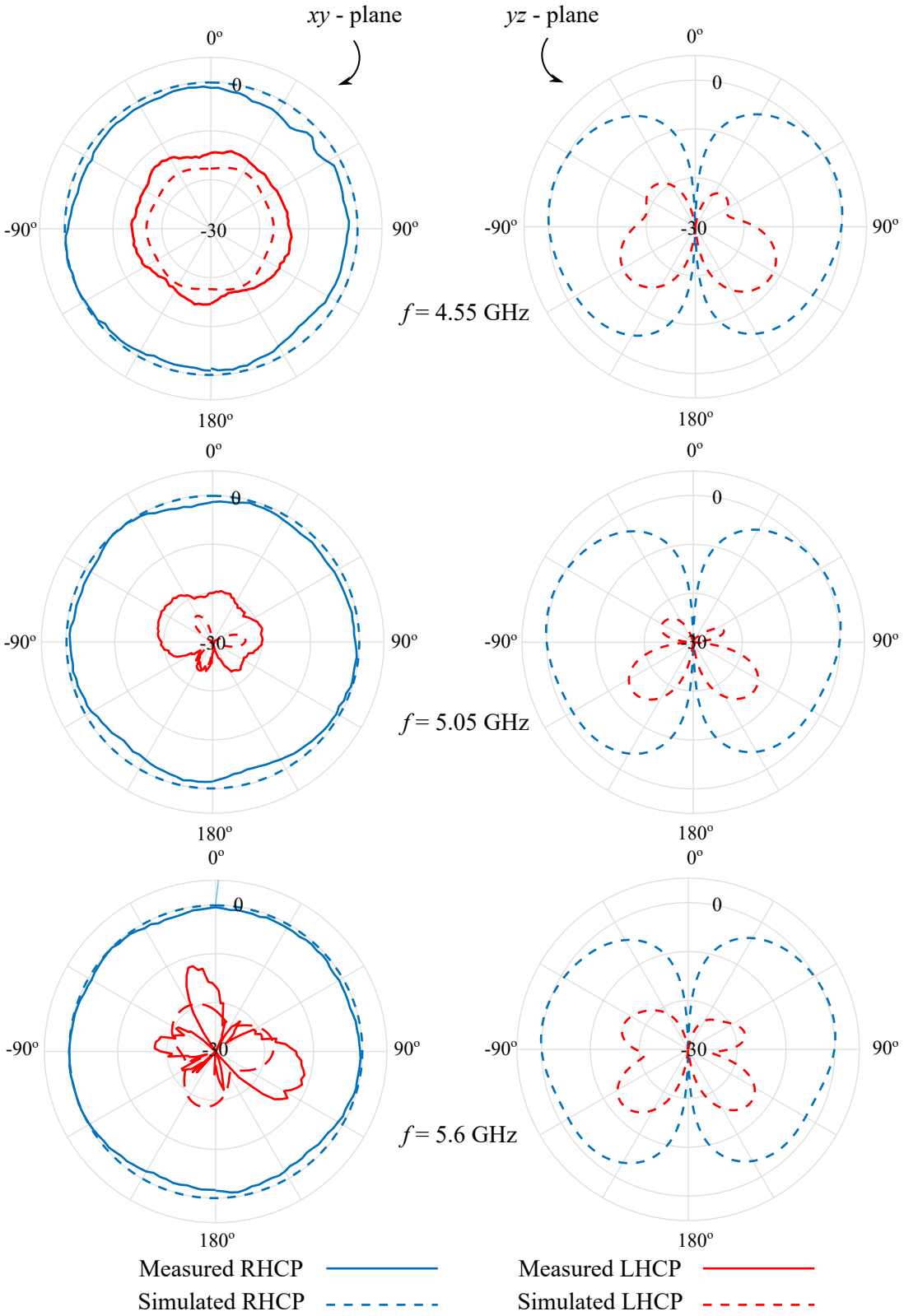

Figure 5.11. Normalized radiation patterns of the antenna. Measured and simulated at low, medium, and high tuning bands. It is noted that only azimuth patterns are measured.

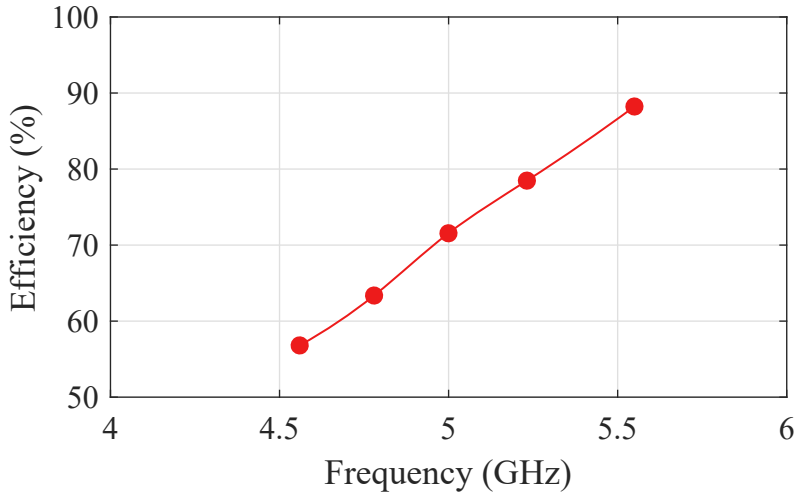

Figure 5.12. Simulated efficiency of the antenna.

5.6 Conclusion

In this chapter, a concept of circularly-polarized frequency-reconfigurable omnidirectional antenna has been presented. The CP antenna is based on a combination of three main elements: magnetic current sources, electric current sources, and phase compensation lines. To obtain the frequency reconfigurability, the patch is etched with three varactor-loaded slots. Coiled biasing wires and sleeve balun have been implemented into the antenna to reduce the parasitic surface currents that may disturb the axial ratio. The realization demonstrates a wide CP tuning range of 22.6% from 4.48 to 5.62 GHz. Stable omnidirectional patterns in the azimuth plane are achieved across the tuning range. All these results suggest that the antenna is suitable for communications systems that require an omnidirectional CP antenna with a frequency-tunable feature.

Chapter 6

Thesis Conclusion

THIS chapter summarizes the contributions that have been presented in the thesis. The achieved results have been described into two main parts mainly associated with the design of omnidirectional antennas realized in substrate-integrated cavities. The first part has focused on the design of passive low-profile monopole antennas, namely with via- and via-less shortings. The second part has introduced novel frequency-reconfigurable omnidirectional antennas with original contributions of multi-band and circularly-polarized designs.

6.1 Part I: Low-Profile Antennas

This part of the thesis consists of Chapter 3, which have placed a focus on the design low-profile omnidirectional antennas. In particular, this chapter has discussed the development of low-profile monopoles with via-less shortings. This section summarizes the original contributions and describes the potential future research of this part.

6.1.1 Summary of Original Contributions

Three different shorting strategies have been investigated for low-profile monopole antennas. These shorting methods include shorting pins, stubs, and complementary split ring resonators (CSRRs). The performance of designed antennas utilizing these three shorting techniques has been compared in terms of size, bandwidth and radiation patterns. From the measurement results, it is found that bandwidth for via-less monopoles are narrower than the via-based version. The narrow bandwidth is particularly because of the high Q factor from the stubs and CSRRs. Nevertheless, the results indicate that the stubs and CSRRs act similarly as physical vias to realize shortings in the antenna. Also, all the designs exhibit omnidirectional radiation patterns in the azimuth plane and conical patterns in the elevation plane.

6.1.2 Future Work

The concept of via-less shortings that is proposed in the thesis can be potentially applied to other types of antenna designs, for example, planar inverted F-antenna (PIFA). A PIFA is a special case of the patch antenna. It consists of a patch parallel to the PCB with short circuit implemented at the edge. This type of antenna is increasingly used in the compact hand-held wireless devices due to its small size. It is noted that the shorting pins take integral parts to the radiation of the PIFA. This thesis shows that the stubs and CSRRs can be potential substitutions to shorting vias. Therefore, it is expected that these two via-less shorting solutions can also be alternatives to shorting mechanism in PIFAs. This is an interesting scenario worth investigating. Furthermore, similar studies can also be conducted for other types of antennas that require shorting wall realization.

As discussed in Chapter 3 and 4, a low-profile monopole with stubs shortings can be extended into a multi-band device. This is obtained by adding additional sets of

stubs into the patch. The technique is simple and can be further explored to design many other types of antenna, such as a broadband stub-loaded low-profile monopole antenna. This particular objective is possible to be achieved by configuring the design parameters of the stubs. The length of the adjacent stubs can be set to be gradually increasing in order to achieve a broad bandwidth instead of a multi-band one.

6.2 Part II: Frequency Reconfigurable Antennas

Chapters 4 and 5 represent the second part of the thesis, which has investigated low-profile monopolar antenna designs with frequency tunability. This section concludes the original contributions and suggests potential directions for future work.

6.2.1 Summary of Original Contributions

First, frequency-reconfigurable low-profile monopole antennas with independently tunable bands have been proposed. The designs are based on the concept of a circular patch with shorting stubs to realize independent magnetic current loops sharing the same thin aperture. Varactor diodes are integrated to obtain the frequency reconfigurability. They are positioned in the gap between the patch and the stubs to control the surface current distributions. The concept is firstly validated with a dual-band reconfigurable prototype and then is extended into a triple-band device. The results have indicated that the tuning independency is attained in both designs. The tuning ranges are 21.2% and 27.1% for the dual-band design, and 22.8%, 22.8%, and 16.7% for the triple-band device. The radiation pattern is omnidirectional and stable across the tuning ranges. The designs are promising for advanced applications such as software-defined radio or carrier aggregation systems.

The second design is a circularly-polarized (CP) frequency-reconfigurable low-profile omnidirectional antenna. The antenna consists of three main elements: magnetic current sources from the slot cavities, electric current sources from the arc-shaped arms, and phase compensation lines between them. By optimizing these three elements, the antenna can radiate with circular polarization. The frequency reconfigurable version of the antenna can be designed with integration of varactor-loaded slots. The variation of the capacitance in these slots enables the resonance frequency to be shifted while still maintaining the axial ratio. The radiation patterns are all omnidirectional across

the tuning range. The proposed design is unique and might be the only one existing CP frequency-reconfigurable antenna that radiates omnidirectionally.

6.2.2 Future Work

The two proposed frequency-reconfigurable antennas mentioned above can be suitable for numerous wireless applications due to their compact configuration. For example, the triple-band antenna in Chapter 4 can be re-designed to be conformal so that it can be mounted onto a helmet. Furthermore, with some modifications, the biasing network can be integrated into the structure of the helmet. Future investigations should study the effect of these adaptations on the performance of the antenna.

Moreover, the feature of these two antennas can be further developed with the integration of additional active elements, such as PIN diodes. For instance, the CP reconfigurable antenna in Chapter 5 can be made frequency- and polarization-reconfigurable. This is possible by placing PIN diodes in between the patch and the phase compensation lines. In the OFF state, the polarization of the antenna will be linear, while in the ON state the polarization is circular.

6.3 Concluding Statement

The research investigated in this thesis has focused on the design of low-profile omnidirectional antennas. Initially, shorting techniques in low-profile monopole antennas were investigated with contributions on the via and via-less monopoles design procedures. Additionally, a novel multi-band reconfigurable low-profile monopolar antennas have been presented and could be deployed in advanced communications systems. Finally, a concept of CP frequency-reconfigurable antenna with an omnidirectional pattern is presented. All these antennas offer many attractive features, making them suitable to be used in numerous communications systems. Furthermore, all the design principles that are proposed in the thesis can be further developed to design many other forms of antennas.

Appendix A

Self-Resonance of Inductors

The capacitance and resistance of ideal inductors are strictly equal to zero. Nevertheless, real inductors have parasitic resistance and capacitance. This will cause the appearance of so-called self-resonances, which can be modelled by a parallel combination of inductance and capacitance. At the self-resonant frequency (SRF), inductors have a peak input impedance. The effective reactance is zero since the negative capacitive reactance ($X_C = 1/j\omega C$) negates the positive inductive reactance ($X_L = j\omega L$). The capacitance of an inductor is generally called "inter-winding capacitance", as a result of charge separation between insulated coil windings. However, because the inductor is usually used over a conducting ground-plane, a capacitance between the coil and the ground plane should also be taken into account. The distance between the coil and the ground plane and the substrate effective relative permittivity affect the capacitance to the ground. As a result, the SRF measurement of inductors can vary from one type to another. The relation between the SRF and the inductance and capacitance of an LC circuit is as follows:

$$\text{SRF} = \frac{1}{2\pi\sqrt{LC}}, \tag{A.1}$$

where L is the inductance in Henries, C is the capacitance in Farads, and the SRF is in Hz. This equation suggests that reducing capacitance or inductance increases the SRF.

A high value of inductance is usually desired when using inductors as an RF choke. In most cases, a high-value inductor has a high level of parasitic capacitance and a low SRF. However, many RF chokes are made of very thin wires so that they can pack a given inductance into a small space. Because of the skin effect of the inductors, these RF chokes cannot have sufficient capacitance to counteract the high-frequency resistance of the wire [84]. This means that they might be useful for a broader frequency

range than the specification, sometimes up to several orders of magnitude higher in frequency.

An investigation of inductors as RF chokes using co-planar waveguide (CPW) transmission lines has been conducted. The configurations are shown in Fig. A.1. The first CPW device is without inductors, as illustrated in Fig. A.1(a), while two 47 nH inductors with SRF of 3.3 GHz are placed between the gap of the second CPW configuration, as depicted in Fig. A.1(b). The objective is to compare the S-parameters between these two configurations of CPW lines. In principle, the inductors should not affect the transmission coefficient S_{21} as they block the RF current travelling to the ground side of the CPW line. As shown from the results illustrated in Fig. A.2 , there are no significant differences between the two S-parameters of the CPW transmission lines. Therefore, we can assume that the inductors will be effectively working as RF chokes for the frequency range of interest.

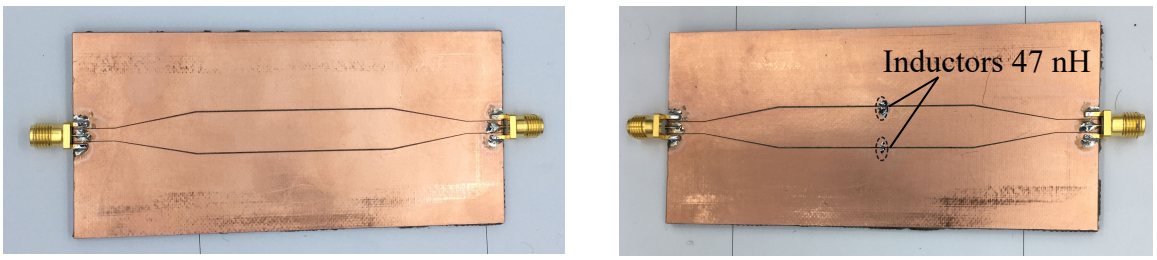

Figure A.1. Photographs of CPW transmission lines (a) without and (b) with inductors. In (b), the inductors bridge the gaps of the CPW line.

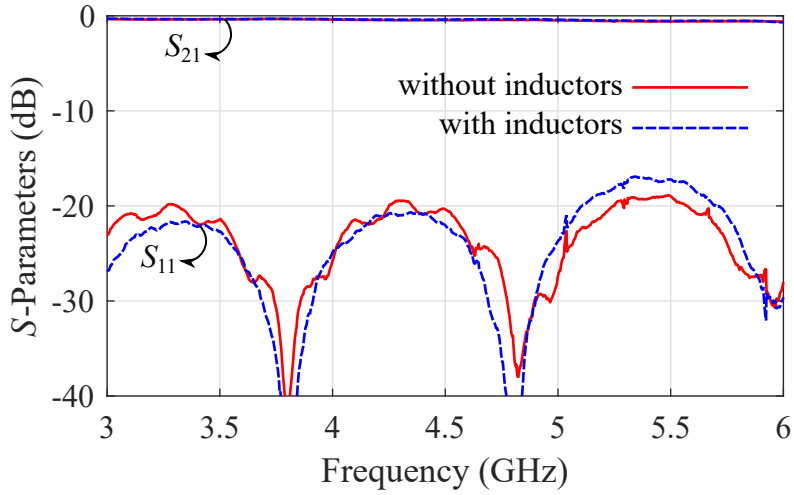

Figure A.2. S-Parameters of CPW transmission lines with and without inductors.

Appendix B

CST Mesh Refinement

All the CST simulations that have been carried out for the thesis are based on finite-element frequency-domain solver with tetrahedral meshing. The accuracy of the simulation is directly dependant on the fineness of the mesh. However, the simulation time increases with the total number of mesh cells. Therefore, it is advisable to manually configure the mesh size to optimize the tradeoff between the accuracy and the simulation time.

Figure B.1 shows an example of the mesh refinement for the simulation of the dual-band antenna design in Chapter 4. The procedure focus on the mesh accuracy in the capacitive gap and the gap between the patch and the stub. Three different meshes are used for the refinement process, namely Mesh 1, 2 and 3. Mesh 1 is automatically generated from CST, while Mesh 2 and Mesh 3 are manually refined with maximum discretization sizes of 0.1 mm and 0.01 mm, respectively. Consequently, Mesh 1 simulation delivered the result in the shortest time (about 30 minutes), while simulation using Mesh 3 requires the longest time of above 2 hours. In terms of the convergence of the S_{11} results, it can be seen from Fig. B.2 that there is a frequency-shifting from Mesh 1 to Mesh 2 simulations. However, there is almost no difference in Mesh 2 and Mesh 3 simulation results. This concludes that Mesh 2 simulation, which took about 1 hour, has satisfied the convergence and can be used for the dual-band design optimization.

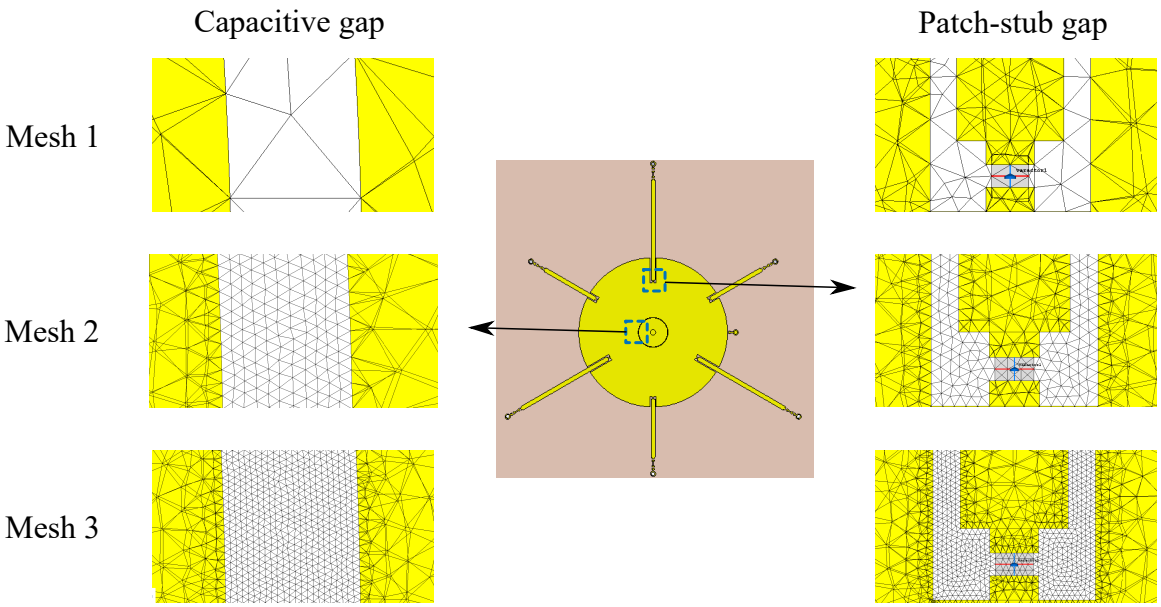

Figure B.1. Mesh refinement steps for the dual-band antenna design from Chapter 4.

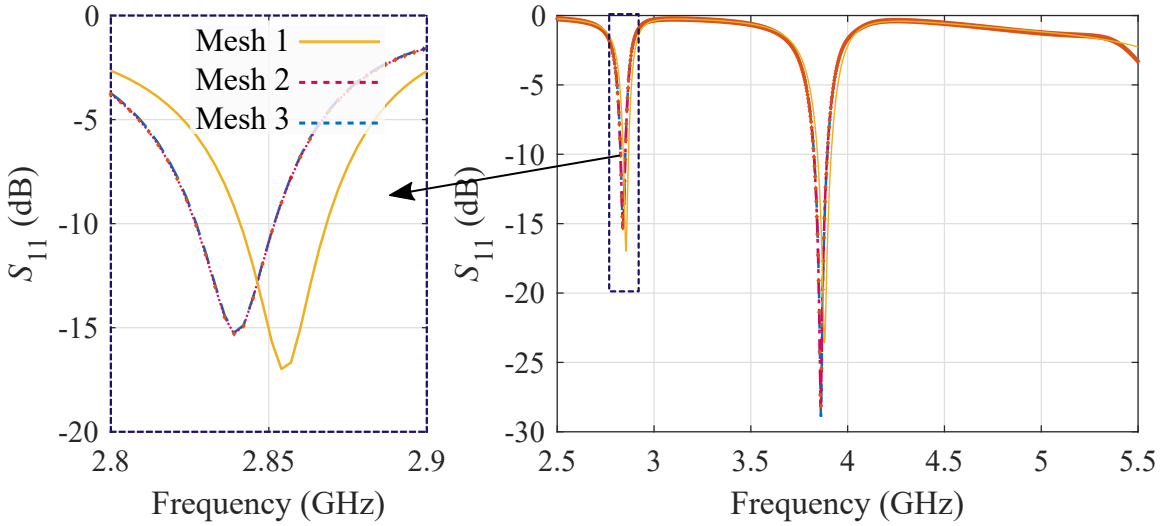

Figure B.2. S_{11} results comparison for different mesh refinement.

Appendix C

Antenna Radiation Boundary Conditions

In antenna design simulations, boundary conditions are typically used to emulate the free space environment. By default, Ansys HFSS uses radiation boundary (RB), while CST uses perfectly-matched layer (PML) boundary condition. In principle, the RB mimics continued propagation beyond the boundary plane. The distance of the boundary plane should place at least $\lambda/4$ from a radiating structure. Figure C.1 depicts the example of a horn antenna simulation that uses this boundary condition. The RB absorbs best when the incident energy flow is normal to surface. This is illustrated in Fig. C.2.

The PML is a lossy and an anisotropic layer which is used to fully absorbs the electromagnetic fields. There are two applications of PML, as a free-space termination and as a transmission line termination. When it is used as a free-space termination, PML objects absorb free radiation. Meanwhile, if PML terminates a transmission line, PML objects mimic a continuation of the guided waves. An example of PML configuration is illustrated in Fig. C.3. PML offers a better absorption at a larger incidence angle compared to the RB, which resulted in better consistency in the patterns. This is shown in Fig. C.4.

LIBRARY NOTE:

This diagram has been removed due to copyright.

Figure C.1. Example of radiation boundary configuration. Adopted from [85].

LIBRARY NOTE:

This diagram has been removed due to copyright.

Figure C.2. Incident angle dependency of radiation boundary condition. Adopted from [85].

LIBRARY NOTE:

This diargram has been removed due to copyright.

Figure C.3. Example of PML configuration. Adopted from [85].

LIBRARY NOTE:

This diagram has been removed due to copyright.

Figure C.4. Incident angle dependency of PML boundary condition. Adopted from [85].

Bibliography

[1] H. A. Wheeler, "Fundamental limitations of small antennas," *Proceedings of the IRE*, vol. 35, no. 12, pp. 1479–1484, 1947.

[2] E. W. Seeley, "An experimental study of the disk-loaded folded monopole," *IRE Transactions on Antennas and Propagation*, vol. 4, no. 1, pp. 27–28, 1956.

[3] C. Delaveaud, P. Leveque, and B. Jecko, "New kind of microstrip antenna: the monopolar wire-patch antenna," *Electronics Letters*, vol. 30, no. 1, pp. 1–2, 1994.

[4] H. Nakano, H. Iwaoka, K. Morishita, and J. Yamauchi, "A wideband low-profile antenna composed of a conducting body of revolution and a shorted parasitic ring," *IEEE Transactions on Antennas and Propagations*, vol. 56, no. 4, pp. 1187–1192, 2008.

[5] T. Kaufmann and C. Fumeaux, "Low-profile magnetic loop monopole antenna based on a square substrate-integrated cavity," *International Journal of Antennas and Propagation*, vol. 2015, 2015.

[6] M. Koohestani, J.-F. Zürcher, A. A. Moreira, and A. K. Skrivervik, "A novel, low-profile, vertically-polarized UWB antenna for WBAN," *IEEE Transactions on Antennas and Propagations*, vol. 62, no. 4, pp. 1888–1894, 2014.

[7] N. P. Lawrence, C. Fumeaux, and D. Abbott, "Wideband substrate-integrated monopole antenna," *Microwave and Optical Technology Letters*, vol. 58, no. 8, pp. 1855–1857, 2016.

[8] N. Nguyen-Trong, A. Piotrowski, T. Kaufmann, and C. Fumeaux, "Low-profile wideband monopolar UHF antennas for integration onto vehicles and helmets," *IEEE Transactions on Antennas and Propagations*, vol. 64, no. 6, pp. 2562–2568, 2016.

[9] A. Elsherbini and K. Sarabandi, "Very low-profile top-loaded UWB coupled sectorial loops antenna," *IEEE Antennas and Wireless Propagation Letters*, vol. 10, pp. 800–803, 2011.

[10] H. F. Abutarboush, R. Nilavalan, S. W. Cheung, and K. M. Nasr, "Compact printed multiband antenna with independent setting suitable for fixed and reconfigurable wireless communication systems," *IEEE Transactions on Antennas and Propagations*, vol. 60, no. 8, pp. 3867–3874, 2012.

[11] A. Khidre, F. Yang, and A. Z. Elsherbeni, "A patch antenna with a varactor-loaded slot for reconfigurable dual-band operation," *IEEE Transactions on Antennas and Propagations*, vol. 63, no. 2, pp. 755–760, 2015.

[12] C. Hung and T. Chiu, "Dual-band reconfigurable antenna design using slot-line with branch edge," *IEEE Transactions on Antennas and Propagations*, vol. 63, no. 2, pp. 508–516, 2015.

[13] N. Behdad and K. Sarabandi, "Dual-band reconfigurable antenna with a very wide tunability range," *IEEE Transactions on Antennas and Propagations*, vol. 54, no. 2, pp. 409–416, 2006.

[14] Q. Bai, R. Singh, K. L. Ford, T. O'Farrell, and R. J. Langley, "An independently tunable tri-band antenna design for concurrent multiband single chain radio receivers," *IEEE Transactions on Antennas and Propagations*, vol. 65, no. 12, pp. 6290–6297, 2017.

[15] N. Nguyen-Trong, A. Piotrowski, and C. Fumeaux, "A frequency-reconfigurable dual-band low-profile monopolar antenna," *IEEE Transactions on Antennas and Propagations*, vol. 65, no. 7, pp. 3336–3343, 2017.

[16] S. Gao, Q. Luo, and F. Zhu, *Circularly Polarized Antennas*. John Wiley & Sons, Ltd, 2014.

[17] R. Szumny, K. Kurek, and J. Modelski, "Attenuation of multipath components using directional antennas and circular polarization for indoor wireless positioning systems," in *2007 European Radar Conference*, 2007, pp. 401–404.

[18] B. A. Witvliet, E. van Maanen, G. J. Petersen, A. J. Westenberg, M. J. Bentum, C. H. Slump, and R. Schiphorst, "The importance of circular polarization for diversity reception and MIMO in NVIS propagation," in *The 8th European Conference on Antennas and Propagation (EuCAP 2014)*, 2014, pp. 2797–2801.

[19] S. Biswas, R. Tatchikou, and F. Dion, "Vehicle-to-vehicle wireless communication protocols for enhancing highway traffic safety," *IEEE Communications Magazine*, vol. 44, no. 1, pp. 74–82, 2006.

[20] K. Sampigethaya, R. Poovendran, S. Shetty, T. Davis, and C. Royalty, "Future E-enabled aircraft communications and security: The next 20 years and beyond," *Proceedings of the IEEE*, vol. 99, no. 11, pp. 2040–2055, 2011.

[21] G. Marrocco, L. Mattioni, and C. Calabrese, "Multiport sensor RFIDs for wireless passive sensing of objects—basic theory and early results," *IEEE Transactions on Antennas and Propagation*, vol. 56, no. 8, pp. 2691–2702, 2008.

[22] C. A. Balanis, *Antenna Theory: Analysis and Design*, 3rd ed. Hoboken, NJ: Wiley-Interscience, 2005.

[23] Y. Huang and K.Boyle, *Antennas: From Theory to Practice*, 1st ed. West Sussex, UK: John Wiley & Sons Ltd, 2008.

[24] J. Bernhard, *Reconfigurable Antennas*, ser. Synthesis Lectures on Antennas and Propagation Series. Morgan & Claypool, 2007.

[25] R. O. Ouedraogo, J. Tang, K. Fuchi, E. J. Rothwell, A. R. Diaz, and P. Chahal, "A tunable dual-band miniaturized monopole antenna for compact wireless devices," *IEEE Antennas and Wireless Propagation Letters*, vol. 13, pp. 1247–1250, 2014.

[26] T. Li, H. Zhai, X. Wang, L. Li, and C. Liang, "Frequency-reconfigurable bow-tie antenna for bluetooth, WiMAX, and WLAN applications," *IEEE Antennas and Wireless Propagation Letters*, vol. 14, pp. 171–174, 2015.

[27] T. . Han and C. . Huang, "Reconfigurable monopolar patch antenna," *Electronics Letters*, vol. 46, no. 3, pp. 199–200, 2010.

[28] H. Boudaghi, M. Azarmanesh, and M. Mehranpour, "A frequency-reconfigurable monopole antenna using switchable slotted ground structure," *IEEE Antennas and Wireless Propagation Letters*, vol. 11, pp. 655–658, 2012.

[29] H. A. Majid, M. K. A. Rahim, M. R. Hamid, N. A. Murad, and M. F. Ismail, "Frequency-reconfigurable microstrip patch-slot antenna," *IEEE Antennas and Wireless Propagation Letters*, vol. 12, pp. 218–220, 2013.

[30] L. Pazin and Y. Leviatan, "Reconfigurable slot antenna for switchable multiband operation in a wide frequency range," *IEEE Antennas and Wireless Propagation Letters*, vol. 12, pp. 329–332, 2013.

[31] P. Qin, F. Wei, and Y. J. Guo, "A wideband-to-narrowband tunable antenna using a reconfigurable filter," *IEEE Transactions on Antennas and Propagations*, vol. 63, no. 5, pp. 2282–2285, 2015.

[32] Y. Tawk, A. El-Amine, S. Saab, J. Costantine, F. Ayoub, and C. G. Christodoulou, "A software-defined frequency-reconfigurable meandered printed monopole," *IEEE Antennas and Wireless Propagation Letters*, vol. 17, no. 2, pp. 327–330, 2018.

[33] A. Zohur, H. Mopidevi, D. Rodrigo, M. Unlu, L. Jofre, and B. A. Cetiner, "RF-MEMS reconfigurable two-band antenna," *IEEE Antennas and Wireless Propagation Letters*, vol. 12, pp. 72–75, 2013.

[34] D. E. Anagnostou, M. T. Chryssomallis, B. D. Braaten, J. L. Ebel, and N. Sepúlveda, "Reconfigurable UWB antenna with RF-MEMS for on-demand WLAN rejection," *IEEE Transactions on Antennas and Propagations*, vol. 62, no. 2, pp. 602–608, 2014.

[35] H. Mirzaei and G. V. Eleftheriades, "A compact frequency-reconfigurable metamaterial-inspired antenna," *IEEE Antennas and Wireless Propagation Letters*, vol. 10, pp. 1154–1157, 2011.

[36] N. Nguyen-Trong, T. Kaufmann, L. Hall, and C. Fumeaux, "Analysis and design of a reconfigurable antenna based on half-mode substrate-integrated cavity," *IEEE Transactions on Antennas and Propagations*, vol. 63, no. 8, pp. 3345–3353, 2015.

[37] V. I. Cojocaru and T. J. Brazil, "A large-signal equivalent circuit model for hyperabrupt p-n junction varactor diodes," in *1992 22nd European Microwave Conference*, vol. 2, 1992, pp. 1115–1121.

[38] S. N. M. Zainarry, N. Nguyen-Trong, and C. Fumeaux, "A frequency- and pattern-reconfigurable two-element array antenna," *IEEE Antennas and Wireless Propagation Letters*, vol. 17, no. 4, pp. 617–620, 2018.

[39] S. J. Chen, D. C. Ranasinghe, and C. Fumeaux, "A robust snap-on button solution for reconfigurable wearable textile antennas," *IEEE Transactions on Antennas and Propagations*, vol. 66, no. 9, pp. 4541–4551, 2018.

[40] N. Nguyen-Trong, L. Hall, and C. Fumeaux, "A frequency- and pattern-reconfigurable center-shorted microstrip antenna," *IEEE Antennas and Wireless Propagation Letters*, vol. 15, pp. 1955–1958, 2016.

[41] N. Behdad and K. Sarabandi, "A varactor-tuned dual-band slot antenna," *IEEE Transactions on Antennas and Propagations*, vol. 54, no. 2, pp. 401–408, 2006.

[42] H. Li, J. Xiong, Y. Yu, and S. He, "A simple compact reconfigurable slot antenna with a very wide tuning range," *IEEE Transactions on Antennas and Propagations*, vol. 58, no. 11, pp. 3725–3728, 2010.

[43] P. Chi, R. Waterhouse, and T. Itoh, "Compact and tunable slot-loop antenna," *IEEE Transactions on Antennas and Propagations*, vol. 59, no. 4, pp. 1394–1397, 2011.

[44] Y. Cai, K. Li, Y. Yin, S. Gao, W. Hu, and L. Zhao, "A low-profile frequency reconfigurable grid-slotted patch antenna," *IEEE Access*, vol. 6, pp. 36 305–36 312, 2018.

[45] P. Qin, A. R. Weily, Y. J. Guo, T. S. Bird, and C. Liang, "Frequency reconfigurable quasi-yagi folded dipole antenna," *IEEE Transactions on Antennas and Propagations*, vol. 58, no. 8, pp. 2742–2747, 2010.

[46] Y. Cai, Y. J. Guo, and T. S. Bird, "A frequency reconfigurable printed Yagi-Uda dipole antenna for cognitive radio applications," *IEEE Transactions on Antennas and Propagations*, vol. 60, no. 6, pp. 2905–2912, 2012.

[47] T. Li, H. Zhai, L. Li, and C. Liang, "Frequency-reconfigurable bow-tie antenna with a wide tuning range," *IEEE Antennas and Wireless Propagation Letters*, vol. 13, pp. 1549–1552, 2014.

[48] M. N. M. Kehn, O. Quevedo-Teruel, and E. Rajo-Iglesias, "Reconfigurable loaded planar inverted-F antenna using varactor diodes," *IEEE Antennas and Wireless Propagation Letters*, vol. 10, pp. 466–468, 2011.

[49] S. Sam and S. Lim, "Compact frequency-reconfigurable half-mode substrate-integrated waveguide antenna," *IEEE Antennas and Wireless Propagation Letters*, vol. 12, pp. 951–954, 2013.

[50] C. Wu and T. Ma, "Pattern-reconfigurable self-oscillating active integrated antenna with frequency agility," *IEEE Transactions on Antennas and Propagations*, vol. 62, no. 12, pp. 5992–5999, 2014.

[51] M. S. Alam and A. Abbosh, "A compact reconfigurable antenna with wide tunable frequency and 360° beam scanning," *IEEE Antennas and Wireless Propagation Letters*, vol. 18, no. 1, pp. 4–8, 2019.

[52] A. Tariq and H. Ghafouri-Shiraz, "Frequency-reconfigurable monopole antennas," *IEEE Transactions on Antennas and Propagations*, vol. 60, no. 1, pp. 44–50, 2012.

[53] L. Ge and K. Luk, "Frequency-reconfigurable low-profile circular monopolar patch antenna," *IEEE Transactions on Antennas and Propagations*, vol. 62, no. 7, pp. 3443–3449, 2014.

[54] D. G. Chen and K. W. Eccleston, "Substrate integrated waveguide with corrugated wall," in *Proceedings of Asia–Pacific Microwave Conference*, 2008, pp. 1–4.

[55] K. W. Eccleston, "Mode analysis of the corrugated substrate integrated waveguide," *IEEE Transactions on Microwave Theory and Techniques*, vol. 60, no. 10, pp. 3004–3012, 2012.

[56] M. Nitas, C. S. Antonopoulos, and T. V. Yioultsis, "E-B eigenmode formulation for the analysis of lossy and evanescent modes in periodic structures and metamaterials," *IEEE Transactions on Magnetics*, vol. 53, no. 6, pp. 1–4, 2017.

[57] M. Nitas, M. . Passia, and T. V. Yioultsis, "Analysis and design of a CSRR-based fully planar substrate-integrated waveguide for millimeter-wave circuits and antennas," in *2017 11th European Conference on Antennas and Propagation (EUCAP)*, 2017, pp. 3501–3505.

[58] C. A. Balanis, *Antenna Theory: Analysis and Design*. Wiley-Interscience, 2005.

[59] J. D. Baena, J. Bonache, F. Martin, R. M. Sillero, F. Falcone, T. Lopetegi, M. A. G. Laso, J. Garcia-Garcia, I. Gil, M. F. Portillo, and M. Sorolla, "Equivalent-circuit models for split-ring resonators and complementary split-ring resonators coupled to planar transmission lines," *IEEE Transactions on Microwave Theory and Techniques*, vol. 53, no. 4, pp. 1451–1461, 2005.

[60] C. Lin, P. Jin, and R. W. Ziolkowski, "Single, dual and tri-band-notched ultrawideband (UWB) antennas using capacitively loaded loop (CLL) resonators," *IEEE Transactions on Antennas and Propagations*, vol. 60, no. 1, pp. 102–109, 2012.

[61] N. Behdad, M. Li, and Y. Yusuf, "A very low-profile, omnidirectional, ultrawideband antenna," *IEEE Antennas and Wireless Propagation Letters*, vol. 12, pp. 280–283, 2013.

[62] Y. M. Pan, S. Y. Zheng, and B. J. Hu, "Wideband and low-profile omnidirectional circularly polarized patch antenna," *IEEE Transactions on Antennas and Propagations*, vol. 62, no. 8, pp. 4347–4351, 2014.

[63] K. Ghaemi and N. Behdad, "A low-profile, vertically polarized ultrawideband antenna with monopole-like radiation characteristics," *IEEE Transactions on Antennas and Propagations*, vol. 63, no. 8, pp. 3699–3705, 2015.

[64] A. A. Omar and Z. Shen, "A compact and wideband vertically polarized monopole antenna," *IEEE Transactions on Antennas and Propagations*, vol. 67, no. 1, pp. 626–631, 2019.

[65] E. Erdil, K. Topalli, M. Unlu, O. A. Civi, and T. Akin, "Frequency tunable microstrip patch antenna using RF-MEMS technology," *IEEE Transactions on Antennas and Propagations*, vol. 55, no. 4, pp. 1193–1196, 2007.

[66] I. Kim and Y. Rahmat-Samii, "RF-MEMS switchable slot patch antenna integrated with bias network," *IEEE Transactions on Antennas and Propagations*, vol. 59, no. 12, pp. 4811–4815, 2011.

[67] C. Chiu, J. Li, S. Song, and R. D. Murch, "Frequency-reconfigurable pixel slot antenna," *IEEE Transactions on Antennas and Propagations*, vol. 60, no. 10, pp. 4921–4924, 2012.

[68] K. Paramayudha, S. J. Chen, W. Withayachumnankul, and C. Fumeaux, "Low-profile monopole antenna with via-less shorting," in *Proceedings of Australian Microwave Symposium (AMS)*, 2018, pp. 11–12.

[69] T. P. Lee, "Evaluation of voltage dependent series resistance of epitaxial varactor diodes at microwave frequencies," *IEEE Transactions on Electron Devices*, vol. 12, no. 8, pp. 457–470, 1965.

[70] M. Niroo-Jazi and T. A. Denidni, "A new triple-band circular ring patch antenna with monopole-like radiation pattern using a hybrid technique," *IEEE Transactions on Antennas and Propagations*, vol. 59, no. 10, pp. 3512–3517, 2011.

[71] E. Brookner, W. M. Hall, and R. H. Westlake, "Faraday loss for l-band radar and communications systems," *IEEE Transactions on Aerospace and Electronic Systems*, vol. AES-21, no. 4, pp. 459–469, 1985.

[72] N. Jin, Fan Yang, and Y. Rahmat-Samii, "A novel patch antenna with switchable slot (pass): dual-frequency operation with reversed circular polarizations," *IEEE Transactions on Antennas and Propagation*, vol. 54, no. 3, pp. 1031–1034, 2006.

[73] C. W. Jung, M. . Lee, and F. D. Flaviis, "Reconfigurable dual-band antenna with high frequency ratio (1.6:1) using MEMS switches," *Electronics Letters*, vol. 44, no. 2, pp. 76–77, 2008.

[74] T.-Y. Lee and J.-S. Row, "Frequency reconfigurable circularly polarized slot antennas with wide tuning range," *Microwave and Optical Technology Letters*, vol. 53, no. 7, pp. 1501–1505, 2011.

[75] J. Row and J. Tsai, "Frequency-reconfigurable microstrip patch antennas with circular polarization," *IEEE Antennas and Wireless Propagation Letters*, vol. 13, pp. 1112–1115, 2014.

[76] H. Gu, J. Wang, and L. Ge, "Circularly polarized patch antenna with frequency reconfiguration," *IEEE Antennas and Wireless Propagation Letters*, vol. 14, pp. 1770–1773, 2015.

[77] M. S. Shakhirul, M. Jusoh, A. H. Ismail, M. R. Kamarudin, H. A. Rahim, and T. Sabapathy, "Reconfigurable frequency with circular polarization for on-body wearable textile antenna," in *2016 10th European Conference on Antennas and Propagation (EuCAP)*, 2016, pp. 1–4.

[78] Q. Chu, M. Ye, and X. Li, "A low-profile omnidirectional circularly polarized antenna using planar sector-shaped endfire elements," *IEEE Transactions on Antennas and Propagation*, vol. 65, no. 5, pp. 2240–2247, 2017.

[79] F. W. Gover, *Inductance Calculations*, ser. Dover Books on Electrical Engineering. Dover Publications, 2009.

[80] C. Icheln, J. Ollikainen, and P. Vainikainen, "Reducing the influence of feed cables on small antenna measurements," *Electronics Letters*, vol. 35, no. 15, pp. 1212–1214, 1999.

[81] C. Icheln, J. Krogerus, and P. Vainikainen, "Use of balun chokes in small-antenna radiation measurements," *IEEE Transactions on Instrumentation and Measurement*, vol. 53, no. 2, pp. 498–506, 2004.

[82] C. Icheln, M. Popov, P. Vainikainen, and S. He, "Optimal reduction of the influence of RF feed cables in small antenna measurements," *Microwave and Optical Technology Letters*, vol. 25, no. 3, pp. 194–196, 2000.

[83] S. A. Saario, J. W. Lu, and D. V. Thiel, "Full-wave analysis of choking characteristics of sleeve balun on coaxial cables," *Electronics Letters*, vol. 38, no. 7, pp. 304–305, 2002.

[84] L. Siebert. When to use an RF choke vs an inductor. [Online]. Available: https://e2e.ti.com/blogs_/b/analogwire/archive/2014/04/23/when-to-use-an-rf-choke-vs-an-inductor

[85] Ansys. Antenna boundary conditions. [Online]. Available: https://www.ansys.com/services/training-center/electronics/ansys-hfss-for-antenna-design

Biography

Ken Paramayudha was born in Bandung, Indonesia in 1987. He received his Bachelor of Engineering in the field of Electrical Engineering from Bandung Institute of Technology, Indonesia in 2009. After obtaining his undergraduate degree, he worked as a Software Modeling Engineer at Indonesia's first IC design house, Versatile Silicon Technologies until 2011. At the end of 2011, he moved to PT. Len Industri to work as a Project Engineer. Since 2014 Ken is a Junior Researcher in a Research Center for Electronics and Telecommunication, Indonesian Institute of Sciences. In 2017, He received the Riset-PRO Scholarship from Indonesian Ministry of Research, Technology, and Higher Degree Education to continue his Master study at the University of Adelaide. He joined the School of Electrical and Electronic Engineering in the area of applied electromagnetics under the supervision of Prof. Christophe Fumeaux and Dr. Withawat Withayachumnankul.

During his candidature, he was the finalist of the best student paper award at Australian Microwave Symposium 2017, Brisbane. His research interests revolve around antennas and microwave devices.

Ken Paramayudha
ken.paramayudha@gmail.com